

論文 / 著書情報
Article / Book Information

題目(和文)	
Title(English)	A Structural Study of Peptides and Proteins by Solid State NMR
著者(和文)	浅川直紀
Author(English)	naoki asakawa
出典(和文)	学位:工学博士, 学位授与機関:東京工業大学, 報告番号:乙第2920号, 授与年月日:1996年7月31日, 学位の種別:論文博士, 審査員:安藤勲
Citation(English)	Degree:Doctor of Engineering, Conferring organization: Tokyo Institute of Technology, Report number:乙第2920号, Conferred date:1996/7/31, Degree Type:Thesis doctor, Examiner:
学位種別(和文)	博士論文
Type(English)	Doctoral Thesis

A Structural Study of Peptides and Proteins by Solid State NMR

A Dissertation
for the Degree of Engineering
Department of Polymer Chemistry,
Faculty of Engineering,
Tokyo Institute of Technology

Naoki Asakawa

1996

Contents

1	Introduction	1
1.1	Conformation-dependent Chemical Shift of Peptides	2
1.2	Hydrogen-bonding in Peptides	3
1.3	The Aim of This Study	4
2	Theory	8
2.1	Theory of NMR Spectrum	8
2.2	Determination of Chemical Shift Anisotropy	9
2.2.1	Powder Spectrum Analysis	9
2.2.2	Herzfeld-Berger Analysis	12
2.3	Theory of NMR Parameters: Inhomogeneous and Homogeneous Interactions	21
2.4	Detection of Dipolar Coupling in Rotating Solids	23
2.5	Molecular Orbital Calculation of Chemical Shielding	25
2.5.1	Finite Perturbation Theory with INDO MO Method (FPT-INDO)	26

2.5.2	Coupled Hartree-Fock Method Employing the 4-31G ab-initio MO Method with Gauge-Invariant Atomic Orbitals(4- 31G-GIAO-CHF)	27
3	Experiment	34
3.1	Peptides syntheses	34
3.2	Solid State ¹³ C NMR Measurements	35
4	Hydrogen-bonding Effect on the ¹³C Chemical Shift for L- Alanine Residue Carbonyl-carbon	37
4.1	Solid State NMR Measurements	37
4.2	¹³ C Shielding Constant Calculation by FPT-INDO Method . .	42
4.3	Verification of Hydrogen-bonding Structure in Proteins: Ba- sic Pancreatic Trypsin Inhibitor(BPTI); Ribonuclease H ^r from E.Coli(RNaseH)	45
5	Correlation Between Chemical Shifts of L-Alanine Residue C_α- and C_β-carbon and the Main-chain Dihedral-angles of Peptides and Proteins	59
5.1	Solid State NMR Measurements	59
5.2	Chemical Shielding Calculation by 4-31G-GIAO-CHF Method	61
5.3	Application to Structural Elucidation of Proteins: Basic Pan- creatic Trypsin Inhibitor(BPTI); Ribonuclease H from E.Coli (RNaseH)	68
6	Determination of Intermolecular Homonuclear Distance of	

α -Glycyl-glycine by XY8-DRAMA Sequence	87
6.1 Solid State NMR Measurements	89
6.2 Determination of Intermolecular Distances of Peptides	90
7 Conclusion	98
8 Future Prospect	101
Appendix	104
Bibliography	112
Acknowledgments	119

Chapter 1

Introduction

NMR chemical shift is one of the most important parameters for providing information about molecular structures.¹ Particularly, chemical shifts observed by the solid state NMR enable one an understanding of the three dimensional electronic structure around a nucleus. It is well known that peptides and proteins are found in almost every biological systems and play an important role in the biological processes. An understanding of how the secondary structure of peptides relates to their biological functions is very important to unravel the many biological systems in nature. The study of their model peptides is of particular interest because they serve as partial model systems for proteins which are too large to crystallize easily for X-ray diffraction studies and are too large to study with conventional solution NMR.

As is well known, both of the X-ray diffraction method and the distance-geometry method with solution NMR techniques are applied to structural

elucidation of proteins.² In the X-ray diffraction study, one must prepare a single crystal sample of a protein. Since it is not generally easy to prepare a single crystal of large protein, the X-ray diffraction method does not necessarily become a powerful methodology for structural elucidation of large proteins. The distance-geometry method gives the structural information on proteins in the solution state. This method employs nuclear Overhauser effect (NOE) and J-coupling obtained by solution NMR experiments. However, as signal enhancement by NOE is proportional to r^{-6} (where r is the inter-proton distance), the larger the inter-proton distance to be determined is, the larger experimental error it inevitably contains. Eventually, the main problem of these two methods is the lack of the number of the experimental data compared to the number of parameters required for determining the structure of a protein; the number of parameters is over ten thousand parameters of bond-lengths, bond-angles, and dihedral-angles. From such situations one seeks a further method for the structural elucidation in addition to these methods.

1.1 Conformation-dependent Chemical Shift of Peptides

Ando et al. have shown that the ^{13}C chemical shift behaviors of poly(L-alanine) can be interpreted in terms of the change in the electronic structure, which occurs by changes in main-chain conformations.³ From these studies, we realized that ^{13}C Chemical shifts of peptides in the solid state give us

information about conformations; from a point of view, we considered the term "conformation" as the main-chain dihedral-angles, (ϕ, ψ) , of a peptide. However, the hydrogen-bond formed in carbonyl-group seemed to be still crucial to understand ^{13}C chemical shift of peptides.

1.2 Hydrogen-bonding in Peptides

It is well-known that the hydrogen-bond plays an important role in forming stable conformations of oligopeptides, polypeptides, and proteins. So far, the nature of the hydrogen-bond has been widely studied by various spectroscopic methods.⁴ High resolution NMR spectroscopy has been also used as one of the most powerful tools for obtaining useful information about details of the hydrogen-bond.^{5, 6, 7, 8, 9, 10, 11, 12} Since the electronic structure around the carbonyl carbon is greatly affected by the nature of hydrogen-bond, ^{13}C NMR chemical shift for the carbonyl-carbon would be sensitive to the spatial arrangement of the nuclei comprising the hydrogen-bond. In fact, it was reported that the formation of the hydrogen-bond causes a downfield shift on the carbonyl-carbon of peptides in solution. It is difficult, however, to estimate exactly the hydrogen-bond effect on the ^{13}C chemical shift because the observed chemical shifts of peptides are often the averaged value for all the rotational isomers owing to an interconversion by rapid rotation about the bonds in solution.

On the other hand, chemical shifts in the solid state provide useful information about the hydrogen-bond of the peptides with a fixed conformation. From such a viewpoint, recently, Ando et al. have studied the hydrogen-

bonding effect on the ^{13}C chemical shifts of carbonyl carbons for peptides containing glycine (Gly) residues in the solid state.¹³ They have reported that the ^{13}C isotropic chemical shifts were determined for a series of oligopeptides containing glycine residues, of which the crystal structures were already available from X-ray diffraction studies. They found that the ^{13}C chemical shifts for the carbonyl carbons in the amide-amide type ($>\text{C}=\text{O}\cdots\text{H}-\text{N}<$) hydrogen-bond move linearly downfield with a decrease of the hydrogen-bond length. Furthermore, Ando et al. explained the ^{13}C chemical shift behavior for the carbonyl carbon in polyglycine with form I (β -sheet) or form II (3_1 -helix) in terms of the differences in their hydrogen-bond length. These experimental results were understood by ^{13}C chemical shielding calculations based on the semi-empirical molecular orbital method.

1.3 The Aim of This Study

Peptides containing Gly residues provide models for proteins. However, since proteins have the other amino acid residues besides glycine residue, of which the α -carbon is chiral, it is necessary to employ such amino acid residues to clarify generally the hydrogen-bonding effect on the ^{13}C chemical shift. Further, it is also important to clarify how changes in the main-chain dihedral-angles would affect on the ^{13}C chemical shift in solid peptides. However, since the knowledge of the effect of the hydrogen-bond and the main-chain dihedral-angles does not seem to be well-established, one needs to accumulate solid state NMR data by using peptides with the well-defined three-dimensional structures. In order to make it, we prepared some pep-

tides by the liquid phase organic synthesis, made ^{13}C solid state NMR measurements. On the basis of the experimental results, we performed the ^{13}C chemical shielding calculations for some model compounds, and investigated the correlation between ^{13}C chemical shift and the molecular structure.

In Chapter 4, we shall describe the results of the correlation between hydrogen-bonded structure and ^{13}C chemical shifts for the carbonyl carbons in amino acid residues such as L-alanine(Ala), L-valine(Val), D- and L-leucine(Leu), L-aspartic acid(Asp) residues in peptides in the solid state. In order to discuss the relationship between the ^{13}C chemical shift and the hydrogen-bond length, we prepared some peptides containing these amino acid residues of which hydrogen-bond lengths and conformations had been determined from X-ray diffraction studies. These results will be compared with those of peptides containing Gly residues as reported previously. We employ peptides of which the L-alanine residue carbonyl-carbon in the amide group is involved in the $>\text{C}=\text{O}\cdots\text{H}-\text{N}<$ type hydrogen-bonds (the carbonyl-carbon is not in the terminal carboxyl group).

However, in order to describe a correlation between the electronic structure and chemical shift, one needs to obtain information about both chemical shift tensor principal values (δ_{11} , δ_{22} , and δ_{33}) and the orientation of chemical shift tensor with respect to the molecular axis system, which can be described by the atomic coordinates, chemical shift tensor principal values (δ_{11} , δ_{22} , and δ_{33}).

Magic-angle spinning(MAS) technique¹⁴ provides a high-resolution spectrum of a solid material that includes nuclei which have a large chemical shift anisotropy(CSA) such as a carbonyl-carbon, by averaging out CSA into

an isotropic chemical shift instead of obtaining the information about CSA. Herzfeld and Berger developed the method for determination of CSA by MAS with low spinning rate relative to the amplitude of CSA.¹⁵ This method is useful for the determination of CSA for the systems that include several nuclei which have different electronic environments and therefore have overlapped powder patterns each other. By using the Herzfeld-Berger analysis, we have measured the principal values of the chemical shift tensor for the L-alanine residue carbonyl-carbon in the solid peptides. In order to understand the correlation between the hydrogen-bonded structure and the behavior of ^{13}C chemical shift for the carbonyl-carbon, we made ^{13}C chemical shielding calculations by the FPT-INDO (finite perturbation theory with intermediate neglect differential overlap) method.¹⁶ From the knowledge from the results, we shall make some discussions on the hydrogen-bonded structure in proteins such as basic pancreatic trypsin inhibitor (BPTI) and ribonuclease H from E. Coli (RNase H).

In Chapter 5, we will propose the possibility of a methodology for structural elucidation of peptides and proteins through the observation of ^{13}C chemical shifts for the L-alanine residue C_α - and C_β -carbons. For this purpose, the combination of ^{13}C solid-state NMR experiments of peptides and the ^{13}C chemical shielding calculations by the 4-31G-GIAO-CHF (gauge-invariant atomic-orbital and the coupled-Hartree-Fock with 4-31G basis set) methods¹⁷ were made. We shall apply this approach to the elucidation of the main-chain structure for proteins in the aqueous solution, such as BPTI and RNaseH. Moreover, we will give as well the possibility of detection regarding the differences in the molecular structures in the crystalline state and the

solution state, and also regarding the solvent effect on the chemical shift for the L-alanine residue C_{β} -carbon.

In Chapter 6, we will describe the results of the sophisticated method for the detection of homonuclear magnetic dipole couplings, hence the detection of internuclear distances. We made the solid state NMR measurements by using the dipolar restoration at the magic-angle with XY-8 π pulse sequences (XY-8 DRAMA), in order to determine the distances between intermolecular carbonyl-carbons in 10 % labeled α -[1- ^{13}C]glycyl-glycine powder sample. We shall also propose a possibility of obtaining the information about the inter-chain distances in large proteins.

Chapter 2

Theory

2.1 Theory of NMR Spectrum

There exist several physical parameters that would affect NMR spectrum.¹⁸ They are indirect dipolar coupling(J-coupling), direct dipolar coupling, quadrupolar coupling, and chemical shift. J-coupling emerges from the interaction mediated by electrons between nuclear spins. J-coupling, particularly ^1H - ^1H J-coupling, has played a crucial role in the liquid state or the solution state NMR spectroscopy, because J-coupling constant gives the main-chain dihedral-angle of a molecule by employing the Karplus equation. A lot of studies regarding protein structure have exploited this scheme. Direct dipolar coupling does not influence on the solution NMR spectrum, since the direct dipolar coupling is a traceless second-rank tensor and rapid molecular motions inevitably average this traceless tensor. In the solid state NMR spectroscopy, on the other hand, direct dipolar coupling had given severe problems onto

the spectrum before MAS¹⁴ and the dipolar decoupling(DD)¹⁹ were performed. Recently, some researchers have tried to develop some methods for detecting the direct dipolar coupling of spin-1/2 pairs in rotating solids; therefore, we can determine internuclear distances of spin pairs by detection of the dipolar coupling. Quadrupolar coupling is an important NMR parameter in systems including spins of which spin quantum number is larger than 1/2. Chemical shift has been exploited to identification of molecules because the different electronic environment around a nuclear spin, i.e., the electron density and three dimensional spreads of electron wave functions, gives the different chemical shift value. Although the quantum mechanical description of chemical shielding, i.e. chemical shift, was established in 1950, highly accurate chemical shielding calculations with employing large molecules could not been carried out because the computational facilities were not enough to make it. However, the recent development on computers enables us to perform the chemical shielding calculations for large molecules with large basis sets.

2.2 Determination of Chemical Shift Anisotropy

2.2.1 Powder Spectrum Analysis

Let us consider the indirect coupling of nuclei to the static magnetic field by interaction with the electrons. This interaction leads to shifts in resonance frequencies that are a reflection of the chemical environment of a nucleus in an atom or a molecule and are therefore important in our understanding of

electronic structures of molecules. This interaction is referred as chemical shift or chemical shielding. The chemical shielding is a tensor that is a 3 by 3 matrix and a representation of the value of a particular function in terms of the coordinates relative to a particular coordinate system(in this case, the coordinates defined by the magnetic field direction). The forms of these functions are typically bilinear and, provided that certain inequalities are satisfied, the values of the function can be represented pictorially by the length of a line parallel to one of the axes of the coordinate system(magnetic field) through the center of an ellipsoid of revolution, like the one shown in Fig. 2.1. For arbitrary orientation in which the coordinate system is oriented such that the magnetic field is not parallel to one of the semi-axes of the ellipsoid, the chemical shift will depend on the angles that specify the orientation of the field direction relative to the semi-axes of the ellipsoid, as well as the absolute magnitudes of the lengths of each semi-axis. These lengths are known as the principal values, and the coordinate system oriented such that the unit vectors determining the system are oriented along the semi-axes of the ellipsoid is known as the principal-axis system.

Consider a nucleus in a molecule with some particular shielding environment. The effect of the environment is to produce a term in the Hamiltonian,

$$\mathcal{H} = \gamma I \cdot \sigma \cdot B \quad (2.1)$$

The NMR experiment measures σ_{zz} in the frame with z axis along the field. If we take B to be in the z-direction, and neglect terms including I_x and I_y since they do not commute with the Zeeman Hamiltonian, we obtain

$$\mathcal{H} = \gamma I_z \sigma_{zz} B \quad (2.2)$$

for the chemical shift Hamiltonian. For powder samples, the NMR experiment consists of determining the chemical shift σ_{zz} for several different orientations of the principal axis system of the sample with respect to the magnetic field. Now, we consider the situation such that a shielding tensor has principal axes oriented with the laboratory frame as indicated in Fig.2.2(a). The acute angle between z' and z is β . A rotation about the axis z by the angle α will place the original y axis in the xy plane of the laboratory system (σ'_y in Fig.2.2(b)). A further rotation by β about y' will align z with the laboratory frame (Fig.2.2(c)). The result of these rotations yields a transformed tensor, initially diagonal because it is described in its principal axis system. The observed resonance frequency associated with this orientation of the tensor is given by

$$\omega = -\gamma B_0 (\sigma_{xx} \cos^2 \alpha \sin^2 \beta + \sigma_{yy} \sin^2 \alpha \sin^2 \beta + \sigma_{zz} \cos^2 \beta) \quad (2.3)$$

where σ_{xx} , σ_{yy} , and σ_{zz} are the principal values of the chemical shift. When integrated over all angles, this line shape represents the absorption spectrum of a powder sample, in which all orientations of the principal axes with respect to the magnetic field are present with equal probability. Bloembergen and Rowland²⁰ derived the line shape function $I(\omega)$ for a powder spectrum. Here, we treat the line shape of a chemical shift tensor with an axially symmetric tensor. The intensity is directly proportional to the number of molecules with chemical shift tensor orientation (α, β) , as

$$\int_{\Omega} P(\alpha, \beta) d\alpha \sin \beta d\beta = \int_{-\infty}^{\infty} I(\omega) d\omega = \int_{-\infty}^{\infty} F(\sigma) d\sigma \quad (2.4)$$

, where $P(\alpha, \beta)$ is the probability that a chemical shift principal axes of a molecule will have the orientation Ω , specified by α, β .

2.2.2 Herzfeld-Berger Analysis

The powder spectrum offers the information about the exact principal values of a chemical shift tensor only when there does not exist any severe overlap between power spectra. In the most case of NMR of organic molecules, however, this situation might not be able to be encountered; powder spectra would be composed of some signals that are derived from several chemically and electronically inequivalent environments. Herzfeld and Berger¹⁵ developed the method for determining the principal values of chemical shift tensors from the accurate measurements of the spinning sideband intensities under the condition of MAS with a low spinning rate. While this method, called as the Herzfeld-Berger analysis, maintains the high-resolution NMR spectrum, one can obtain principal values of several chemical shift tensors at once. From a viewpoint of computation, the original Herzfeld-Berger analysis was not necessarily suitable to write the simulation program. Fenzke et al. made an improvement for determination of the principal values of a chemical shift tensor from MAS sideband intensities.²¹ In the method by Fenzke et al., one should calculate the mean square deviation of the calculated sideband intensities from the experimental results and minimize the deviation.

Here, we describe Floquet theory for spinning sideband spectra.²² The

chemical shift MAS Hamiltonian in the rotating frame for a single orientation spin packet can be written in frequency units as

$$H_M(t) = -\Delta\omega I_z - \omega_I [g_1 \cos(\omega_r t + \phi_1) + g_2 \cos(2\omega_r t + \phi_2)] I_x, \quad (2.5)$$

where $\omega_r = 2\pi\nu_r$ is the rotor frequency, $\Delta\omega = 2\pi\Delta\nu$ is the sum of the isotropic chemical shift ω_I^0 plus the off-resonance ω_{off} :

$$\Delta\omega = \frac{1}{3}\omega_0(\sigma_{11} + \sigma_{22} + \sigma_{33}) + \omega_{off} = \omega_I^0 + \omega_{off}. \quad (2.6)$$

ω_I is the anisotropic part of the chemical shift tensor σ_{iso} , and is given by

$$\omega_I = \omega_0\delta = \omega_0\left\{\sigma_{33} - \frac{1}{3}\text{Tr}[\bar{\sigma}]\right\} = \omega_0\sigma_{33} - \omega_I^0, \quad (2.7)$$

where $\omega_0 = \gamma H_0$ and H_0 is the external magnetic field. The coefficients g_1 and g_2 are functions of the Euler angles, β and γ , relating the principal axes of the chemical shift tensor of a spin packet to a coordinate system fixed on the rotor (Fig.2.3). Their explicit forms are expressed as

$$g_1 = \sqrt{\frac{3}{2}} \frac{\sin 2\theta_M \sin \beta}{2} \{(\eta \cos 2\gamma + 3)^2 \cos^2 \beta + \eta^2 \sin^2 2\gamma\}^{\frac{1}{2}} \quad (2.8)$$

$$g_2 = \sqrt{\frac{3}{2}} \frac{\sin^2 \theta_M}{2} \left\{ \left[\frac{3}{2} \sin^2 \beta - \frac{\eta}{2} \cos 2\gamma (1 + \cos^2 \beta) \right]^2 + \eta^2 \cos^2 \beta \sin^2 2\gamma \right\}^{\frac{1}{2}}, \quad (2.9)$$

where the phase angle ϕ_1 and ϕ_2 in Eq.(2.5) are functions of all three Euler angle and are given by

$$\phi_1 = \alpha + \psi_1 \quad (2.10)$$

$$\phi_2 = 2\alpha + \psi_2, \quad (2.11)$$

where

$$\tan \psi_1 = \eta \frac{\sin 2\gamma}{(\eta \cos 2\gamma + 3) \cos \beta}, \quad (2.12)$$

$$\tan \psi_2 = -\eta \frac{\cos \beta \sin 2\gamma}{\frac{3}{2} \sin^2 \beta - \frac{\eta}{2} \cos 2\gamma (1 + \cos^2 \beta)}. \quad (2.13)$$

Note that for an axially symmetric ($\eta = 0$) s tensor, $\psi_1 = \psi_2 = 0$. This Hamiltonian can be rewritten in terms of its Fourier components with respect to the rotor frequency ω_r :

$$H_M(t) = -\Delta\omega I_z - 2\{X_1 e^{i\omega_r t} + X_1^* e^{-i\omega_r t}\} I_z - 2\{X_2 e^{i2\omega_r t}\} I_z \quad (2.14)$$

with

$$X_1 = \frac{1}{4} \omega_I g_1 \exp i\phi_1 \quad (2.15)$$

$$X_2 = \frac{1}{4} \omega_I g_2 \exp i\phi_2. \quad (2.16)$$

The time evolution of a spin packet can be described in terms of its density matrix $\rho(0)$ which evolves in time according to

$$U(t) = U(t)\rho(0)U^{-1}(t) \quad (2.17)$$

where $U(t)$ is the time evolution operator and is defined by

$$U(t) = \hat{T} \exp[-i \int_0^t H_m(t') dt'] \quad (2.18)$$

\hat{T} is the Dyson time evolution operator. The expectation value of any operator A can be obtained from the trace of r_A :

$$\langle A \rangle = Tr[\rho(t)A]. \quad (2.19)$$

The elements of $U(t)$ are obtained by the integration of the coefficients of the Hamiltonian (Eq.2.14). The calculation of analytic expressions for the elements of $U(t)$ is straightforward for time-dependent Hamiltonians $H_m(t)$ which commute with themselves at all times. In the general case, where the Hamiltonian does not self-commute at all times, it is convenient to use special techniques in order to evaluate Eq.2.18. Here we employ the Floquet formalism to solve the problem. The Floquet Formalism for the solution of the spin density matrix for periodic time-dependent Hamiltonians was extensively discussed by Shirley^{23, 24} and was recently employed to explain multi-photon²⁵ and pulse spin locking NMR experiments.²⁶ The results of these papers will be used here to treat the MAS experiment.

The elements of the evolution operator $U_{pq}(t)$ with $p, q = \alpha, \beta$ can be evaluated by expanding $U_{pq}(t)$ in terms of the matrix elements of an infinite Floquet Hamiltonian H_f in a manifold of dressed spin states $|p, n\rangle$, where $|p\rangle$ are the spin eigenstates of the Hamiltonian $H_M(t)$ and n is the Fourier expansion coefficients

$$U_{pq}(t) = \sum_n \langle pn | \exp(-iH_f t) | q0 \rangle e^{in\omega_r t}. \quad (2.20)$$

The elements of H_F are defined by

$$\langle pn|H_f|rm\rangle = H_{pr}^{n-m} + n\omega_r\delta_{pr}\delta_{nm} \quad (2.21)$$

and H_{pr}^n are the Fourier components of $\langle p|H_n(t)|r\rangle$ defined by

$$\langle p|H_M(t)|r\rangle = \sum_{n=-\infty}^{\infty} H_{pr}^n e^{in\omega_r t}. \quad (2.22)$$

For the MAS Hamiltonian $H_m(t)$, the elements of H_F are determined using Eqs. 2.14 and 2.21 to give

$$\langle \alpha, n|H_f|\alpha, n+1\rangle = -\langle \beta, n|H_f|\beta, n+1\rangle = X_1, \quad (2.23)$$

$$\langle \alpha, n+1|H_f|\alpha, n\rangle = -\langle \beta, n+1|H_f|\beta, n\rangle = X_1^*, \quad (2.24)$$

$$\langle \alpha, n|H_f|\alpha, n+2\rangle = -\langle \beta, n|H_f|\beta, n+2\rangle = X_2, \quad (2.25)$$

$$\langle \alpha, n+2|H_f|\alpha, n\rangle = -\langle \beta, n+2|H_f|\beta, n\rangle = X_2^*, \quad (2.26)$$

$$\langle \alpha, n|H_f|\alpha, n\rangle = n\omega_r - \frac{1}{2}\Delta\omega \quad (2.27)$$

$$\langle \beta, n|H_f|\beta, n\rangle = n\omega_r + \frac{1}{2}\Delta\omega. \quad (2.28)$$

The H_F Hamiltonian for MAS experiment is shown in the followings.

$$H_f = \begin{pmatrix} H_F^{\alpha\alpha} & H_F^{\alpha\beta} \\ H_F^{\beta\alpha} & H_F^{\beta\beta} \end{pmatrix} \quad (2.29)$$

$$H_F^{\alpha\alpha} = -\frac{1}{2}\Delta\omega\mathbf{1} + H_F^+(p = \alpha) \quad (2.30)$$

$$H_F^{\beta\beta} = \frac{1}{2}\Delta\omega\mathbf{1} + H_F^-(p = \beta) \quad (2.31)$$

$$H_F^{\alpha\beta} = 0 \quad (2.32)$$

$$H_F^\pm(p) = \begin{pmatrix} -4\omega_r & \pm X_1 & \pm X_2 & 0 & 0 & 0 & 0 & 0 & 0 \\ \pm X_1^* & -3\omega_r & \pm X_1 & 0 & 0 & 0 & 0 & 0 & 0 \\ \pm X_2^* & \pm X_1^* & -2\omega_r & \pm X_1 & \pm X_2 & 0 & 0 & 0 & 0 \\ 0 & \pm X_2^* & \pm X_1^* & -\omega_r & \pm X_1 & \pm X_2 & 0 & 0 & 0 \\ 0 & 0 & \pm X_2^* & \pm X_1^* & 0 & \pm X_1 & \pm X_2 & 0 & 0 \\ 0 & 0 & 0 & \pm X_2^* & \pm X_1^* & \omega_r & \pm X_1 & \pm X_2 & 0 \\ 0 & 0 & 0 & 0 & \pm X_2^* & \pm X_1^* & 2\omega_r & \pm X_1 & \pm X_2 \\ 0 & 0 & 0 & 0 & 0 & \pm X_2^* & \pm X_1^* & 3\omega_r & \pm X_1 \\ 0 & 0 & 0 & 0 & 0 & 0 & \pm X_2^* & \pm X_1^* & 4\omega_r \end{pmatrix} \quad (2.33)$$

In order to calculate the elements of $U_{pq}(t)$, one must diagonalize H_F and evaluate $\exp(-iH_F)$. H_F is diagonalized with the transformation as

$$D_M H_F D_M^{-1} = H_F^d. \quad (2.34)$$

The resulting matrix H_F^d has the eigenvalues of H_F along the diagonal. For the H_F Hamiltonian shown in Eq.2.29, the elements of H_F^d are equal to the diagonal elements of H_F itself

$$\langle \alpha, n | H_f^d | \alpha, n \rangle = \langle \alpha, n | H_f | \alpha, n \rangle, \quad (2.35)$$

$$\langle \beta, n | H_f^d | \beta, n \rangle = -\langle \beta, n | H_f | \beta, n \rangle = X_1, \quad (2.36)$$

The eigenvalues of H_F as a function of D_M are shown in Eq.2.42. The elements of the diagonalization matrix D_M are given by

$$\langle \alpha, n | D_M | \alpha, m \rangle = \delta_{m-n}, \quad (2.37)$$

$$\langle \beta, n | D_M | \beta, m \rangle = \delta_{m-n}^*, \quad (2.38)$$

$$\langle \alpha, n | D_M | \beta, m \rangle = 0, \quad (2.39)$$

$$\delta_n = \sum_k J_{n-2k}(\Omega_1) J_k(\Omega_2) e^{i(n-2k)\phi_1} e^{ik\phi_2}, \quad (2.40)$$

where

$$\Omega_1 = -2 \frac{|X_1|}{\omega_r}, \Omega_2 = -\frac{|X_2|}{\omega_r}. \quad (2.41)$$

The form of the diagonalization matrix D_M is shown in the followings.

$$D_M = \begin{pmatrix} D_M^\alpha & 0 \\ 0 & D_M^\beta \end{pmatrix} \quad (2.42)$$

$$D_M^\alpha = \begin{pmatrix} \delta_0 & \delta_1 & \delta_2 & \delta_3 & \delta_4 & \delta_5 & \delta_6 & \delta_7 & \delta_8 \\ \delta_{-1} & \delta_0 & \delta_1 & \delta_2 & \delta_3 & \delta_4 & \delta_5 & \delta_6 & \delta_7 \\ \delta_{-2} & \delta_{-1} & \delta_0 & \delta_1 & \delta_2 & \delta_3 & \delta_4 & \delta_5 & \delta_6 \\ \delta_{-3} & \delta_{-2} & \delta_{-1} & \delta_0 & \delta_1 & \delta_2 & \delta_3 & \delta_4 & \delta_5 \\ \delta_{-4} & \delta_{-3} & \delta_{-2} & \delta_{-1} & \delta_0 & \delta_1 & \delta_2 & \delta_3 & \delta_4 \\ \delta_{-5} & \delta_{-4} & \delta_{-3} & \delta_{-2} & \delta_{-1} & \delta_0 & \delta_1 & \delta_2 & \delta_3 \\ \delta_{-6} & \delta_{-5} & \delta_{-4} & \delta_{-3} & \delta_{-2} & \delta_{-1} & \delta_0 & \delta_1 & \delta_2 \\ \delta_{-7} & \delta_{-6} & \delta_{-5} & \delta_{-4} & \delta_{-3} & \delta_{-2} & \delta_{-1} & \delta_0 & \delta_1 \\ \delta_{-8} & \delta_{-7} & \delta_{-6} & \delta_{-5} & \delta_{-4} & \delta_{-3} & \delta_{-2} & \delta_{-1} & \delta_0 \end{pmatrix} \quad (2.43)$$

$$\langle \beta, n | D^\beta | \beta, m \rangle = \langle \alpha, n | D^\alpha | \alpha, m \rangle^* \quad (2.44)$$

Insertion of Eqs.2.34-39 in the expressions for $U_{pq}(t)$ in Eq.2.20 results in

$$U_{\alpha\alpha}(t) = \sum_{n=-\infty}^{\infty} A_n e^{in\omega_r t} e^{i\Delta\omega t/2}, \quad (2.45)$$

$$U_{\beta\beta}(t) = \sum_{n=-\infty}^{\infty} A_n^* e^{-in\omega_r t} e^{-i\Delta\omega t/2}, \quad (2.46)$$

where the complex coefficients A_n are defined as

$$A_n = \left[\sum_{m=-\infty}^{\infty} \delta_m \right] \delta_n^*. \quad (2.47)$$

Eqs. 2.45 and 2.46 show that the diagonal elements of $U(t)$ can be written as an infinite sum of exponential terms with coefficients A_n . These expressions for $U_{pq}(t)$ together with Eqs.2.40 and 2.41 could also be derived using

the Bessel function expansion. The form of the elements of $U(t)$ allows this operator to be written as

$$U(t) = \sum_{n=-\infty}^{\infty} |A_n| \exp\{i[(2n + \Delta\omega)t + 2\alpha_n]I_z\} \quad (2.48)$$

where α_n is the phase angles of A_n ;

$$A_n = |A_n|e^{i\alpha_n}. \quad (2.49)$$

The signal $S(\alpha, \beta, \gamma, t)$ of a spin packet following a 90 degree pulse is proportional to the expectation value of $\langle I_x \rangle$:

$$S(\alpha, \beta, \gamma) = U_{\alpha\alpha}(t)U_{\beta\beta}^{-1}(t) + U_{\alpha\beta}(t)U_{\beta\alpha}^{-1}. \quad (2.50)$$

Using the results of Eqs.2.45 and 2.46, this gives

$$S(\alpha, \beta, \gamma) = \sum_{n=-\infty}^{\infty} \left(\sum_{k=-\infty}^{\infty} A_k A_{n-k} \right) \exp\{i(n\omega_r + \Delta\omega)t\} \quad (2.51)$$

Fourier transformation of $S(\alpha, \beta, \gamma, t)$ results, as expected, in a sideband frequency spectrum, in which the n th sideband has a frequency of $n\omega_r + \Delta\omega$ and a complex amplitude of

$$I_n(\alpha, \beta, \gamma) = \sum_{k=-\infty}^{\infty} A_k A_{n-k}, \quad (2.52)$$

which defines the intensity of the sideband and its phase.

The actual experimental intensities in MAS experiments originate from powder samples and are therefore obtained by integration of $I_n(\alpha, \beta, \gamma)$ amplitudes over all possible values of the Euler angles. Herzfeld and Berger

performed these integrations and used them to construct the contour plots. The values of $I_n(\alpha, \beta, \gamma)$ averaged over selected sets of orientations have been utilized (Fig. 2.4).

2.3 Theory of NMR Parameters: Inhomogeneous and Homogeneous Interactions

The basic issue which a theoretical treatment must address is the general failure of magic-angle spinning to average out homonuclear dipolar interactions. Maricq and Waugh distinguish between systems having a spin Hamiltonian whose eigenstates are time independent within a phase factor (called inhomogeneous systems) and those with time-dependent eigenstates (homogeneous systems).²⁷ For an inhomogeneous system, even slow magic-angle spinning can lead to considerable line narrowing, whilst for a homogeneous system, spinning more rapid than the differences in the relevant eigenvalues is necessary. The case of a coupled nonequivalent spin pair is homogeneous, since the flip-flop part of the dipolar interaction does not commute with the chemical shift term, as examined below. Hence, it is necessary to use rotation speeds much faster than the size of the Hamiltonian (including the chemical shift term) to remove the effects of the dipolar coupling. Maricq and Waugh treated a case of this type with two nonequivalent ^{13}C sites having identical isotropic shifts but anisotropic shift tensors of different orientations. Under these conditions, the dipolar coupling leads to considerable broadening except at high spinning speeds.

Under the condition of MAS, the Hamiltonian is described as the time-independent average Hamiltonian, defined over one rotational period $2\pi/\omega_r$ as follows:

$$\langle H_0 \rangle = \sum_{\mu=0}^{\infty} H_{0\mu}, \quad (2.53)$$

$$H_{00} = \frac{\omega_r}{2\pi} \int_0^{2\pi/\omega_r} H_0(t') dt', \quad (2.54)$$

$$H_{01} = -\frac{i\omega_r}{4\pi} \int_0^{2\pi/\omega_r} \int_0^{t'} [H_0(t''), H_0(t')] dt' dt'', \quad (2.55)$$

etc. Let us consider the situation so that the H_0 should contain only chemical shifts of various spins i . Equation 2.54 is particularly simple:

$$H_{00} = \sigma_{iso}\omega_0 I_z + \frac{1}{2}(3 \cos^2 \theta - 1)(\sigma_{zz} - \sigma_{iso})\omega_0 I_z. \quad (2.56)$$

Under the condition of MAS ($3 \cos 2\theta - 1 = 0$), the second term of this equation is vanished.

As regards higher-order H_{0m} , since one can observe chemical shifts at any time, the commutator, $[H_0(t''), H_0(t')]$, will be zero. Then, all higher-order H_{0m} , which depend on the same commutator, disappear.

Therefore, the average Hamiltonian for this condition is the following:

$$\langle H_0 \rangle = \sigma_{iso}\omega_0 I_z. \quad (2.57)$$

This corresponds to the results by observations made "stroboscopically," synchronized with the rotational period of the sample spinning, $2\pi/\omega_r$. This

means that one can average out chemical shifts even when one use the MAS speed below the strength of the interaction, chemical shift anisotropies ($\omega_r/2\pi < \delta_{aniso}$).

The same will not be true for the homonuclear dipolar coupling:

$$H_0^{ij,D} = \omega_D(t)[I_{iz} \cdot I_{jz} - \frac{1}{4}(I_i^+ I_j^- + I_i^- I_j^+)] \quad (2.58)$$

because the operators for different spin pairs, ij and ik , do not commute. For a Hamiltonian including homonuclear dipolar couplings, the average Hamiltonian should be taken account of the higher terms as well. These two interactions fall into the classes called "inhomogeneous" and "homogeneous." These terms are used to identify the situations where H_0 provides, or does not provide, an exact description of the system for low spinning speeds.

2.4 Detection of Dipolar Coupling in Rotating Solids

High-resolution, high-sensitivity NMR of rare spins-1/2 in solids demands rapid rotation of the sample at the magic angle with respect to the static magnetic field in order to suppress broadening due to chemical shift anisotropy(CSA). Normally this procedure also suppresses the dipolar interactions, which carry clear information as to the molecular geometry. Many recent developments involve the recovery of selected dipolar interaction between neighboring spin-1/2, in order to obtain molecular geometric information. When the molecular site of interest is labeled with pairs of rare spins

such as ^{13}C or ^{15}N , methods such as rotational resonance (R^2),^{28, 29, 30, 31, 32, 33} dipolar recovery at the magic-angle (DRAMA),³⁵ rotary resonance,^{36, 37} rotational-echo double-resonance (REDOR),^{38, 39, 40, 41, 42, 43, 44} transfer echo double resonance (TEDOR),⁴⁵ Simple excitation for rotational echo amplitude (SEDRA),⁴⁶ controlled-SEDRA (CEDRA),⁴⁷ transverse-echo SEDRA (t-SEDRA),⁴⁸ and so on, allow examination of molecular structure in systems lacking long-range order, such as polymers and many biomolecules. For detection of homonuclear dipolar coupling, one exploits R^2 phenomenon, which arises when there are large chemical shift differences between the two members of the coupled spin pair. Here, the partial recovery of dipole interaction is accomplished when the sample rotation frequency ω_r matches a submultiple of the isotropic chemical shift difference $\omega_{iso}^A - \omega_{iso}^B = n\omega_r$, where n is a small integer. DRAMA uses two $\pi/2$ pulses of opposite phase, for every rotor cycle. This method partially recovers the dipolar couplings in a case where the two coupled spins have identical isotropic chemical shifts and small chemical shift anisotropies. In this thesis, we modified the DRAMA with XY-8 π pulse sequence that compensates the large chemical shift anisotropy and effects of carrier offset on the signal intensities and phases, in order to enable to determine homonuclear dipolar coupling.

2.5 Molecular Orbital Calculation of Chemical Shielding

^{13}C chemical shift obtained from solid state NMR is closely related to electronic structure of a molecule, and therefore has information about the three-dimensional structure of the molecule. In order to reveal the correlation between the structure of peptides and the ^{13}C chemical shifts, we carried out the ^{13}C shielding calculations by the finite perturbation theory with the intermediate neglect of differential overlap semi-empirical molecular orbital method(FPT-INDO)¹⁶ and the coupled-Hartree-Fock method with the ab-initio gauge-invariant-atomic-orbitals (GIAO-CHF).¹⁷

The FPT-INDO calculation enables us to understand what kinds of physical phenomena fundamentally occur on chemical shifts of molecules; it is much easier to perform the calculation than the ab-initio methods. On the other hand, ab-initio GIAO-CHF method is suitable for highly accurate chemical shielding calculation, hence comes to give a methodology for determination of a molecular structure through the observation of chemical shifts.

In each procedures, the total shielding constants are estimated as a sum of the diamagnetic($\sigma_{B\alpha\beta}^d$) and paramagnetic($\sigma_{B\alpha\beta}^p$) contributions. The diamagnetic contribution is largely due to geometrical parameters(r_ν, R_B, ϕ_ν ; see Fig.2.5) of a molecule and a unperturbed bond-order($P_{\nu\lambda}^{(0)}$) when the external magnetic field is not applied. On the other hand, the paramagnetic contribution is largely due to not only its geometrical parameters and the

unperturbed bond-order but also a perturbed bond-order($P_{\nu\lambda}^{(0,1)}\rangle_\alpha$) when the molecule is in the magnetic field B_α .

$$\sigma_{B\alpha\beta} = \sigma_{B\alpha\beta}^d + \sigma_{B\alpha\beta}^p \quad (2.59)$$

$$\sigma_{B\alpha\beta}^d = \frac{1}{2c^2} \sum_{\nu\lambda} P_{\nu\lambda}^{(0)} \langle \phi_\nu | \frac{\mathbf{r}_\lambda \cdot \mathbf{r}_B \delta_{\alpha\beta} - (\mathbf{r}_\lambda)_\alpha (\mathbf{r}_B)_\beta}{r_B^3} | \phi_\lambda \rangle \quad (2.60)$$

$$\sigma_{B\alpha\beta}^p = \frac{1}{2c^2} \sum_{\nu\lambda} P_{\nu\lambda}^{(0)} \{ (\mathbf{Q}_{\nu\lambda})_\alpha \langle \phi_\nu | \frac{\mathbf{L}_{B\beta}}{r_B^3} | \phi_\lambda \rangle + \langle (\mathbf{T}_{\nu\lambda})_\alpha \phi_\nu | \frac{\mathbf{L}_{B\beta}}{r_B^3} | \phi_\lambda \rangle \} \quad (2.61)$$

$$- \frac{1}{c} \sum_{\nu\lambda} (P_{\nu\lambda}^{(0,1)})_\alpha \langle \phi_\nu | \frac{\mathbf{L}_{B\beta}}{r_B^3} | \phi_\lambda \rangle \quad (2.62)$$

$$\mathbf{r}_B = \mathbf{r}_\nu - \mathbf{R}_B \quad (2.63)$$

$$\mathbf{Q}_{\nu\lambda} = \mathbf{R}_\nu \otimes \mathbf{R}_\lambda \quad (2.64)$$

2.5.1 Finite Perturbation Theory with INDO MO Method (FPT-INDO)

In this section, we describe the finite perturbation theory (FPT) within the INDO (Intermediate Neglect of Differential Overlap) framework for calculating the ^{13}C shielding constant. The FPT INDO theory has an advantage in permitting the calculation of the paramagnetic term without the explicit wave functions of excited states and the one-electron excitation energies, which are hardly obtained in high accuracy by the usual semiempirical MO approximations. According to the FPT-INDO framework, the ^{13}C shielding constant can be estimated by a sum of $\sigma_{B\alpha\beta}^d$ (diamagnetic term) and $\sigma_{B\alpha\beta}^p$ (paramagnetic term).

In the FPT-INDO calculations, however, the contributions from AOs centered on two different nuclei are not involved. Also, the first term of Eq.2.61 was neglected because the contribution of this term by FPT-INDO method is quite small. We adopted N-acetyl-N'-methyl-L-alanine amide (having the same skeletal bonds as peptide) forming hydrogen-bonds with two formamide molecules as a model supermolecule as will be shown below. The bond lengths and bond angles proposed by Momany et al.⁴⁹ were used. The calculation was performed as a function of hydrogen-bond length (the distance between nitrogen and oxygen atoms, abbreviated as $R_{N...O}$) for the right-handed form α -helix, anti-parallel β -sheet, and 3_1 -helix form with the three dihedral angles, ($\phi = -57^\circ, \psi = -47^\circ$), ($\phi = -139^\circ, \psi = 135^\circ$), and ($\phi = -88^\circ, \psi = 155^\circ$), respectively.

A HITAC M660 computer at the Computer Center of the Tokyo Institute of Technology and a HITAC 280H computer at the Computer Center of the Institute for Molecular Science, Okazaki, were used for the calculation.

2.5.2 Coupled Hartree-Fock Method Employing the 4-31G ab-initio MO Method with Gauge-Invariant Atomic Orbitals(4-31G-GIAO-CHF)

In this thesis, we adopted a model molecule, N-acetyl-N'-methyl L-alanine amide(Ac-L-Ala-NHMe) as shown Figure 5.2. All the bond lengths in this model molecule were optimized except for the C-H bond lengths in the methyl-groups, by the ab-initio 4-31G molecular orbital method. And all the bond angles except for the methyl-groups were also optimized by the

same method. The calculated chemical shifts are given in ppm relative to methane(The calculated ^{13}C shielding of methane by 4-31G/4-31G basis set⁵⁰ is 207.2 ppm and the observed ^{13}C chemical shift is -2.1 ppm relative to TMS.). Finally, the calculated chemical shifts are given relative to TMS.

Sun 4 Sparc Station 2 was used for the calculations. For the optimization of the geometrical parameters and the nuclear shielding constant calculation, it took for about 26 hours (the initial guess used here was Momany's standard values.⁴⁹ and 6 hours, respectively.

Nuclear shielding calculation also offers information about the relative orientation of the principal axis system(PAS) of a chemical shielding tensor with respect to the molecular frame. Each of tensor elements has information about three-dimensional electronic structure around a nucleus. Thus, in this thesis, we also calculated the relative orientation of principal axes of the shielding tensors for the carbonyl-, C_α -, and C_β -carbons in L-alanine residue.

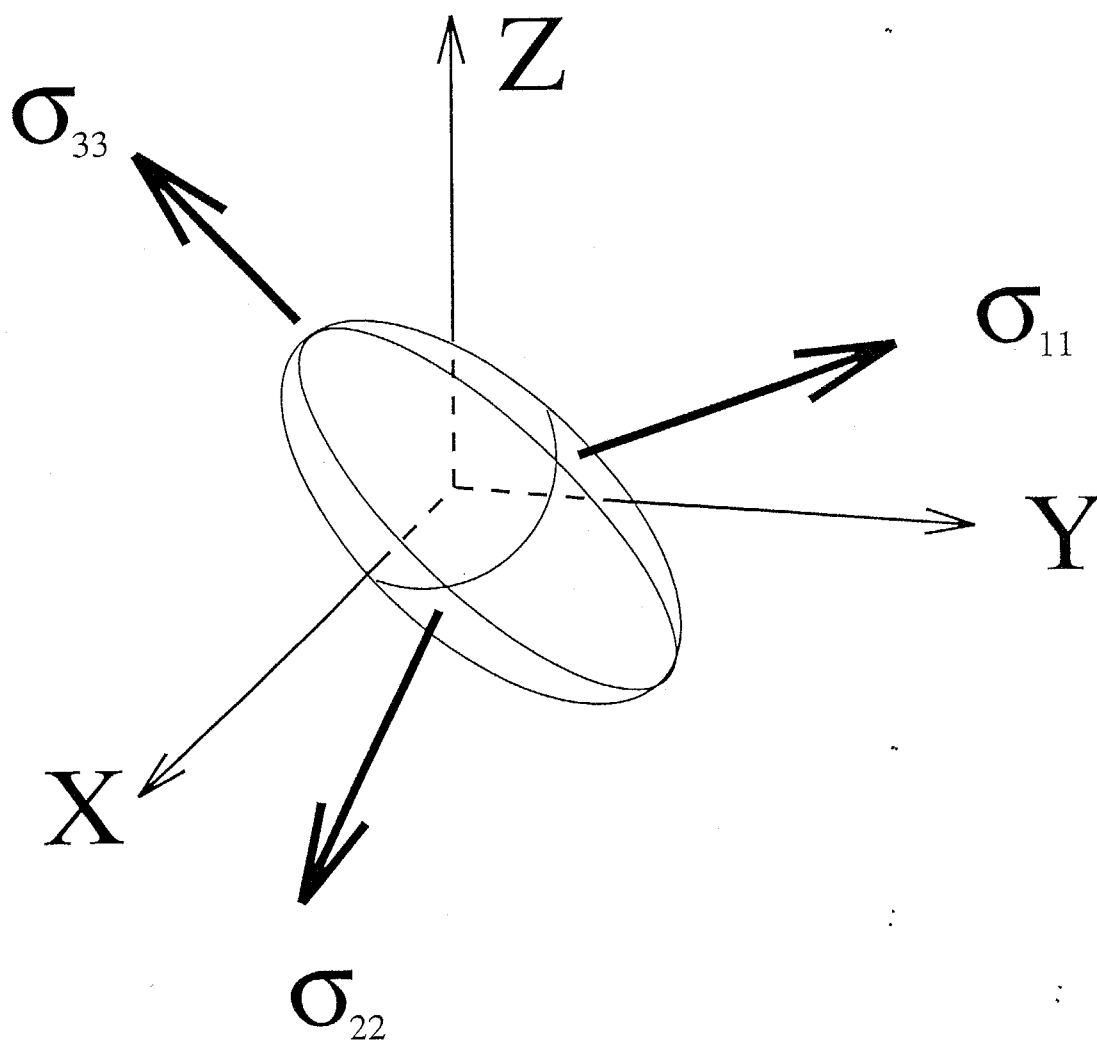


Figure 2.1: The chemical shielding ellipsoid, which is used to indicate that different orientations of the magnetic field relative to the molecular fixed frame results in different resonance position for the same chemical species.

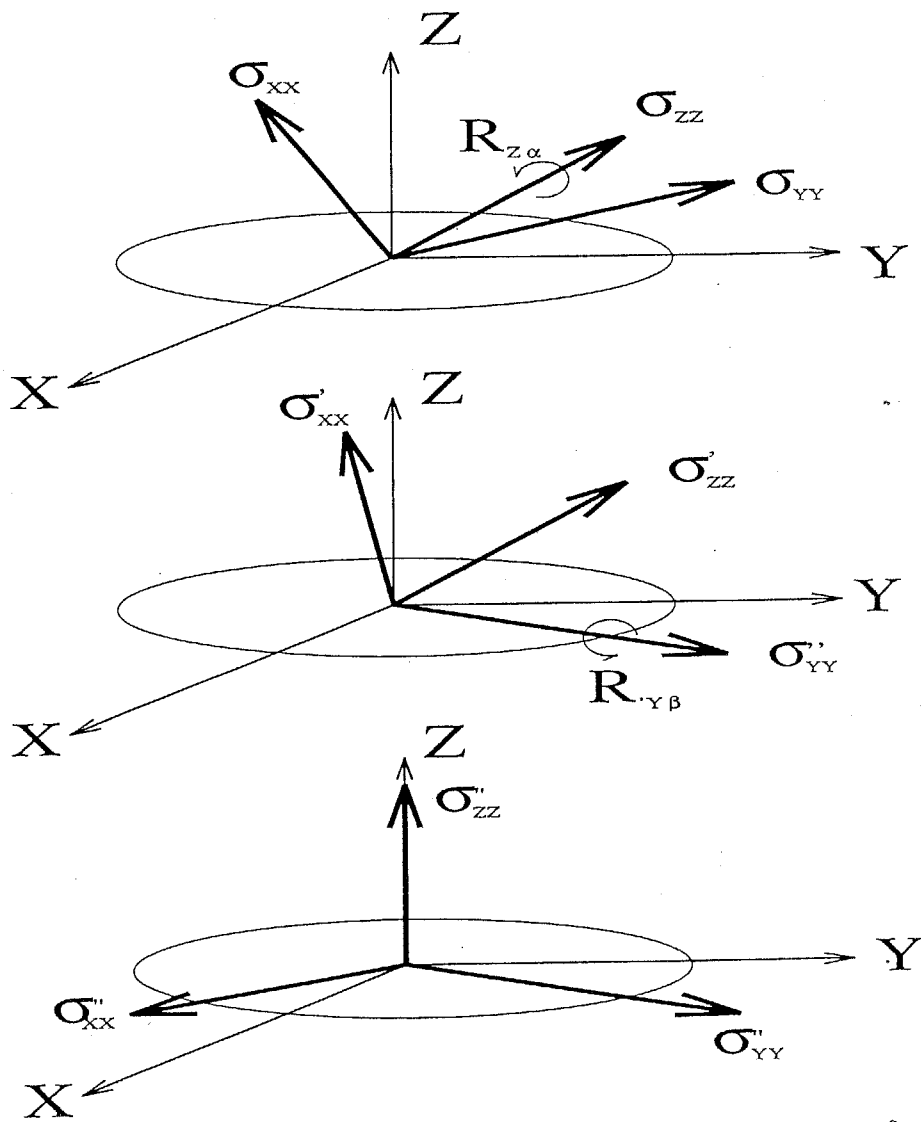


Figure 2.2: The two step processes for bringing two arbitrarily oriented coordinate systems into a situation such that the two axes are parallel. a) before $R_{Z\alpha}$ rotation, b) before $R_{Y\beta}$ rotation, and c) after $R_{Y\beta}$ rotation.

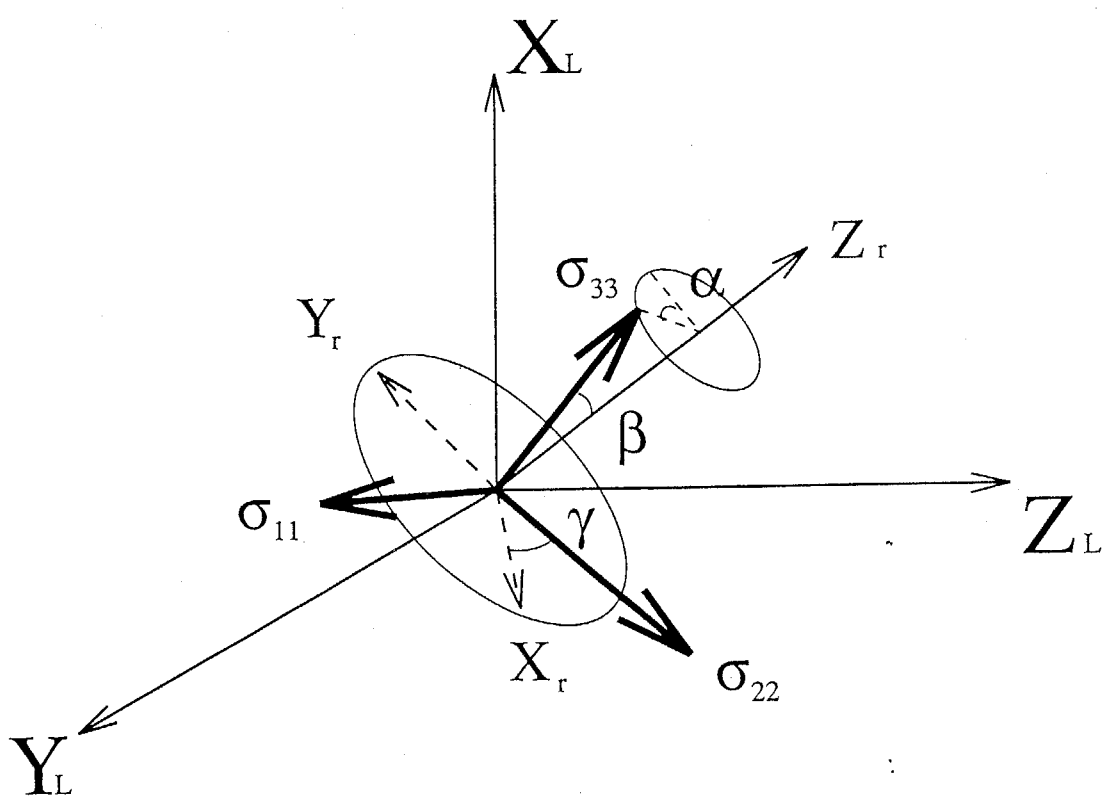
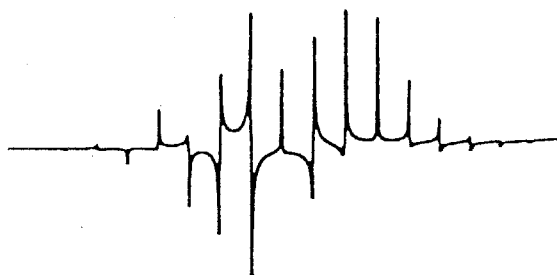


Figure 2.3: The definition of the orientation of the principal axis system for the chemical shift tensor with respect to the rotor fixed frame (X_r , Y_r , Z_r).

a)



b)

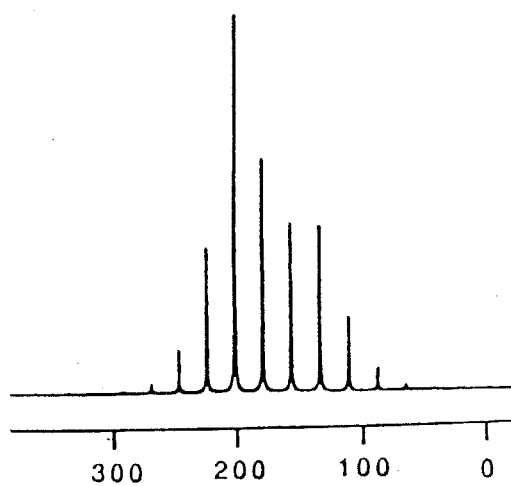


Figure 2.4: The examples of the spectrum simulation for the magic-angle spinning sideband. The principal values of the chemical shift tensor are 243, 193, and 94 ppm. The magic-angle spinning rate is 1.6 kHz. a) $\alpha = 30^\circ$, $\beta = 45^\circ$, and $\gamma = 60^\circ$, and b) powder averaged.

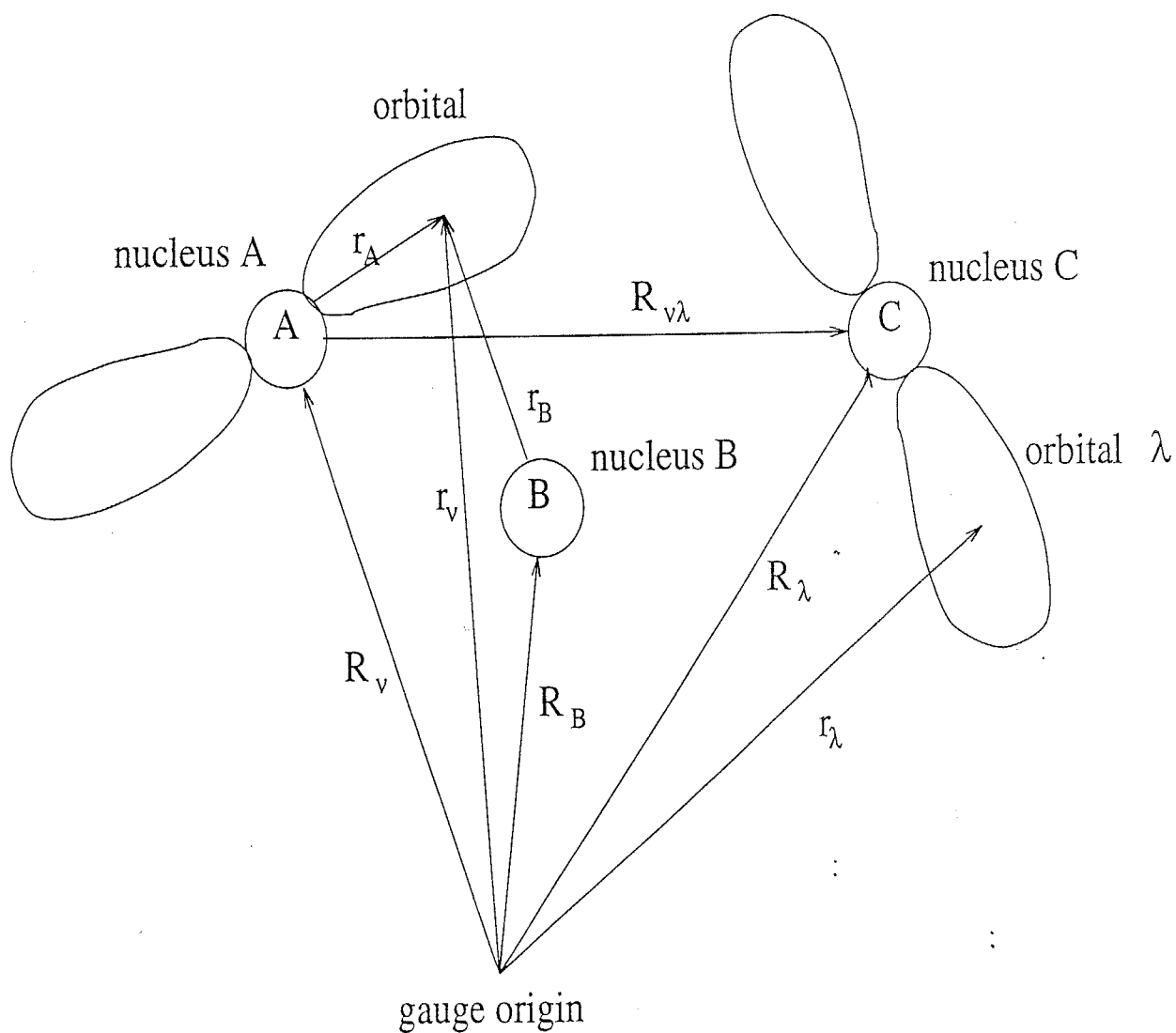


Figure 2.5: The schematic representation of molecular orbital needed to calculate the chemical shielding constant for nucleus B.

Chapter 3

Experiment

3.1 Peptides syntheses

A series of peptides containing L-alanine residue, except L-alanyl-L-prolyl-glycine monohydrate (Ala-Pro-Gly·H₂O) were synthesized according to a fragment condensation between N-hydroxysuccinimide ester of N-terminal protected amino acid and an amino acid.⁵¹ o-Nitrophenylsulphenyl-group(Nps) or t-butyloxycarbonyl-group(Boc) was used as a N-terminal-protect group. N-terminal protect groups were de-protected by dioxane / HCl solution. A mixture of ¹³C labeled L-[1-¹³C]alanine (Merck Inc., isotope purity 99 atom of L-alanine(Nihon-Rika Co.) was used to observe the accurate ¹³C chemical shift value of L-alanine carbonyl-carbon in the ¹³C NMR spectrum. L-[1-¹³C]alanyl-glycylglycine (Ala*-Gly-Gly·H₂O), L-[1-¹³C]alanyl-L-serine (Ala*-Ser), Boc-L-alanyl-α-aminoisobutyric acid (Boc-Ala-Aib-OH), and Boc-L-alanyl-L-proline (Boc-Ala-Pro-OH) were synthe-

sized by this procedure. Nps-Ala-OH and methylamine were used for the synthesis of Nps-N¹-methyl-L-alanine-amide(Nps-Ala-NHMe) by dicyclohexylcarbodiimide method (DCC). Nps-L-alanyl-a-aminoisobutyric acid methyl ester (Nps-Ala-Aib-OMe; not ¹³C labeled) was prepared by DCC method by using Nps-Ala-OH and Aib-OMe. HCl·Ala-NHMe and HCl·Ala-Aib-OMe were de-protected by HCl/dioxane solution. N-acetyl-Ala-NHMe(Ac-Ala-NHMe) and N-acetyl-Ala-Aib-OMe(Ac-Ala-Aib-OMe) was prepared in pyridine by reacting anhydrous acetate with HCl·Ala-NHMe and HCl·Ala-Aib-OMe, respectively. Poly(L-[1-¹³C]alanine) ((Ala)_n) was prepared by polymerization of L-[1-¹³C]alanine-N-carboxy anhydride (Ala-NCA). The peptides synthesized here were recrystallized according to the same procedures as those in the X-ray diffraction studies. The obtained polycrystalline samples were ground by agatemortar before the NMR measurements were carried out to eliminate the orientation anisotropy of crystals in the spinning rotor.

3.2 Solid State ¹³C NMR Measurements

The solid state ¹³C NMR measurements were performed on a JEOL GSX-270WB spectrometer operating at 67.80 MHz equipped with a CP-MAS accessory. The rf field intensity for ¹³C channel was 57 kHz. The matched Hartmann-Hahn cross-polarization(CP) was carried at the condition of 57kHz rf intensity; the CP contact time was 2 ms. The repetition time for pulse sequences was 5 s, and the spectral width was 27.0 kHz. The number of sampling points was 2k, and zero-filled to 8k. Samples were placed in a cylindrical rotor and spun as fast as 1.5-4.5 kHz. ¹³C powder pattern spectra

are often recorded in order to determine principal values of a ^{13}C chemical shift tensor, but we adopted the spinning-sidebands analysis², which allows a determination of these parameters from MAS NMR spectra in a more direct way and with a higher accuracy by using simultaneously all the information contained in the spinning sidebands. Spectra were usually accumulated 200-800 times to achieve a reasonable signal-to-noise ratio. The ^{13}C chemical shifts were calibrated in directly through the adamantane peak observed at upperfield (29.5 ppm relative to tetramethylsilane ($(\text{CH}_3)_4\text{Si}$)).

Chapter 4

Hydrogen-bonding Effect on the ^{13}C Chemical Shift for L-Alanine Residue Carbonyl-carbon

4.1 Solid State NMR Measurements.

Figure 4.1 shows 67.80 MHz ^{13}C CP-MAS NMR spectra of Ala-Ser in the solid state as a typical example. The carbonyl-carbon of the C-terminal carboxylic group appears downfield by several ppm as a rather sharp peak relative to the internal amide carbonyl-carbon.⁵² The isotropic ^{13}C chemical shifts of L-Ala carbonyl-carbons measured are listed in Table 4.1, together with the geometrical parameters obtained by X-ray diffraction

studies.^{53, 54, 55, 56, 57, 58} Some of the geometrical parameters were calculated by using the unit-cell parameters and fractional coordinates in the literature.

Figure 4.2 shows the plots of the observed isotropic ^{13}C chemical shifts (δ_{iso}) of L-Ala carbonyl-carbon against the $\text{N}\cdots\text{O}$ hydrogen-bond length ($R_{\text{N}\cdots\text{O}}$). It is found that a decrease of $R_{\text{N}\cdots\text{O}}$ leads to a downfield shift, and there exists approximately a linear relationship between the ^{13}C chemical shift and $R_{\text{N}\cdots\text{O}}$. It is noted that not only in oligopeptides (dimer or trimer) but also in polypeptide ((L-Ala) $_n$ with the α_R -helix form) the L-Ala carbonyl-carbon chemical shifts give a similar hydrogen-bond dependence. This suggests that the ^{13}C chemical shifts of any L-Ala carbonyl-carbon taking the hydrogen-bond which is formed between the amide $>\text{C}=\text{O}$ and amide $>\text{N}-\text{H}$ are predominantly determined by the hydrogen-bond length. The expression for this relationship is

$$\delta_{iso}(\text{ppm}) = 237.5 - 21.7R_{\text{N}\cdots\text{O}}(\text{\AA}). \quad (4.1)$$

This relationship indicates that the hydrogen-bond length can be determined through the observation of ^{13}C chemical shift of the L-Ala carbonyl-carbon in peptides and polypeptides.

On the other hand, the relationship between the observed ^{13}C chemical shifts in the solid state of Gly carbonyl-carbon and $R_{\text{N}\cdots\text{O}}$ has already determined by Ando et al.¹³ as expressed by

$$\delta_{iso}(\text{ppm}) = 206.0 - 12.4R_{\text{N}\cdots\text{O}}(\text{\AA}). \quad (4.2)$$

As can be seen from these two relationships, the slope of the variation of

the ^{13}C chemical shift of L-Ala carbonyl-carbon against the hydrogen-bond length is 1.7 times larger than that of Gly carbonyl-carbon. This shows the $R_{N...O}$ dependence of the former is much larger than that of the latter. Recently, we have performed the same NMR experiments for several peptides that contains the bulky side-chain such as L-valine(Val), D and L-leucine(Leu), and L-aspartic acid(Asp) residues. These data are added to Figure 4.2. From these investigations, we obtained that the expressions for these relationships as determined by the least-mean squares methods are given in ppm relative to tetramethylsilane(TMS) in the following;

$$\delta_{iso}(ppm) = 206.0 - 12.4R_{N...O}(\text{\AA}) \text{ for Gly} \quad (4.3)$$

$$\delta_{iso}(ppm) = 237.5 - 21.7R_{N...O}(\text{\AA}) \text{ for L-Ala} \quad (4.4)$$

$$\delta_{iso}(ppm) = 215.4 - 14.2R_{N...O}(\text{\AA}) \text{ for L-Val} \quad (4.5)$$

$$\delta_{iso}(ppm) = 202.2 - 10.0R_{N...O}(\text{\AA}) \text{ for L-Leu} \quad (4.6)$$

$$\delta_{iso}(ppm) = 199.0 - 9.6R_{N...O}(\text{\AA}) \text{ for L-Asp.} \quad (4.7)$$

We found that the slope of the variation of δ_{iso} against the hydrogen-bond length for these amino acid residues decreases in the order L-Ala > L-Val > Gly > L-Leu \approx L-Asp. The magnitude of the intercept decreases in the same order as the slope. Therefore, we can say that the equation for the relationship is quite characteristic of individual amino acid residues.

The Principal Values of ^{13}C Chemical Shift Tensor of the L-Alanine Carbonyl Carbon in Peptides

It is expected that the principal values of ^{13}C chemical shift tensors (δ_{11} , δ_{22} and δ_{33} , from the downfield to upfield) are, in principle, more valuable as parameters for obtaining detailed information of hydrogen-bonding to be related with electronic structure compared with the isotropic ^{13}C chemical shift ($\delta_{iso} = (\delta_{11} + \delta_{22} + \delta_{33})/3$). Figures 4.3 a and b show 67.80 MHz ^{13}C NMR powder pattern spectrum of [5%,1- ^{13}C]Ala-Ser measured by CP-MAS and the dipolar dephasing (DDph) pulse technique,⁵⁹ as a typical example. From Figures 4.3 a and b, one can see the severe overlap between the carbonyl-carbon and C_α -carbon powder spectra. Even when one use the DDph pulse sequence, one realize that it is not necessarily easy to determine the exact principal values for ^{13}C chemical shift tensor because of the overlap of powder patterns of more than two sites of carbonyl-carbons for several amino acid residues, which comes out from the low concentration of carbonyl- ^{13}C -labeled L-Ala residue. For this, we adopt the spinning-sidebands analysis,^{15, 22, 21} namely, Herzfeld-Berger analysis, to determine the exact principal values of ^{13}C labeled L-Ala carbonyl-carbons?

Figures 4.4a-e show the 67.80 MHz ^{13}C CP-MAS spectra for the several peptides with the spinning frequency of around 1.6 kHz. The above-mentioned spinning-sideband analysis was carried out to determine the principal values of the ^{13}C chemical shift tensor. Figures 4.4f-j show the calculated MAS SSB spectra for these peptides. The errors of δ_{11} , δ_{22} , and δ_{33} come out from the SSB spectrum simulation were estimated as $< 1.5\text{ppm}$, $< 0.7\text{ppm}$, and $< 1.5\text{ppm}$, respectively.

Table 4.1 lists the determined principal values of ^{13}C chemical shift tensors of peptides as well. The plots of δ_{11} , δ_{22} , and δ_{33} against the N...O hydrogen-bond length ($R_{N...O}$) are shown in Figures 4.5 a-c, respectively. Cross and his co-worker has made solid state NMR measurements of Gramicidin A, and determined principal values for the chemical shift tensor of L-alanine carbonyl-carbon. The data are added to Figure 4.5. Cross and his co-workers has made solid state NMR measurements of Gramicidin A, and determined principal values for the chemical shift tensor of L-alanine carbonyl-carbon. The data are added to Figure 4.5. From this plot, we found that the experimental δ_{22} s are the most sensitive to $R_{N...O}$, and the δ_{22} s shift linearly downfield with a decrease of $R_{N...O}$ except for the δ_{22} of Ala-Pro-Gly·H₂O; as for Ala-Pro-Gly·H₂O, the covalent bond between the Ala and Pro residues does not form the peptide bond but the imide bond. For this, it is thought that the electronic structure of the L-Ala carbonyl-carbon in Ala-Pro-Gly·H₂O is different from that of the L-Ala carbonyl-carbon forming the peptide bond, and, hence, the chemical shift for the L-Ala carbonyl-carbon is sensitive to both $R_{N...O}$ and the nature of the bonds. A decrease of $R_{N...O}$ leads to a slight upfield shift on δ_{11} except for Ala-Pro-Gly·H₂O. The experimental δ_{33} s are almost independent of $R_{N...O}$ with some scatter of the data. From the above results, we can say that the large downfield shift of the isotropic ^{13}C chemical shifts, δ_{iso} , with a decrease of $R_{N...O}$ comes from the behavior of the δ_{22} in overcoming that of the δ_{11} .

4.2 ^{13}C Shielding Constant Calculation by FPT-INDO Method

Figures 4.7a-d show the calculated isotropic shielding constants (σ_{iso}) and their paramagnetic terms of tensor components (σ_{11} , σ_{22} , and σ_{33}) for L-Ala carbonyl-carbon of the model compounds (Figure 4.6) as a function of $R_{N...O}$. The calculated values are all expressed in parts per million (ppm) with an opposite sign to that of the experimental. Note that negative sign for the calculated shielding constant denotes de-shielding, in contrast to the positive sign of the experimental chemical shift values. A isotropic shielding constant and its tensor component are usually represented as a sum of the diamagnetic and the paramagnetic terms. However, the relative change for the ^{13}C shielding tensors is predominantly governed by the paramagnetic term.

Figure 4.7a shows the $R_{N...O}$ dependence of the calculated isotropic ^{13}C shielding constant (σ_{iso}) of the central L-Ala carbonyl-carbon of the model compound with the helix or β_A -sheet form. In the large $R_{N...O}$ region, the values of σ_{iso} significantly depend on the conformational changes. On the other hand, in the short $R_{N...O}$ region, the changes in $R_{N...O}$ dominate the change in σ_{iso} . Therefore, the experimental finding that the isotropic ^{13}C chemical shift moves linearly downfield with a decrease of $R_{N...O}$ should be explained by the calculated results in the short $R_{N...O}$ region. As the semiempirical INDO MO approximation adopted here neglects some two-center electron integrals, the intermolecular interactions are considered to be reproduced reasonably in

the short $R_{N...O}$ region.⁶⁰ The variation of the total energy also supports this view as shown in Figure 4.8, where the total energy minimum appears around the $R_{N...O}$ value of 2.3-2.5 Å.

As shown Figure 4.7a, a decrease of $R_{N...O}$ leads to a decrease of σ_{iso} in the short $R_{N...O}$ region ($R_{N...O} = 2.3 - 2.5$ Å). In this region, the effect of changes in "hydrogen-bond length" on the ^{13}C chemical shift is much larger than that in the "main-chain dihedral-angles". These agree with the experimental results.

Figures 4.7b-d show the $R_{N...O}$ dependence of the calculated principal values of ^{13}C shielding tensor (σ_{11} , σ_{22} , and σ_{33}). It is shown that a decrease of $R_{N...O}$ leads to reduce in shielding of σ_{22} and increase in that of σ_{11} . σ_{33} is not sensitive to changes in $R_{N...O}$. The magnitude of change for σ_{22} is much larger than that for σ_{11} and σ_{33} . These results agree with the experimental ones. If we look at the calculations and experiments carefully, it can be said that the effect of changes in main-chain dihedral-angles on σ_{11} and σ_{22} in the calculation is relatively larger than that in the experimental results. The difference between the experiment and the calculation is probably due to the fact that the calculation was carried out under the assumption which the hydrogen-bonding angle ($\angle N - O - C$) is 180 degrees. In order to explain the experimental behavior, we need calculate the magnetic shielding by using a more accurate model which takes account of not only the main-chain dihedral-angles and the hydrogen-bond length, but also the hydrogen-bond angle.

$R_{N...O}$ Dependence of the Calculated Electron Densities on the Carbonyl-Carbons of L-Ala and Gly

Figures 4.9 a and b show the $R_{N...O}$ dependence of the calculated electron densities on the carbonyl carbons of L-Ala and Gly residue, respectively. The ^{13}C chemical shift is closely related to the electron density on the carbon atom. The smaller electron density on the carbon atom leads to the lower field shift. As shown in this figure, the decrease of the $R_{N...O}$ renders the electron density decrease. It, however, appears that the variation in the electron density on the L-Ala carbonyl-carbon is smaller than that on the Gly, and on the contrary, the change of the experimental ^{13}C chemical shifts of L-Ala carbonyl-carbons is larger than that of the Gly. Therefore, discussion must be done by ^{13}C chemical shielding calculation.

The Direction of the Principal Axes of the L-Ala Carbonyl-Shielding Tensor

Figures 4.10a-c show the direction of the principal axes system of ^{13}C shielding tensor for L-Ala carbonyl-carbon which were determined by theoretical calculations in this thesis, where the value of $R_{N...O}$ of the model compounds considered here is 2.3Å and the main-chain dihedral-angles are the α_R -helix ($\phi = -57^\circ, \psi = -48^\circ$), β_A -sheet ($\phi = -139^\circ, \psi = 135^\circ$), and 3_1 -helix ($\phi = -88^\circ, \psi = 155^\circ$) forms, respectively. Figure 4.10d shows the direction of principal axes for chemical shift tensor determined by the NMR study of $[1-^{13}\text{C}]\text{Ala}[^{15}\text{N}]\text{Ala}$ powder sample.⁶¹ The δ_{22} component nearly lies along the amide carbonyl-bond, and the δ_{11} is in the amide sp^2 plane and lies along the direction normal to the carbonyl-bond. The δ_{33} component is aligned in the direction perpendicular to the amide sp^2 plane. This calculated direction of the principal axes does not conflict with the previous experimental results¹⁴. Therefore, it is found that the δ_{22} value for the prin-

cipal axis parallel to the carbonyl-bond is the most sensitive to changes of $R_{N...O}$.

4.3 Verification of Hydrogen-bonding Structure in Proteins: Basic Pancreatic Trypsin Inhibitor(BPTI); Ribonuclease H from E.Coli(RNaseH)

Using the two and three dimensional NMR and the isotopic labeling techniques, Yamazaki and Nagayama carried out the assignments of backbone carbons of a large protein, ribonuclease H (RNase H) extracted from E.coli, which consists of 155 amino acid residues and has a molecular mass of 17.6kDa.⁶² The sample were dissolved in a 0.1M deuterated acetate buffer of 80It was also found that the structure of RNase H determined by NMR agreed with that obtained from the X-ray diffraction study.^{63, 64} From these results, it is obvious that the main-chain conformation of RNase H in the solution state is quite similar to that of the crystalline RNase H.

¹³C Chemical Shifts of the Carbonyl-carbons of the L-Ala Residues in RNase H

Figure 4.11 shows the plots for the ¹³C chemical shifts of the L-alanine residue carbonyl carbons in RNase H against the $R_{N...O}$ s obtained from the X-ray diffraction study. A solid straight line in Figure 4.11 was obtained from equation 4.2. In this figure, there are many data which have large deviations

from the a solid straight line by equation 4.2. It is thought that this is not caused by the difference between the secondary structure in the solid state and that in the aqueous solution, but by lack of the accuracy of $R_{N...O}$ as determined by the X-ray diffraction study. Since structural analysis of proteins by X-ray diffraction study gives covalent-bond length and bond angle related in the accuracy of 10^{-2} Å, then the main-chain dihedral-angles can be determined in the sufficient accuracy.⁶⁴ In the case of a small protein such as BPTI, the hydrogen-bond length can be accurately determined.^{65, 66} Therefore, the datum for the carbonyl-carbon of A48 in BPTI lies on a solid straight line by the equation 4.2 as shown in Figure 4.11. However, through-space internuclear distances such as hydrogen-bond length in larger proteins (such as RNaseH) determined by the X-ray diffraction study may include the large experimental error (about 0.3 Å) which results in by accumulated errors of the main-chain dihedral-angles.⁶⁴ This means that for structural elucidation of larger proteins, it is useful to utilize chemical shifts of the carbonyl-carbon as indications of hydrogen-bond lengths.

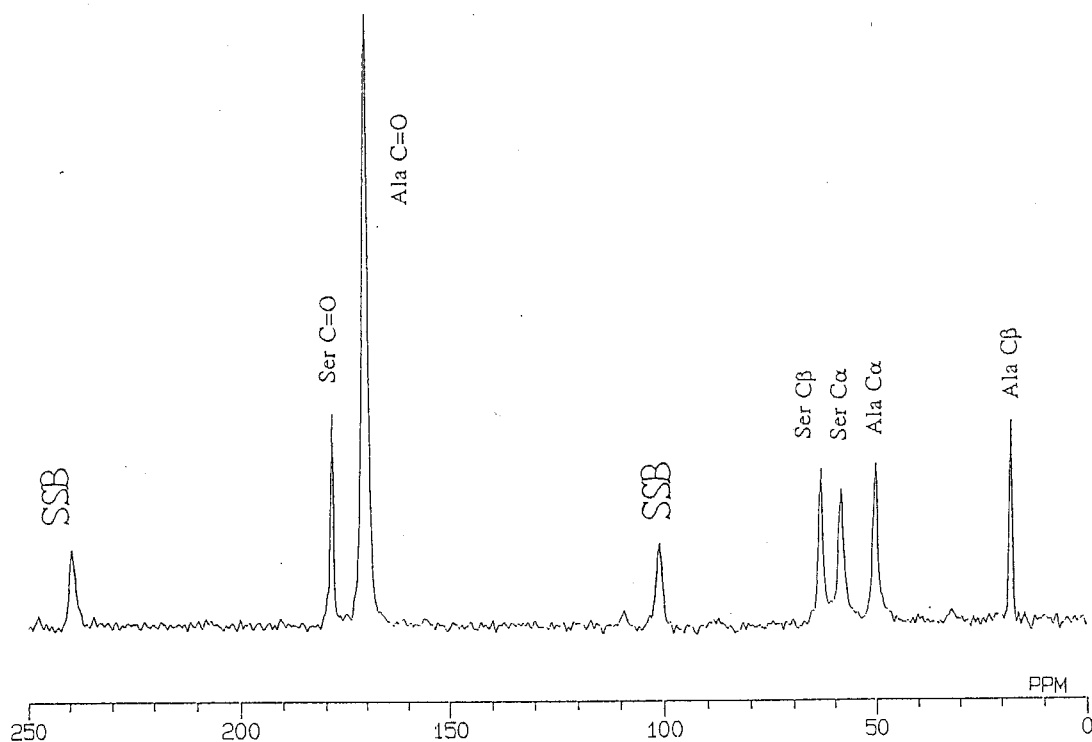


Figure 4.1: 67.8MHz cross-polarization magic-angle spinning(CP-MAS) NMR spectrum for [5%,1-¹³C]Ala-Ser, as a typical example. The solid state NMR measurements were performed under the condition of the following. The rf-field intensity for the carbon channel was 56kHz; the contact time for the matched cross-polarization between ¹H and ¹³C was 2ms; the heteronuclear dipolar decoupling during acquisition period was carried out at the intensity of 56kHz. The number of data collection was 2048;before Fourier transform, the FID were zerofilled the total data points were 8192. SSB denotes the spinning sideband.

Table 4.1 Observed ^{13}C chemical shifts of L-Alanine-residue carbonyl-carbons for oligopeptides containing L-Alanine residue in the solid state as determined by ^{13}C CP-MAS NMR and their geometrical parameters.

sample	^{13}C chemical shift(ppm)						geometrical parameters			
	δ_{iso}	δ_{11}	δ_{22}	δ_{33}	N··O	Hydrogen bond length (Å)	Hydrogen bond angle (deg.)	dihedral angle (deg.)	ϕ	ω
Ac-Ala-NHMe	175.9	245	186	96	2.92	138.3	-84.3	159.0	173.3	
	177.0	241	196	94	2.72	132.4	-87.6	154.8	171.9	
Ac-Ala-Aib-OMe	174.7	-	-	-	2.93	154.5	-134.0	122.2	-174.1	
	171.7	-	-	-	2.97	152.2	-129.8	121.5	-179.5	
Ala-Gly-Gly·H ₂ O	172.6	245	179	93	3.00	150.2	-	160.0	172.4	
Ala-Ser	170.1	249	172	89	3.04	156.3	-	124.8	-178.0	
Ala-Pro-Gly·H ₂ O	169.3	235	178	95	3.157	155.2	-	153.2	177.0	
Poly(Ala) ^a	176.8	243	194	94	2.87	-	-57.4	-47.5	-179.8	

a) with the α -helix

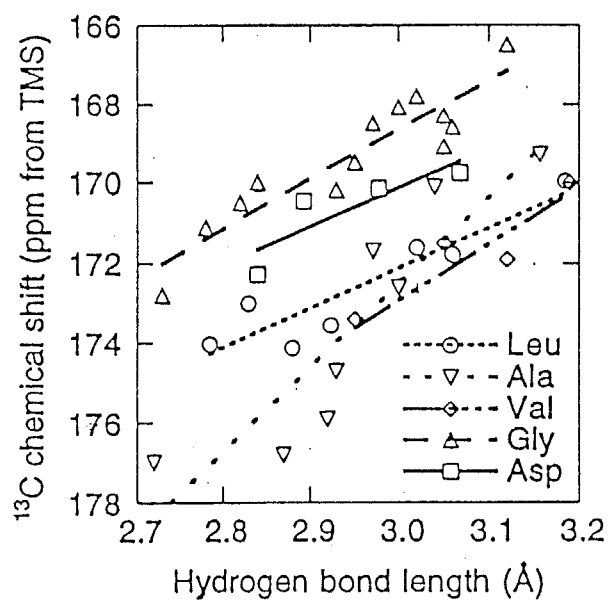


Figure 4.2: Plots of ^{13}C chemical shifts for the carbonyl-carbons in Gly, L-Ala, L-Val, D,L-Leu, and L-Asp residues in peptides in the solid state, against hydrogen-bond length ($R_{N\dots O}$).

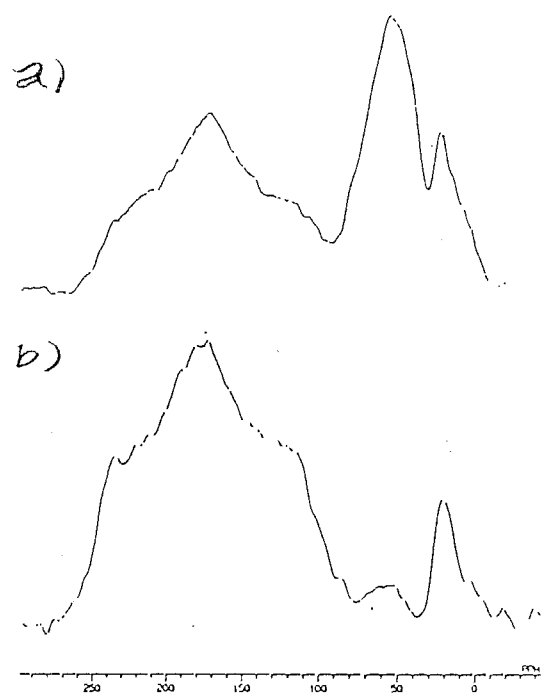


Figure 4.3: 67.8MHz a) CP-static and b) the dipolar-dephased CP-static spectra for [5%,1-¹³C]Ala-Ser in the solid state, as a typical example. The other conditions for NMR measurements were the same as those in Figure 4.1.

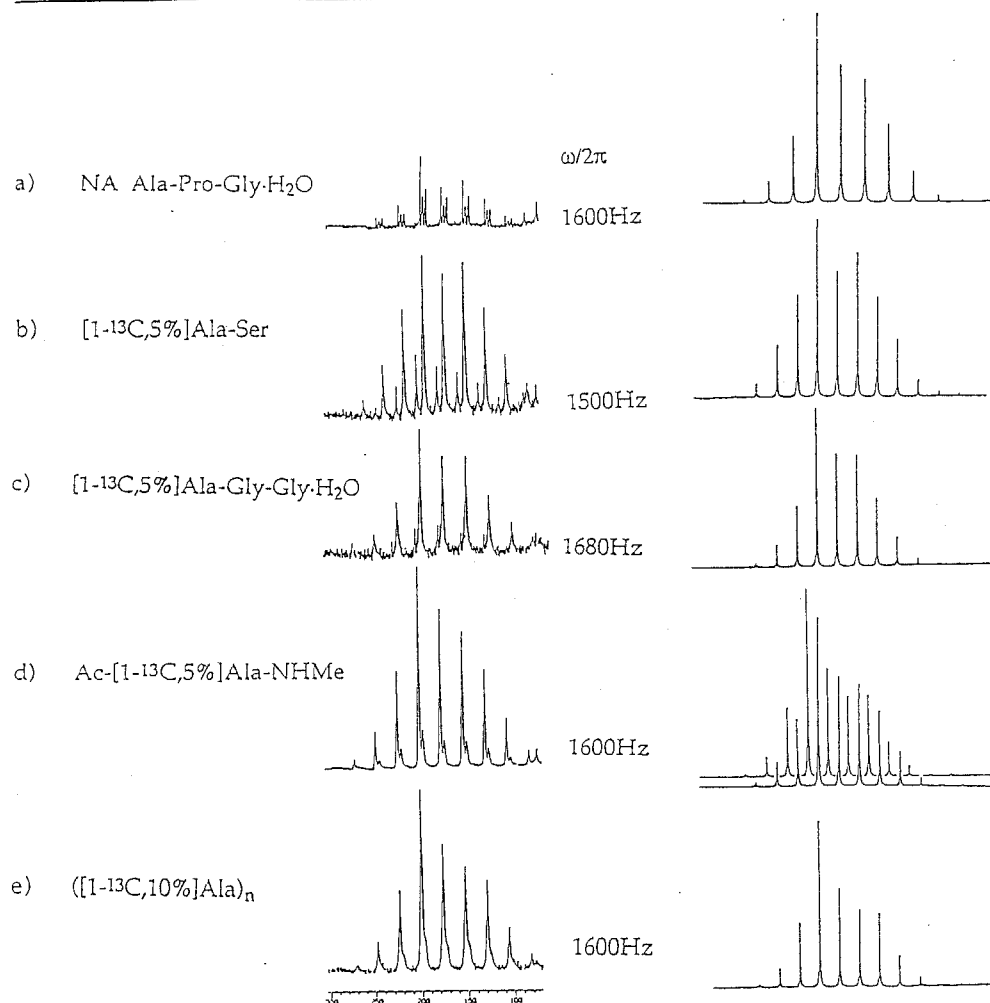


Figure 4.4: ¹³C cross-polarization magic-angle spinning (CP-MAS) NMR spectra (left) for the several peptides that contain L-alanine residues, and the MAS spectrum simulation (right) for each L-alanine residue carbonyl-carbon by using the principal values of determined chemical shift tensors. The rf field intensity for the carbon channel was 56kHz; the contact time for the matched cross-polarization between ¹H and ¹³C was 2ms; the heteronuclear dipolar decoupling during acquisition period was carried out at the intensity of 56kHz. The delay time before acquisition was set at 34.8μs; the gate for ¹³C channel was opened at 20.0μs after CP contact duration. The number of data collection was 2048; before Fourier transformation, the FIDs were zero-filled and the total data points were 8192. a) Natural abundance Ala-Pro-Gly-H₂O, b) [5%, 1-¹³C]Ala-Ser, c) [5%, 1-¹³C]Ala-Gly-Gly-H₂O, d) Ac-[5%, 1-¹³C]Ala-NHMe, and e) ([10%, 1-¹³C]Ala)_n. In the spectrum simulation procedures, 4851 orientations of chemical shift tensors with respect to the external magnetic field were accumulated.

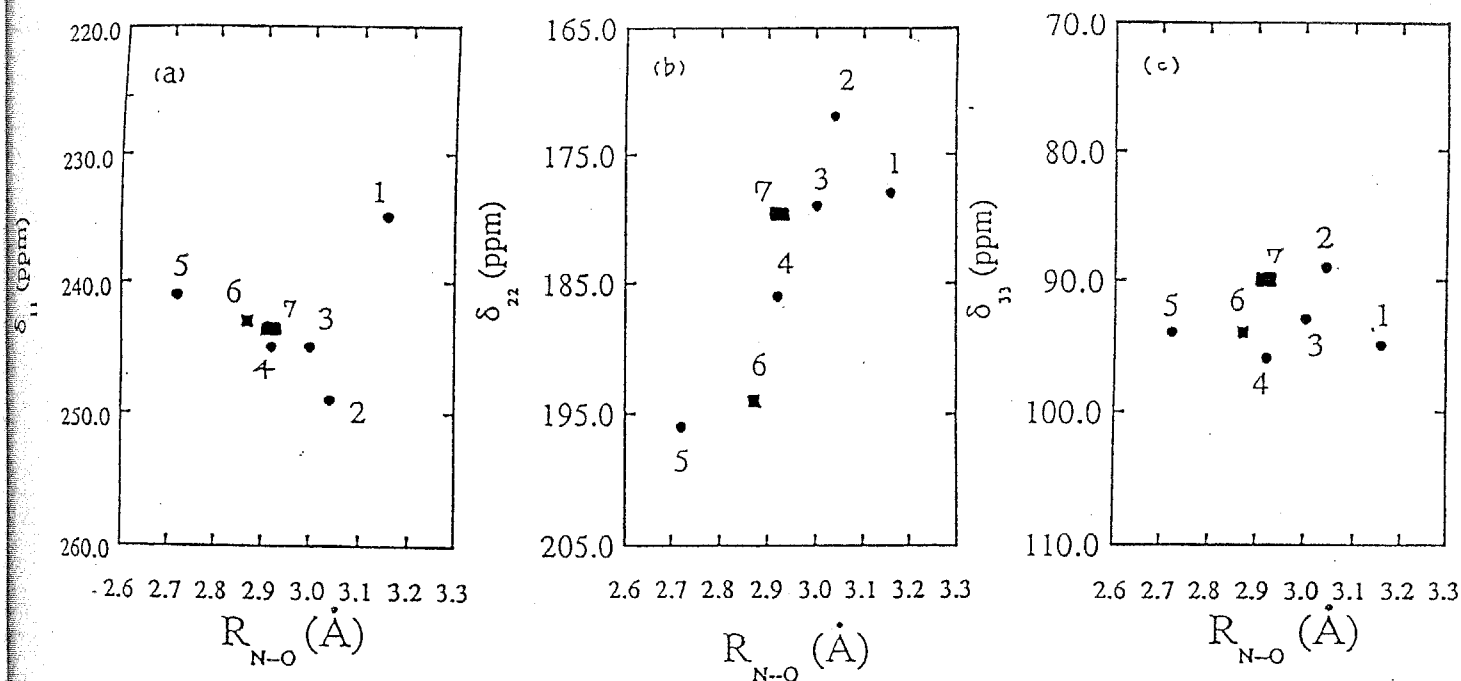


Figure 4.5: Plots of the observed principal values for ^{13}C chemical shift tensor for (a) δ_{11} , (b) δ_{22} , and (c) δ_{33} against the N...O hydrogen-bond length ($R_{\text{N}\cdots\text{O}}$): 1) Natural abundance Ala-Pro-Gly·H₂O, 2) [5%,1- ^{13}C]Ala-Ser, 3) [5%,1- ^{13}C]Ala-Gly-Gly·H₂O, 4,5) Ac-[5%,1- ^{13}C]Ala-NHMe, 6) ([10%,1- ^{13}C]Ala)_n, 7) Ala-5 in Gramicidin A.

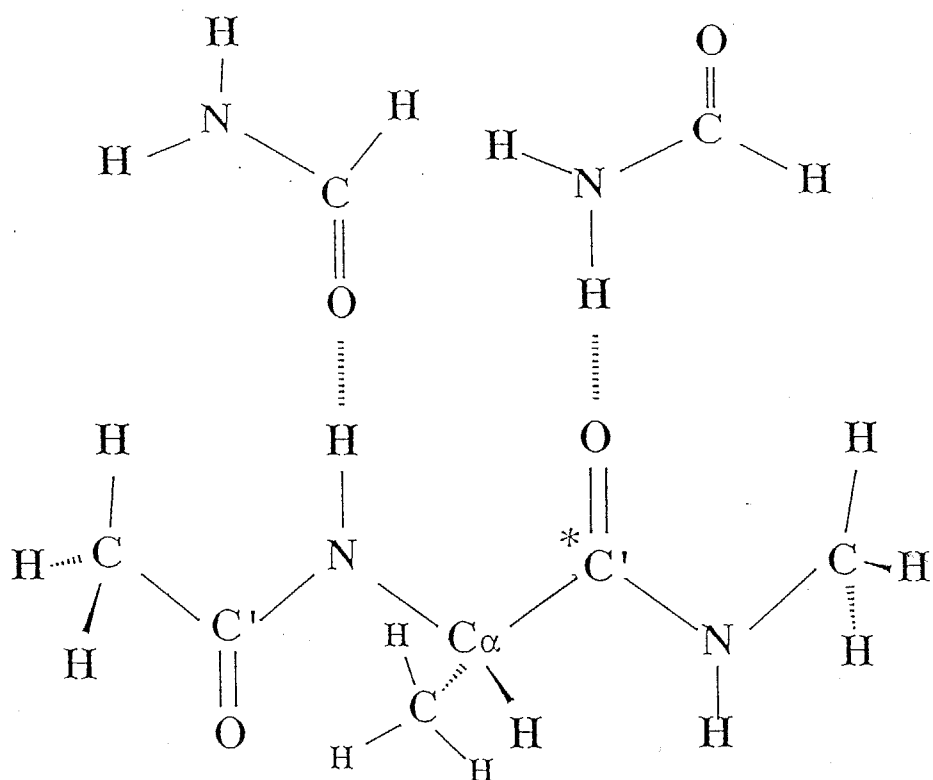


Figure 4.6: Molecular structure of N-acetyl-N'-methyl-L-alanine amide hydrogen-bonded with two formamide molecules. The chemical shielding calculation was made for the carbonyl marked by asterisk.

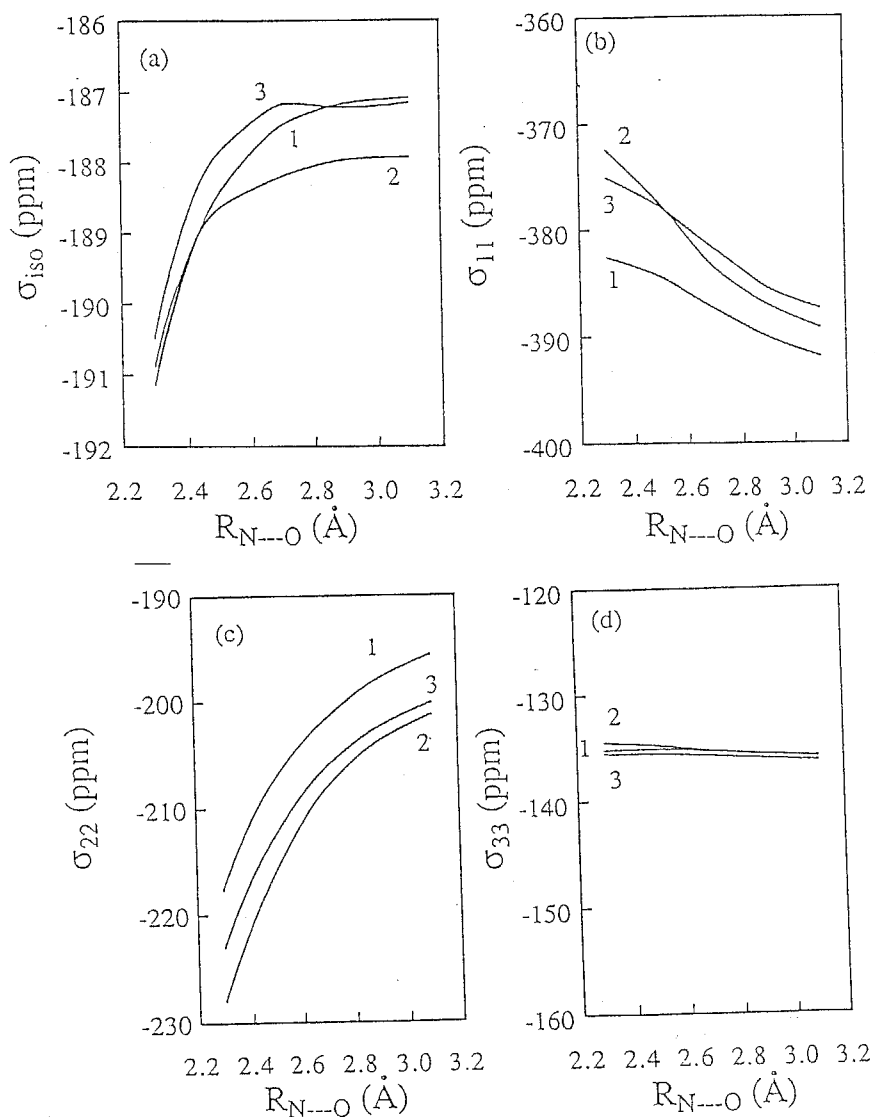


Figure 4.7: Variation of the calculated ^{13}C shielding constants and the tensor components of the paramagnetic term with respect to the $\text{N} \cdots \text{O}$ hydrogen-bond length $R_{\text{N} \cdots \text{O}}$ for (a) isotropic shielding constant σ_{iso} , (b) σ_{11} (c) σ_{22} (d) σ_{33} : (1) α_R -helix, (2) β_A -sheet, and (3) 3_1 -helix.

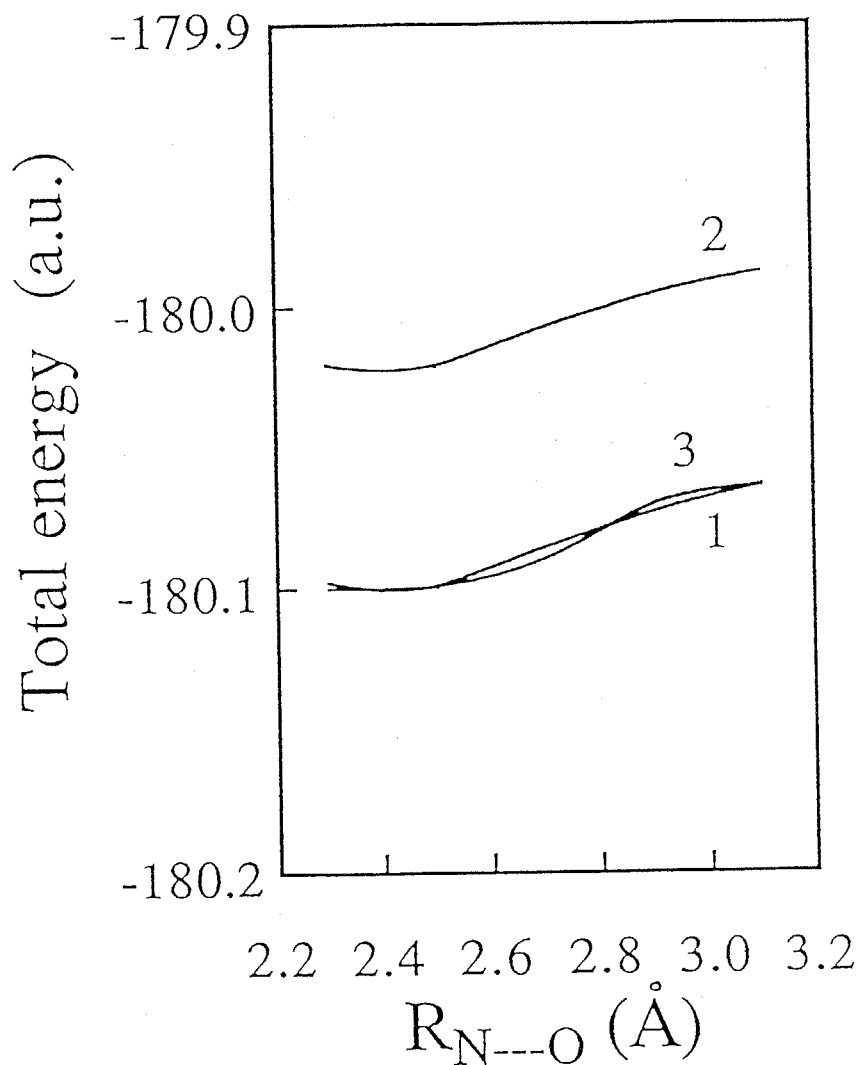


Figure 4.8: Variation of the calculated total energy against the N ... O hydrogen-bond length $R_{N...O}$ for N-acetyl-N'-methyl-L-alanine amide forming hydrogen-bonds with two formamide molecules: (1) α_R -helix, (2) β_A -sheet, and (3) 3_1 -helix.

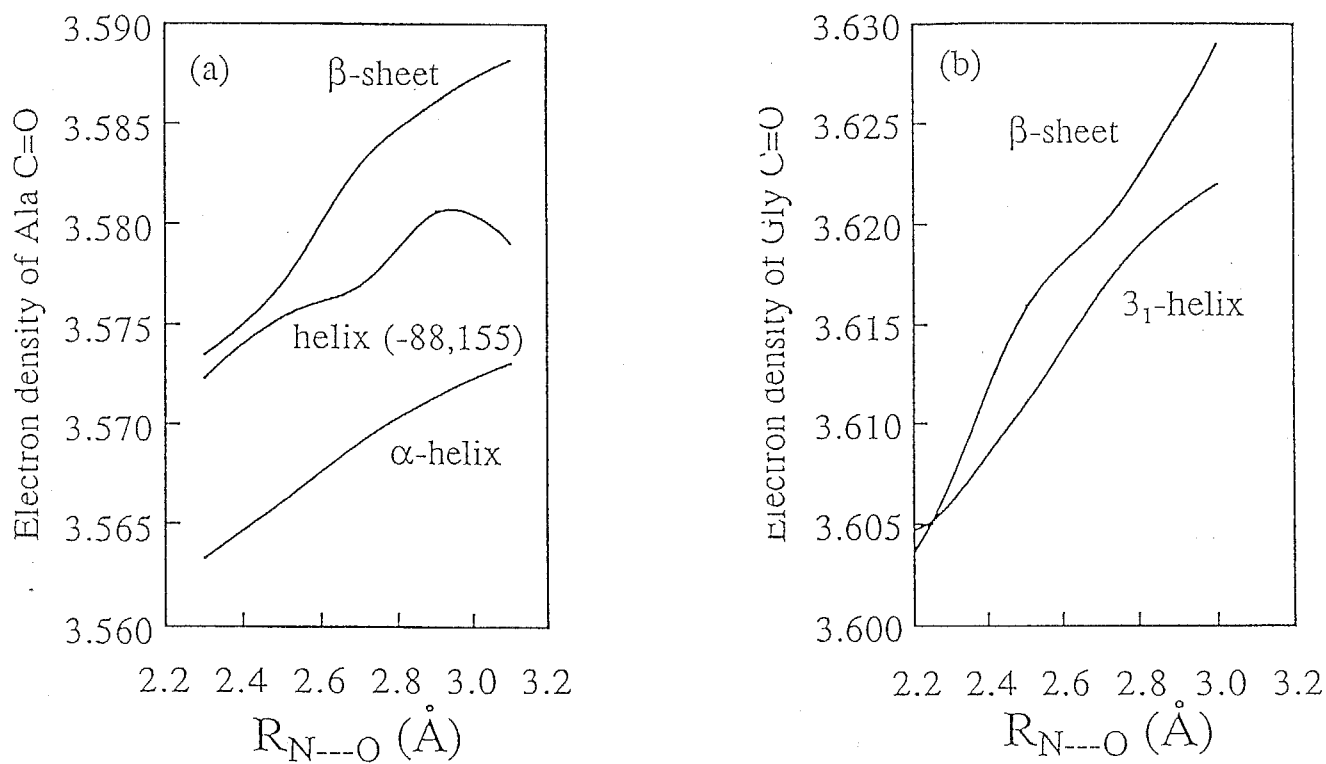


Figure 4.9: Variation of the calculated electron density against $R_{N...O}$ for (a) L-Ala carbonyl-carbon and (b) Gly carbonyl-carbon, respectively.

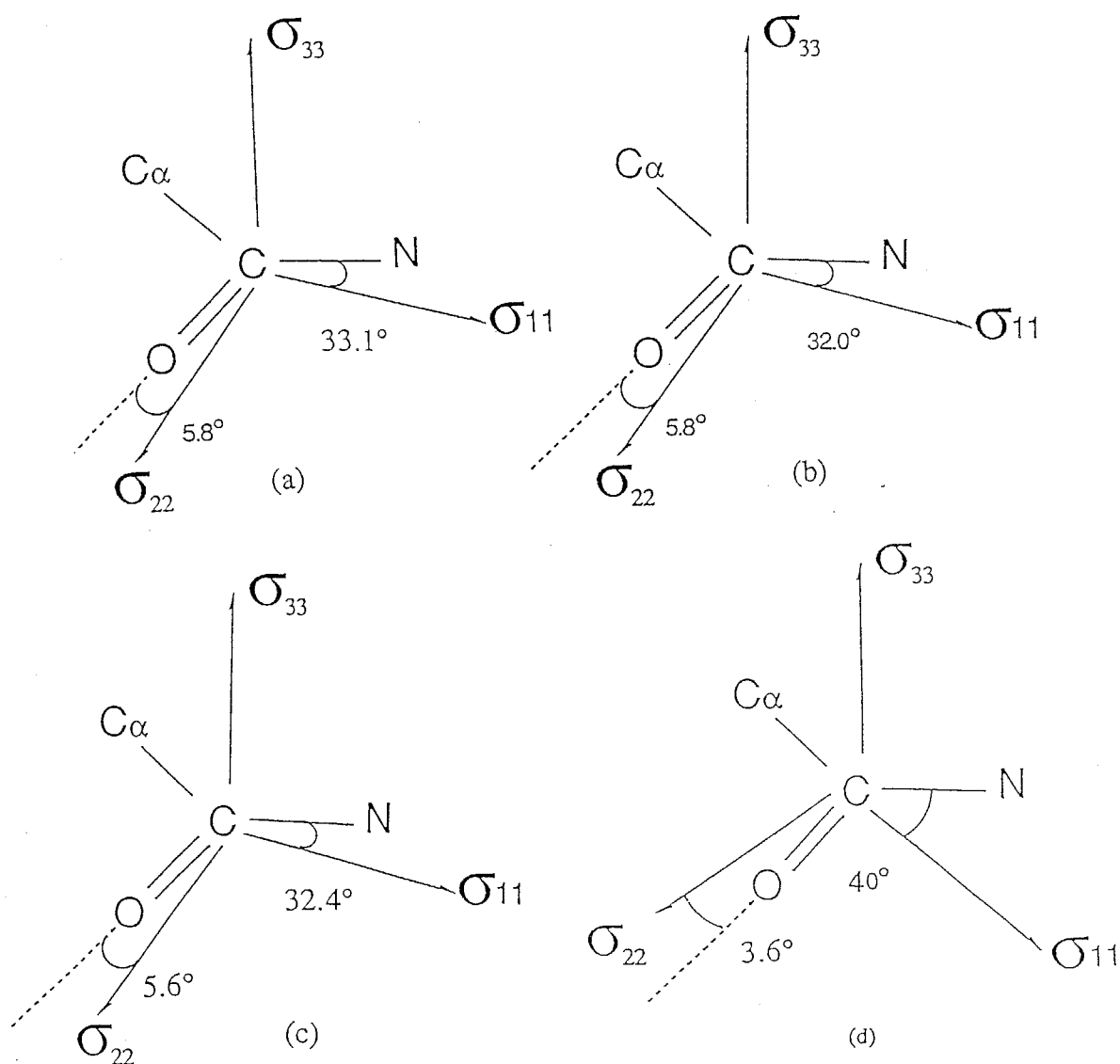


Figure 4.10: Orientation of the principal axes of the calculated and the observed ^{13}C chemical shift tensors for L-alanine residue carbonyl-carbon: (a) α_R -helix, (b) β_A -sheet, (c) 3_1 -helix, and (d) $[1-^{13}\text{C}]\text{Ala}-[^{15}\text{N}]\text{Ala}$.

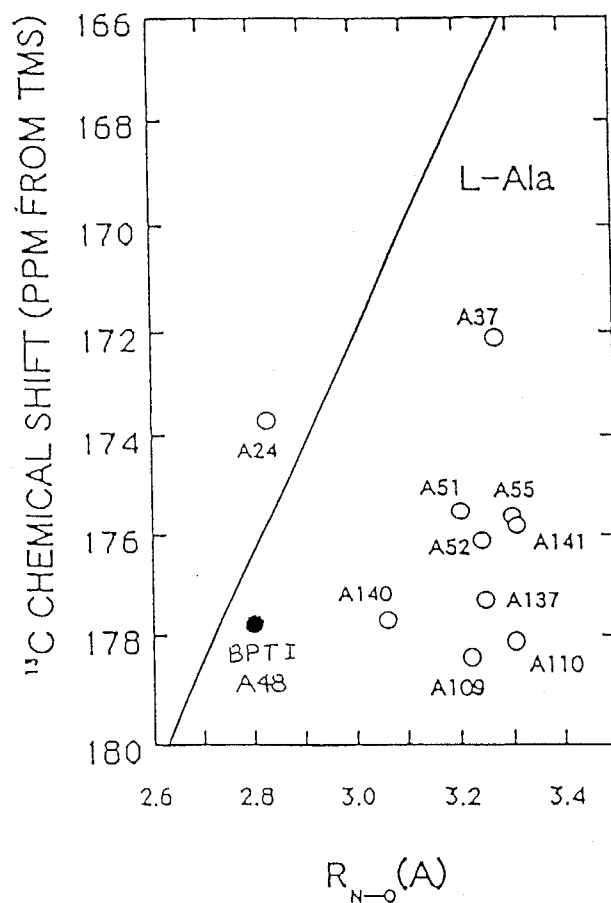


Figure 4.11: Plots of the observed chemical shifts of the L-alanine residue carbonyl-carbons in RNaseH and BPTI in the aqueous solution against the hydrogen-bond lengths ($R_{N...O}$). The straight lines is the correlation between the observed ^{13}C chemical shifts of the L-alanine residue carbonyl-carbons in some peptides in the solid state and their $R_{N...O}$ values reported previously.

Chapter 5

Correlation Between Chemical Shifts of L-Alanine Residue C_{α} - and C_{β} -carbon and the Main-chain Dihedral-angles of Peptides and Proteins

5.1 Solid State NMR Measurements

^{13}C Chemical Shifts of the L-Alanine C_{α} - and C_{β} -Carbons in Peptides in the Solid State

Figures 5.1a-d show the 67.8 MHz CP-MAS spectra for several peptides containing L-alanine residues of which the main-chain dihedral-angles

can be defined; in the other word, L-alanine portions are not terminal amino acid residue in peptides. From the X-ray diffraction study, it had been found that the unit cell of Ac-L-Ala-NHMe crystal contains two molecules of which conformations are not identical. In Figure 5.1c, for the carbonyl-, C_α - and C_β -carbons, the two signals which come from two different conformations were observed. In Figure 5.1d, we can see the signals derived from the α_R -helix and β_A -sheet. From Figure 5.1a-d and the data from previous works, we summarized in Table 5.1 the observed chemical shift for L-alanine residue C_α - and C_β -carbons, with their geometrical parameters as determined by the X-ray diffraction studies.^{67, 68, 69, 70} Some of the geometrical parameters were calculated by using the unit cell parameters and the fractional coordinates. Table 5.1 shows that L-alanine residue in the peptides takes the dihedral-angles, (ϕ, ψ) , corresponding to several conformations such as α_R -helix, β_A -sheet, 3_{10}^R -helix, etc. The ^{13}C signal of the L-alanine C_α -carbon in poly(L-alanine) which forms the α_R -helix conformation appears at upperfield by several ppm relative to the other conformations; on the other hand, the ^{13}C chemical shift of the L-alanine C_β -carbon in the β_A -sheet conformation is 21.0 ppm, which appears at downfield relative to the other conformations. The ^{13}C chemical shift of the L-alanine C_α -carbon for the β_A -sheet conformation is 48.7 ppm, which appears upfield relative to the other conformations; on the other hand, the ^{13}C chemical shift for poly(L-alanine) which forms the α_R -helix conformation is 53.0 ppm, which appears upfield by several ppm relative to the other conformations. The ^{13}C chemical shifts of the L-alanine C_α - and C_β -carbons for the other specified conformations were almost intermediate values between those for the α_R -helix and the β_A -sheet conformations.

We can recognize from these results that ^{13}C chemical shifts of the C_α - and C_β -carbons in L-alanine residue in peptide closely relates with the main chain conformation. However, since the term "the main chain conformation" of peptide implies not only the main-chain dihedral-angles, (ϕ, ψ) , but also its hydrogen-bonding structure (hydrogen-bond length and angles), it is not apparent yet whether ^{13}C chemical shifts of the L-alanine C_α - and C_β -carbons should be governed by the dihedral-angles for the L-alanine residue moiety.

5.2 Chemical Shielding Calculation by 4-31G-GIAO-CHF Method

Dihedral-angle, (ϕ, ψ) , Dependence of Chemical Shift for the L-alanine Residue C_α - and C_β -carbons

We shall estimate the correlation between the chemical shifts and the main-chain dihedral-angles of peptides, by carrying out chemical shielding calculations by the GIAO-CHF with ab-initio 4-31G basis set.

The total chemical shielding tensor is represented by a sum of the diamagnetic and paramagnetic contributions. The diamagnetic contribution is largely affected by the geometrical parameters of a molecule and an unperturbed bond order when the external magnetic field is not applied. On the other hand, the paramagnetic contribution is influenced not only by the geometrical parameters and the unperturbed bond order, but also a perturbed bond order when the molecule is in the magnetic field.

A N-acetyl-N'-methyl-L-alanine amide (Ac-L-Ala-NHMe) molecule was

employed as a model molecule (Figure 5.2). All the geometrical parameters of this molecule, except for the C-H bond lengths in the acetyl methyl-group and the amide-methyl-group, were energy-optimized by the ab-initio molecular orbital method with the 4-31G basis set. By using the optimized geometries of this molecule, we calculate carbon chemical shielding constants.¹⁷ Sun 4 Sparc Station 2 was used for the calculations.

Table 5.1 shows the main-chain conformation and the observed ¹³C chemical shifts for series of peptides that contain the L-alanine residue. The term "main-chain conformation" of peptides implies not only the main-chain dihedral-angles but also the hydrogen-bonding structure. Since the L-alanine residue in a protein does not necessarily form the hydrogen-bond, it would be still important to estimate the contribution of the main-chain dihedral-angles to chemical shift of the L-alanine residue C_α- and C_β-carbons. Figure 5.3a shows the (φ, ψ) dependence of the calculated isotropic chemical shift for the L-alanine residue C_β-carbon. The isotropic shielding constants for the C_β-carbon are 186.4 ppm for the main-chain dihedral-angles that correspond to the β_A-sheet conformation, 189.4 ppm for the α_R-helix, 189.6 ppm for the α_L-helix, 188.7 ppm for the 3₁-helix, and 186.5 ppm for silk I and (Ala-Gly)_n form II; on the other hand, the observed isotropic chemical shifts are 21.0 ppm for the β_A-sheet, 15.5 ppm for the α_R-helix, 15.9 ppm for the α_L-helix, 18.4 for 3₁-helix (we employed the chemical shift values for (Ala-Gly-Gly)_n that forms a collagen-like helix.), and 17.6 ppm for (Ala-Gly)_n form II. It is found that the change of the main-chain dihedral angles dominates the isotropic chemical shift behavior of the L-alanine residue C_β-carbon; however, except for Silk I and (Ala-Gly)_n form II. Saito, Ando, and

their co-workers had already argued against the structure model of silk I and (Ala-Gly)_n form II that is known as a crankshaft model,⁷¹ and predicted that the structure of silk I and (Ala-Gly)_n form II might be a loose fourfold helical conformation, which is originally proposed by the X-ray diffraction study of Konishi and Kurokawa.⁷³ From our calculation, the loose helix model could not be accepted either; at this point, it is, however, difficult to determine the main-chain dihedral-angle yet.

In order to understand the isotropic chemical shift behavior, we calculated principal values of the chemical shift tensor. The (ϕ, ψ) dependences of the σ_{11} , σ_{22} , and σ_{33} (that are defined from the least shielding to the most shielding, respectively.) are shown in Figures 5.3b-d. From Figures 5.3b-d, the fact that the isotropic C_β chemical shift for the α_R -helix appears in a higher field (15.5 ppm) than that for the β_A -sheet (21.0 ppm) is understood by the explicit differences in the σ_{11} ($\Delta\sigma_{11} \approx 9$ ppm). The careful investigation of chemical shielding tensor shows that the paramagnetic term for the σ_{11} dominates the total σ_{11} value. The 2p-orbital for the C_α -carbon, which corresponds to the angular momentum operator of electron and which contributes to the $C_\alpha - C_\beta\sigma$ -bond, is the most effective to the paramagnetic term for the σ_{11} , since the magnetic dipole coupling integral of electrons, $\langle \phi_\nu | L_{B\beta} / r_B^3 | \phi_\lambda \rangle$ (here, $\beta = 1$), is dominantly estimated by the 2p-orbital perpendicular to the σ_{11} . Because, in the 4-31G optimized geometries, the distance between the C_α - and C_β -carbons is 1.51 Å for β_A -sheet and 1.53 Å for α_R -helix, the changes in the σ_{11} is explained as the differences in the distances for the $C_\alpha - C_\beta$ bond, which come out from the changes in the main-chain dihedral-angles.

Figure 5.3e shows the dependence of isotropic chemical shielding for the C_α -carbon against the main-chain dihedral-angles. From Figure 5.3e, the isotropic chemical shieldings for the C_α -carbon are 160.4 ppm for the β_A -sheet, 159.6 ppm for the α_R -helix, 159.2 ppm for the α_L -helix, 161.4 ppm for the 3_1 -helix, and 157.9 ppm for silk I and $(\text{Ala-Gly})_n$ form II; for these calculated shielding, the observed isotropic chemical shifts are 48.7 ppm for the β_A -sheet, 53.0 ppm for the α_R -helix, 50.1 ppm for the α_L -helix, 49.7 ppm for the 3_1 -helix, and 51.5 ppm for $(\text{Ala-Gly})_n$ form II, respectively. Although it is obvious that there exists the main-chain dihedral-angle dependence on chemical shift for the C_α -carbon, it seems more complicated than that for the C_β -carbon, because the orientation of the chemical shift tensor for the C_α -carbon with respect to the molecular fixed frame is different from one (ϕ, ψ) to another, and also because, in a case in which the L-alanine residue carbonyl- or amide-group would form the hydrogen-bond, the hydrogen-bonding structure can also affect on the behavior of chemical shift for the C_α -carbon. As regards the structure of $(\text{Ala-Gly})_n$ form II and silk I, it needs chemical shift calculation that is taken into consideration of the hydrogen-bonding; the investigation of chemical shift carbonyl-carbon will be needed.

In order to give a further insight to the C_α chemical shift behavior, we calculated principal values of the chemical shielding tensor as well. From Figures 5.3f-h, it is obvious that all the principal values are quite sensitive to the (ϕ, ψ) differences; particularly, the σ_{33} is the most sensitive to the (ϕ, ψ) differences. For almost all (ϕ, ψ) s, the principal axis of the σ_{33} is aligned to the C_α -C' bond but with about 30 degrees deviation and is also nearly perpen-

dicular to the C_α - C_β bond. Since it is generally known that bond extension makes shieldings decrease,⁷³ then it is predicted that the C_α -C' bond length differences associated with dihedral-angles variations would dominately contribute to the σ_{33} differences. However, the C_α -C' bond lengths in the 4-31G energy-optimized geometry are 1.512 Å for the β_A -sheet and 1.516 Å for the α_R -helix; the bond length difference is 0.004 Å. It seems that this bond length difference is too small to understand the behavior of σ_{33} . The notice of the shielding calculation procedures leads us to know where a chemical shift change comes out from. As for the σ_{33} for the C_α -carbon, we found that the diamagnetic contribution for the σ_{33} dominates the changes in the total σ_{33} , therefore the most crucial factor for this behavior is changes in geometric parameters of the C_α -carbon moiety along to the σ_{33} axis for model compounds with the several main-chain dihedral-angles.

It should be noted that the other principal values, σ_{11} and σ_{22} , changes their orientation of principal axes for one (ϕ, ψ) to another.

One of the complexities, the orientation of the chemical shift tensor, will be discussed in the next section. The other complexity, the hydrogen-bonding effect, seems rather intricated because the chemical shift for the C_α -carbon, especially the principal values of the chemical shift tensor, would be greatly affected by differences in not only the hydrogen-bond length ($R_{N...O}$ and $R_{H...O}$) but also in the hydrogen-bond angles (for example, $\angle N...O = C$, $\angle H...O = C$, and so on). We are trying to determine the chemical shift tensor anisotropies and orientations for the L-alanine residue C_α -carbon in peptides. The hydrogen-bonding effect on the C_α chemical shift will be estimated by the solid state NMR measurement combined with the GIAO-CHF

chemical shielding calculation.

The Orientation of the Principal Axis System of the Calculated Chemical Shift Tensor with respect to the Molecular Fixed Frame

As mentioned above, the principal values of chemical shift tensor give information about three dimensional electronic structure of a molecule. However, in order to understand behavior of the principal values, one should obtain information about the orientation of the principal axis system of a chemical shift tensor with respect to the molecular fixed frame. Figures 5.4 a-d show the calculated orientations of the principal axis systems of the chemical shift tensors of L-alanine C_β -carbons in some peptides whose L-alanine moieties have different main-chain dihedral-angles, $(\phi, \psi) = (-57.4^\circ, -47.5^\circ)$ [α_R -helix], $(-138.8^\circ, 134.7^\circ)$ [β_A -sheet], $(-66.3^\circ, -24.1^\circ)$ [3_{10}^R -helix], and $(-84.3^\circ, 159.0^\circ)$ [3_1 -helix]. Figures 5.4 a-d show that the σ_{33} component nearly lies along the C_α - C_β bond for all peptides considered here, and also show that the σ_{11} is nearly perpendicular to the plane which is defined by the C_β , the C_α , and the N atoms in L-alanine residue; on the other hand, the σ_{22} is parallel with regard to the plane. These results agree with the experimentally determined direction of σ_{33} of the C_β -carbon in L-alanine amino acid by Naito et al.⁷⁴ As is seen from Table 5.2, the σ_{11} component for the dihedral-angles corresponding to the β_A -sheet conformation is 37.01 ppm. This shows downfield shift of about 9 ppm with respect to that for the α_R -helix conformation. This result means that the σ_{11} dominates downfield shift on the isotropic chemical shift of the C_β -carbon for the β_A -sheet conformation. Since the σ_{11} does not orient to a specified chemical bond, it is not easy to comprehend intuitively the chemical shift tensor behavior of the C_β -

carbon. However, it is obvious that the through-space interaction between the C_β -methyl group and its surrounding is important to understanding the σ_{11} behavior. Figures 5.4 a-d show the calculated orientations of the principal axis systems of the chemical shift tensors of L-alanine C_α -carbons in the peptides with respect to the molecular frames. As is seen from these figures, the calculated orientation of the principal axis system for the C_α -carbon is quite different from sample to sample. For all the dihedral-angles employed in the calculations, the σ_{33} component of ^{13}C chemical shift tensor in L-alanine C_α -carbon always lies along the C_α - C' bond. However, for the dihedral-angles, $(\phi, \psi) = (-57.4^\circ, -47.5^\circ)[\alpha_R\text{-helix}]$, $(-66.3^\circ, -24.1^\circ)[3_{10}^R\text{-helix}]$, and $(-84.3^\circ, 159.0^\circ)$, the σ_{11} component lies along the slightly deviated direction from the C_α - C_β bond; while, for $(\phi, \psi) = (-138.8^\circ, 134.7^\circ)[\beta_A\text{-sheet}]$, the σ_{22} component is along this direction. As is shown in Table 5.2, the principal value which is nearly along with regard to C_α - C_β bond is 47.53 ppm for the β_A -sheet form, 61.93 ppm for the α_R -helix form, 64.74 ppm for the 3_{10}^R -helix form, and 65.79 ppm for $(\phi, \psi) = (-84.3^\circ, 159.0^\circ)[3_1\text{-helix}]$. The change of the dihedral-angles causes the large deviation on the chemical shift tensor element which is along the C_α - C_β bond. Moreover, since the σ_{33} depends on changes from one dihedral-angles to another, it is obvious that there exists the explicit dihedral-angle dependence on the σ_{33} . Then, it is thought that if the carbonyl-group in the L-alanine residue forms a hydrogen-bond, the σ_{33} will be probably affected. The principal values of chemical shift tensor of the L-alanine C_α -carbon in peptides have not been measured yet, because the chemical shift anisotropy is not so large that we can accurately evaluate it. The measurements of principal values of chemical shift tensor for the

L-alanine C_{α} -carbon still remain as a future work.

5.3 Application to Structural Elucidation of Proteins: Basic Pancreatic Trypsin Inhibitor(BPTI); Ribonuclease H from E.Coli (RNaseH)

^{13}C Chemical Shift of the C_{β} -carbons of the L-Alanine Residues in RNaseH

The correlation between the ^{13}C chemical shifts of peptides and its backbone conformation is of great interest for structural elucidation. We carried out calculation of the isotropic ^{13}C chemical shift of the C_{β} -carbons in the L-alanine residue by applying the GIAO-CHF method. The calculated shift shifts are shown in Table 5.3. A comparison of the calculated and experimental ^{13}C chemical shifts are in Figure 5.5. From this, it is clear that the isotropic ^{13}C chemical shift of the L-alanine C_{β} -carbon is apparently related to the main-chain dihedral-angles of the L-alanine residue moiety of RNase H in the aqueous solution. In this figure, the observed chemical shift behavior of the L-alanine residue C_{β} -carbon is generally similar to that of the RNase H in the aqueous solution. Moreover, by using this comparison between the experimental and the calculated chemical shifts, one can elucidate interaction between L-alanine C_{β} -carbon and its surrounding, solvent molecules(H_2O) or side chains of the adjacent amino acid residues. For example, the data for

the A58 and A125 as shown in Figure 5.5 are deviated from the correlation curve. These L-alanine residues do not form any hydrogen-bond in the protein; that is, the solvent molecules or side-chains of adjacent residues can be proximate to the C^β -methyl group. From such situation, it is thought that the isotropic chemical shifts for the A58 and A125 C^β -carbons are affected by not only their main-chain dihedral-angles but also by the above mentioned interactions. It is important for studying of functional aspect of a protein to detect these interactions. The detection of such interactions in the solution can be only done by both solid state NMR measurements and chemical shift calculations, as well as solution NMR and X-ray diffraction studies.

^{13}C Chemical Shifts of the C_α -carbons of the L-Ala Residues in RNase H

We also carried out the chemical shift calculations of the L-alanine residue C_α -carbons by the GIAO-CHF method with 4-31G basis set. In this calculation, N-acetyl-N'-methyl-L-alanine amide (Ac-L-Ala-NHMe) with the dihedral-angles, (ϕ, ψ) , is employed. The experimental and calculated isotropic chemical shifts are shown in Table 5.3. A comparison between the experimental and the calculated ^{13}C chemical shifts is shown in Figure 5.6. From this figure, it is found that there is no clear relationship between the experimental and the calculated chemical shifts. This is because we carried out the calculation without taking account of the hydrogen-bonding effect. Although we tried to make calculation taking into account of the hydrogen-bonding, we have suffered from the difficulty of obtaining the self-consistent field(SCF) solution yet.

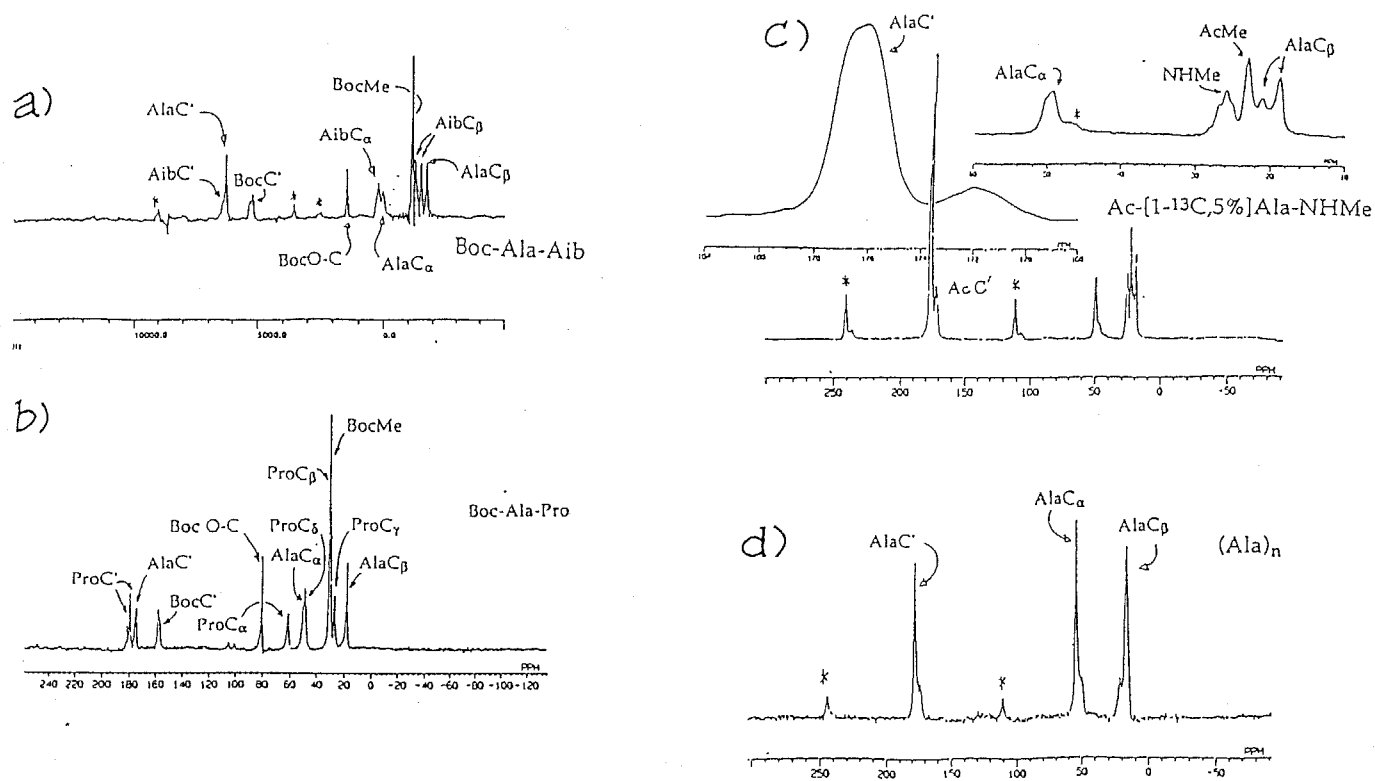


Figure 5.1: 67.8MHz CP-MAS spectra for some peptides containing L-alanine residue in the solid state. The condition for NMR measurements were the same as those in Figure 4.1. a) Boc-Ala-Aib, b) Boc-Ala-Pro, c) Ac-[5%,1- ^{13}C]Ala-NHMe, and d) (Ala) $_n$.

Table 5.1 Observed chemical shifts for solid peptides that contain L-alanine residue by ^{13}C CP-MAS NMR Measurements, and their main-chain dihedral angles for the L-alanine residue portions that were determined by the X-ray diffraction studies

sample	chemical shift (ppm from TMS)		ϕ (deg.)	ψ (deg.)	secondary structure
	$\text{C}\alpha$	$\text{C}\beta$			
(Ala) _n	53.0	15.5	-54.7	-47.5	α R-helix
	48.7	21.0	-138.8	134.7	β A-sheet
(D,L-Ala) _n ^a	50.1	15.9	54.7	47.5	α L-helix
(Ala-Gly-Gly) _n I	49.7	22.6			β -sheet
(Ala-Gly-Gly) _n II	49.7	18.4	-90	150	3_1 -helix ^e
(Ala-Ala-Gly) _n	50.1	21.4			β -sheet
(Ala-Gly) _n I ^b	49.5	21.0			β -sheet
(Ala-Gly) _n II ^c	51.5	17.6			unknown ^f
(Pro-Ala-Gly) _n	49.3	18.6			triple-helix ^e
Ac-Ala-NHMe ^d	49.3	18.8	-84.3	159.0	3_1 -helix like ^g
	50.4	21.2	-87.6	154.8	
Boc-Ala-Aib-OH	52.3	17.4	-66.3	-24.1	3_{10} ^R -helix
Boc-Ala-Pro-OH	49.2	17.2	-95.4	153.6	3_1 -helix like ^g

a. (D,L-Ala)_n denotes copolymer of D- and L-alanines.

b. (Ala-Gly)_n form I is a model compound for Silk II.

c. (Ala-Gly)_n form II is a model compound for Silk I.

d. There exist two conformers in a unit cell.

e. (Ala-Gly-Gly)_n form II and (Pro-Ala-Gly)_n are model compounds for Collagen.

f. Some X-ray crystallographic structures^{13,14} was presented by other groups. However, some arguments about the structure for (Ala-Gly)_n and Silk I have been raised⁷.

g. The secondary structure for these samples are not exactly 3_1 -helix conformation, because the hydrogen-bonding structures are not the same to that for the 3_1 -helix for polypeptides.

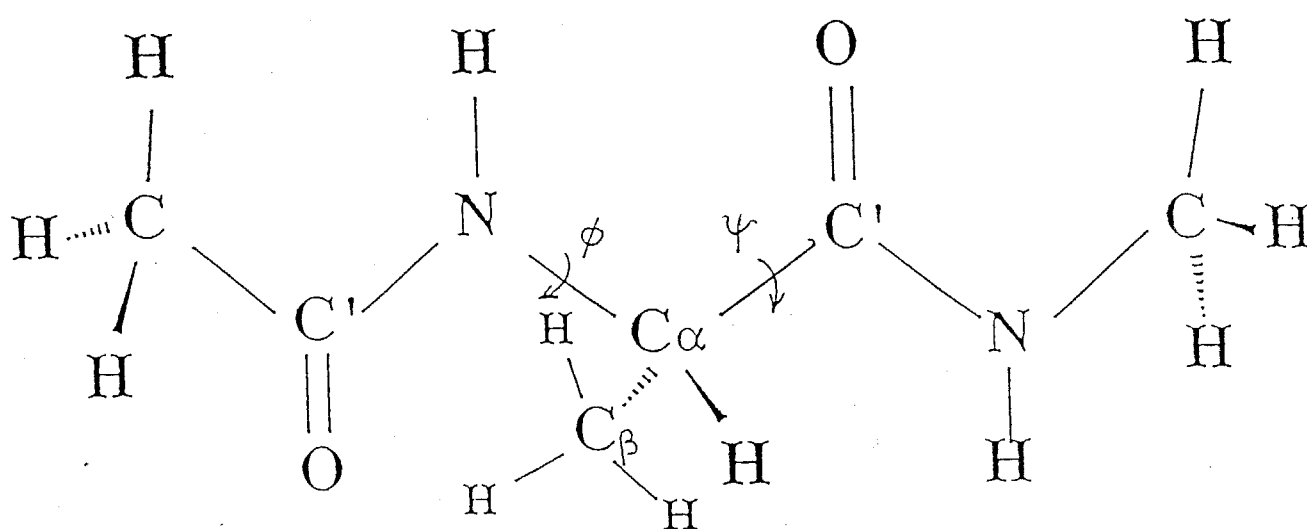


Figure 5.2: Molecular structure of N-acetyl-N'-methyl-L-alanine amide. The chemical shielding calculation was made for the C_α- and C_β-carbons by using the 4-31G GIAO-CHF method.

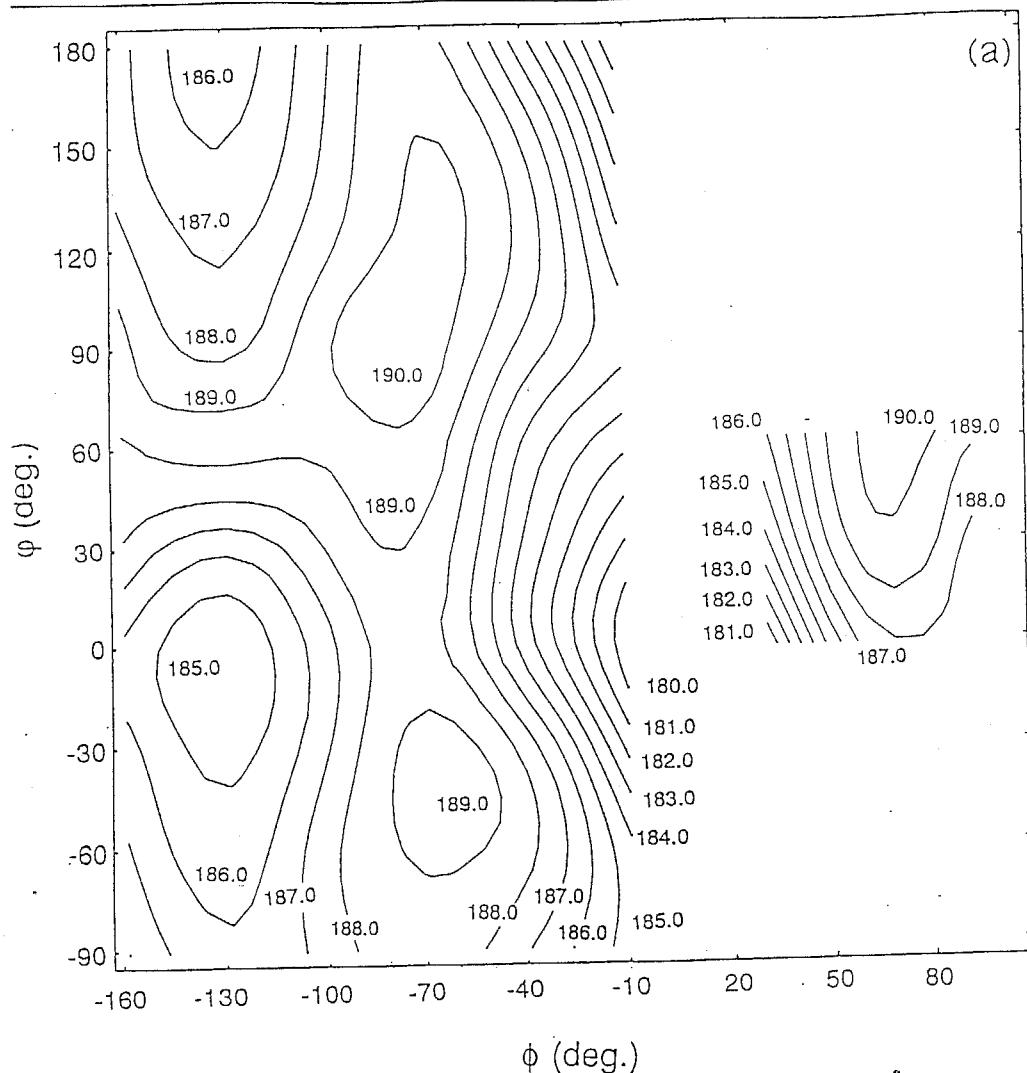


Figure 5.3: The dependences on the dihedral angles (ϕ, ψ), of the chemical shielding constants for the L-alanine residue C_{α} - and C_{β} -carbons in peptides. Chemical shielding calculations were carried out using the GIAO-CHF method with the 4-31G ab initio basis set. The 4-31G optimized geometries for the model molecules, N-acetyl-N'-methyl-L-alanine amide, were employed. (a) Isotropic, (b) σ_{11} , (c) σ_{22} , and (d) σ_{33} for the C_{β} -carbon (unit in ppm). (e) Isotropic, (f) σ_{11} , (g) σ_{22} , and (h) σ_{33} for the C_{α} -carbon (unit in ppm).

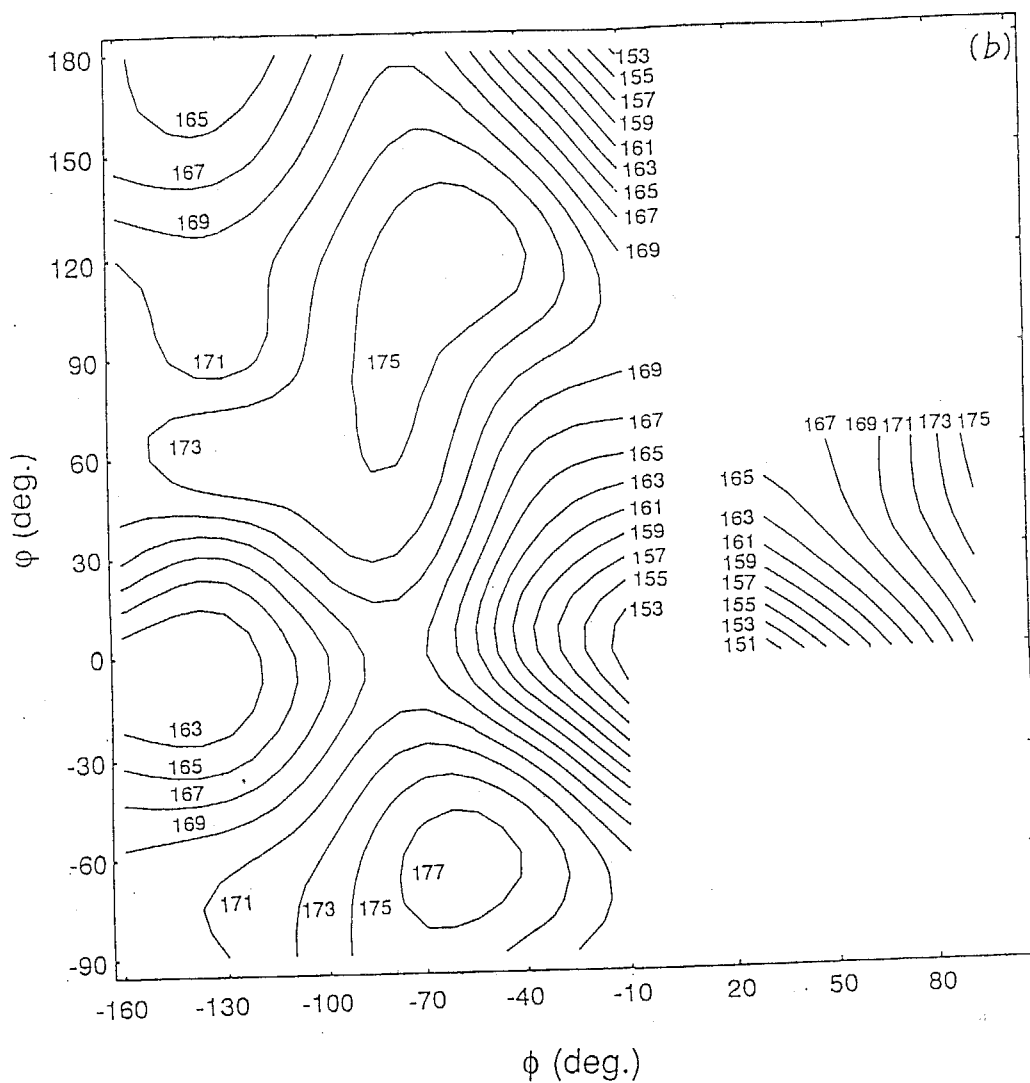


Figure 5.3: (continued.)

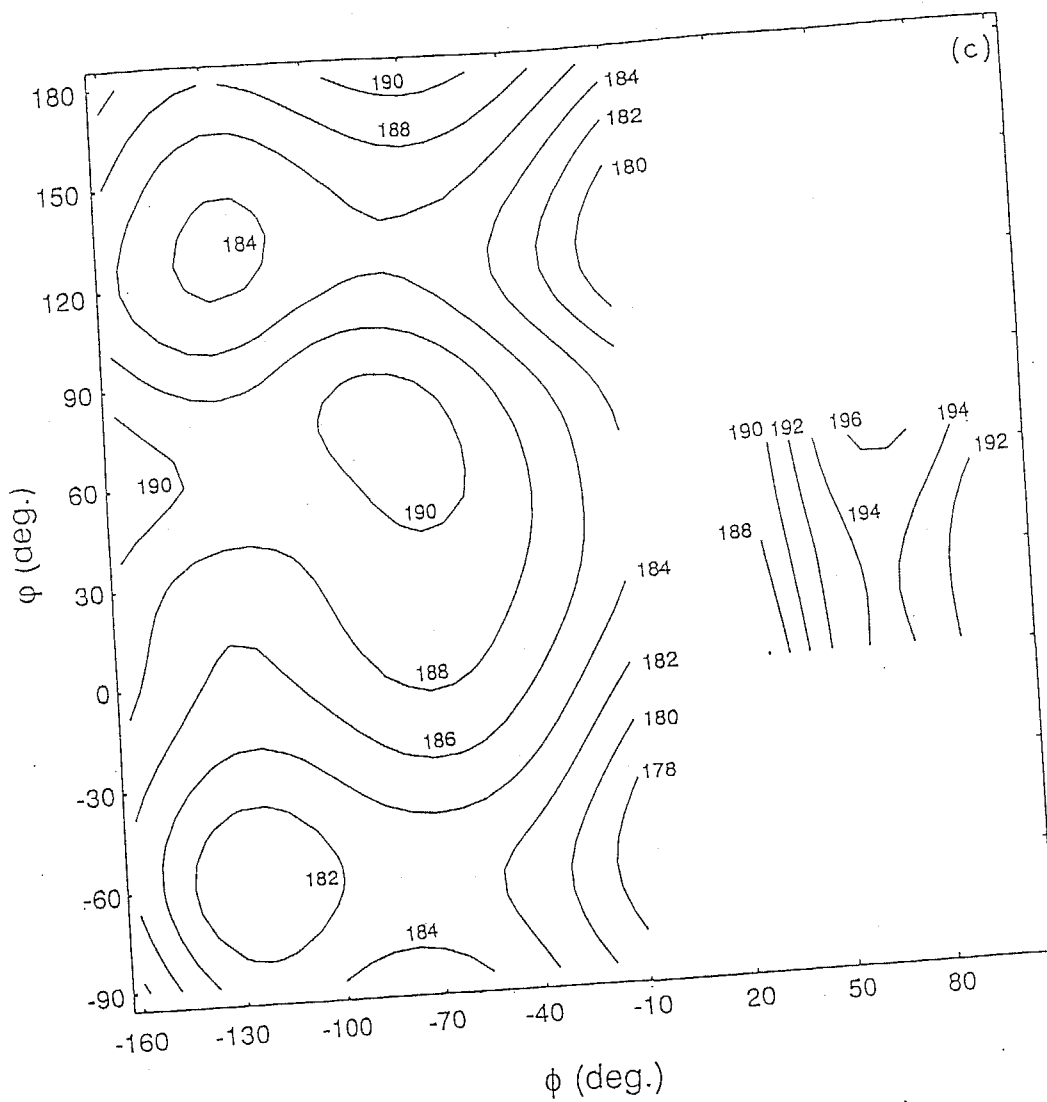


Figure 5.3 (continued.)

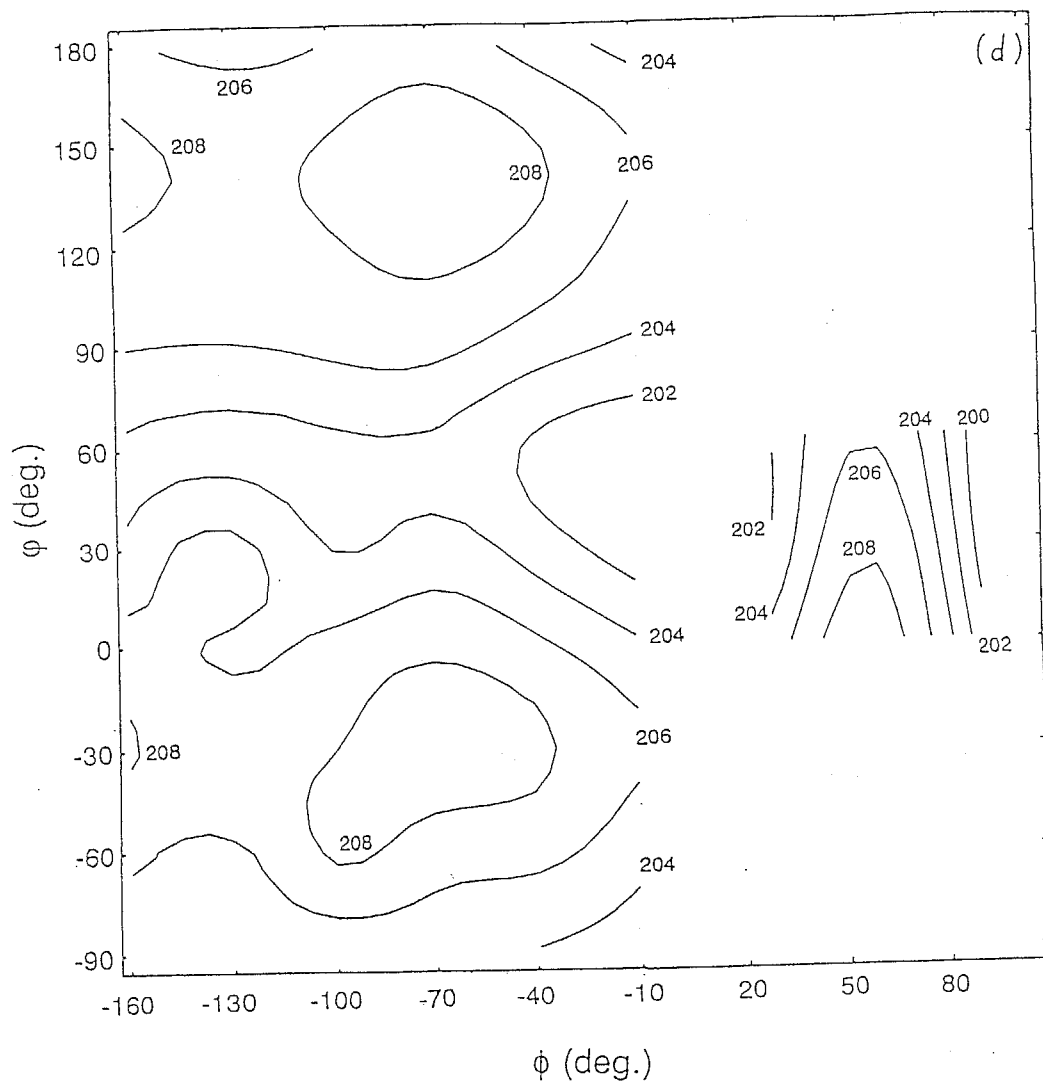


Figure 5.3 (continued.)

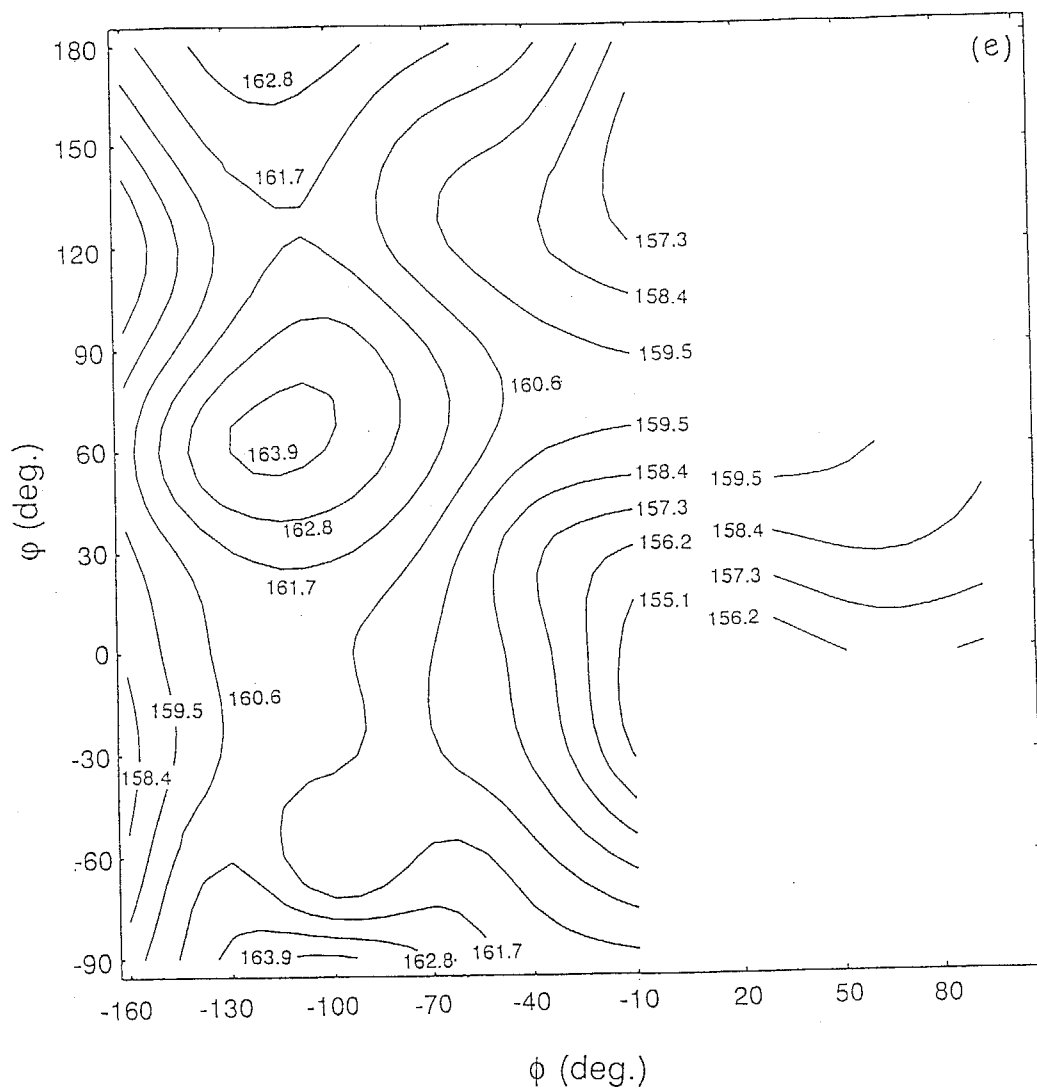


Figure 5.3 (continued.)

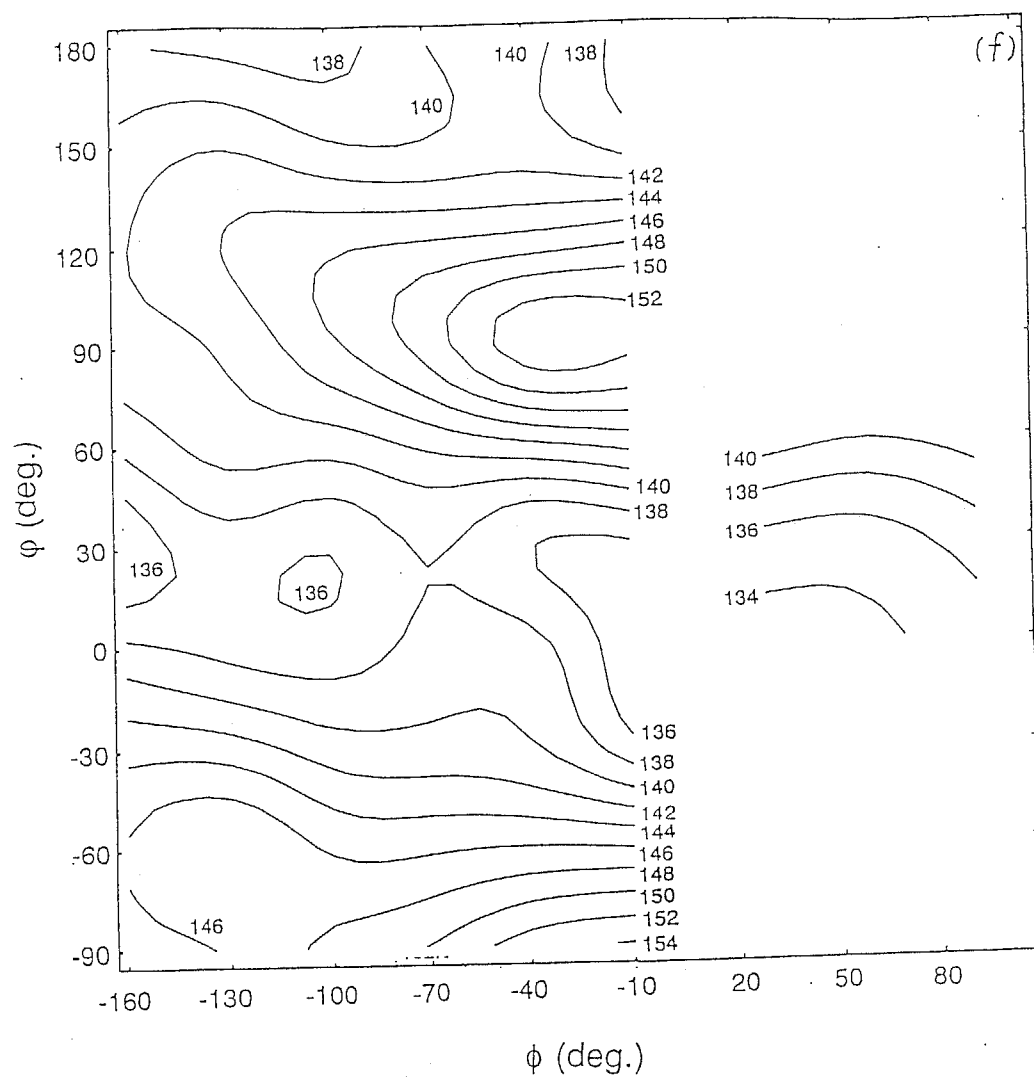


Figure 5.3 (continued.)

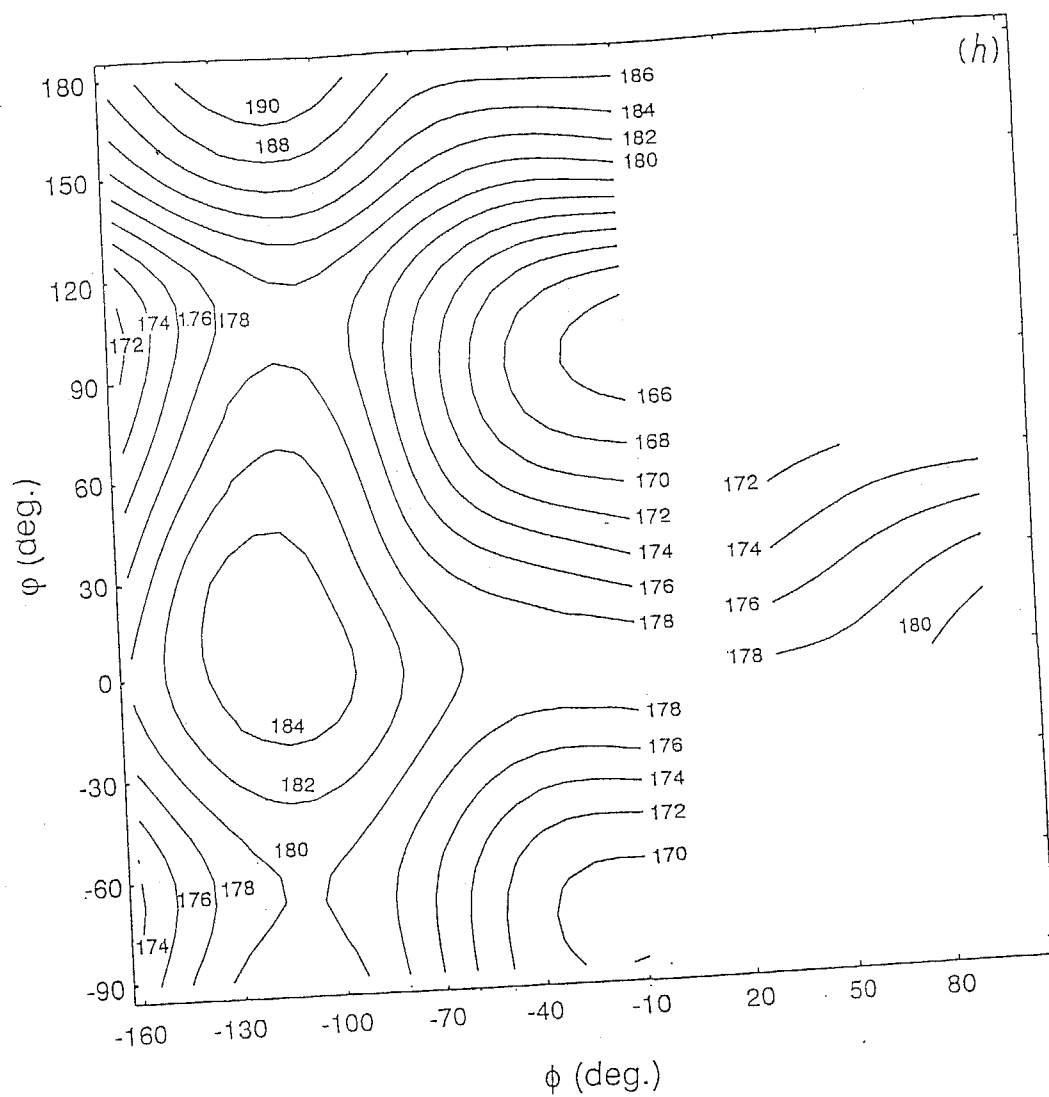


Figure 5.3 (continued.)

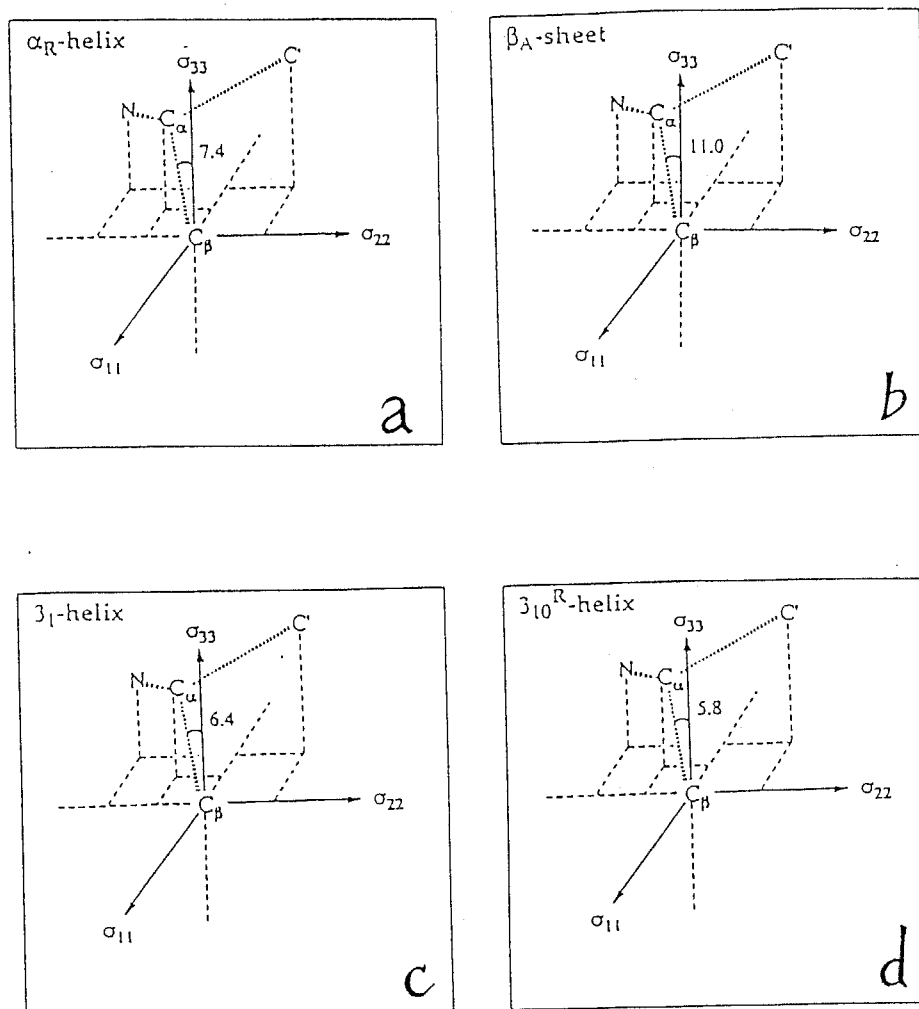


Figure 5.4: Orientation of the principal axes of the calculated ^{13}C chemical shift for the L-alanine residue C_β -carbons: (a) $(\phi, \psi) = -57.4^\circ, -47.5^\circ$ (α_R -helix); (b) $-138.8^\circ, 134.7^\circ$ (β_A -sheet); (c) $66.3^\circ, -24.1^\circ$ (3_{10}^R -helix); (d) $-84.3^\circ, 159.0^\circ$ (3_1 -helix), and for the C_α -carbon: (e) $(\phi, \psi) = -57.4^\circ, -47.5^\circ$ (α_R -helix); (f) $-138.8^\circ, 134.7^\circ$ (β_A -sheet); (g) $66.3^\circ, -24.1^\circ$ (3_{10}^R -helix); (h) $-84.3^\circ, 159.0^\circ$ (3_1 -helix).

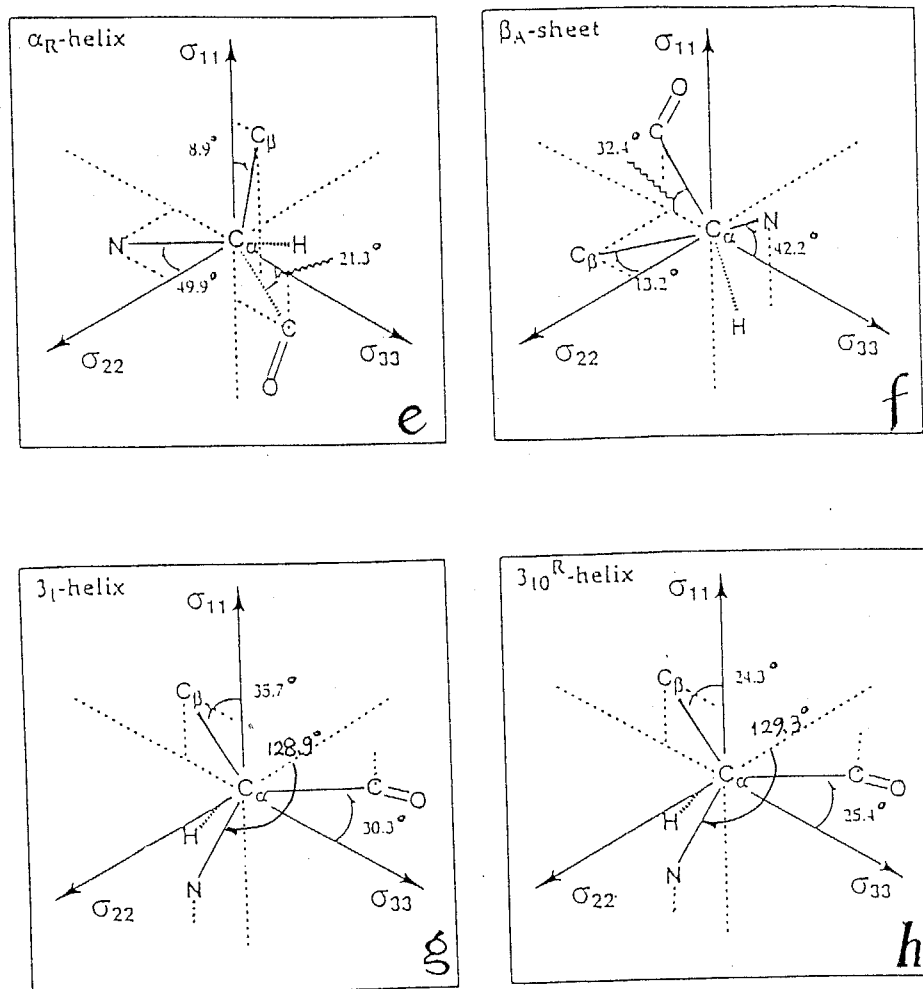


Figure 5.4 (Continued.)

Table 5.2 Calculated ^{13}C Chemical Shifts of L-Alanine Residue C_α - and C_β -Carbons by 4-31G-GIAO-CHF Method

sample	^{13}C chemical shift (ppm)							
	C_α				C_β			
	σ_{iso}	σ_{11}	σ_{22}	σ_{33}	σ_{iso}	σ_{11}	σ_{22}	σ_{33}
αR -helix	45.52	61.93	43.69	30.93	15.72	28.16	22.14	-3.16
βA -sheet	44.73	62.02	47.53	24.64	18.74	37.06	21.70	-2.53
3_1 -helix	43.62	65.79	46.46	18.91	15.94	33.80	17.97	-3.49
3_{10}R -helix	45.71	64.74	45.04	26.37	15.84	32.47	19.03	-4.00

Table 5.3 Geometrical parameters of L-alanine residues in RNase H and BPTI determined by the X-ray diffraction study and ^{13}C NMR chemical shift of the carbonyl-, C_α -, C_β -carbons in the corresponding residues

amino acid residue	dihedral angles (deg.)			hydrogen-bond length(Å) $\text{R}_{\text{N}..\text{O}}$	observed chemical shift(ppm)			calculated chemical shift(ppm)	
	ϕ	ψ	ω		C'	C_α	C_β	C_α	C_β
A24	-144.6	134.7	178.7	2.83	173.7	49.2	21.3	49.55	22.74
A37	-160.5	150.4	179.9	3.27	172.1	50.2	19.7	50.13	21.61
A51	-55.2	-46.1	-179.1	3.20	175.5	53.3	19.3	49.76	19.88
A52	-71.3	-35.4	-178.6	3.24	176.1	52.7	15.3	49.52	19.90
A55	-65.8	-49.2	178.1	3.30	175.6	52.7	17.2	49.27	19.83
A58	-81.0	-11.5	176.8	-	176.1	51.2	17.2	49.34	20.93
A93	-62.4	-22.9	-179.0	-	175.8	53.1	16.0	50.07	20.14
A109	-53.5	-49.9	-177.5	3.22	178.4	52.9	15.8	49.66	20.00
A110	-72.2	-25.6	180.0	3.30	178.1	52.7	16.5	49.66	20.11
A125	-66.5	123.7	-179.8	-	176.1	50.8	16.4	49.74	19.06
A137	-53.7	-57.3	179.8	3.25	177.3	53.5	16.6	49.29	20.17
A139	-67.4	-38.4	177.7	-	178.9	52.9	15.7	49.60	19.77
A140	-67.6	-41.7	-179.0	3.06	177.7	52.7	15.3	49.51	19.76
A141	-60.5	-22.9	-178.9	3.31	175.8	52.7	16.0	50.14 ₆	20.20
A16	-76.2	172.0	170.6	-	-	50.5	18.5		
A25	-62.3	-28.0	177.0	-	-	53.0	17.5		
A27	-82.9	-23.1	-178.7	-	176.3	50.5	19.0		
A40	-62.5	151.1	170.6	-	176.9	52.5	18.5		
A48	-61.7	-35.9	-179.4	2.80	177.9	53.5	16.0		

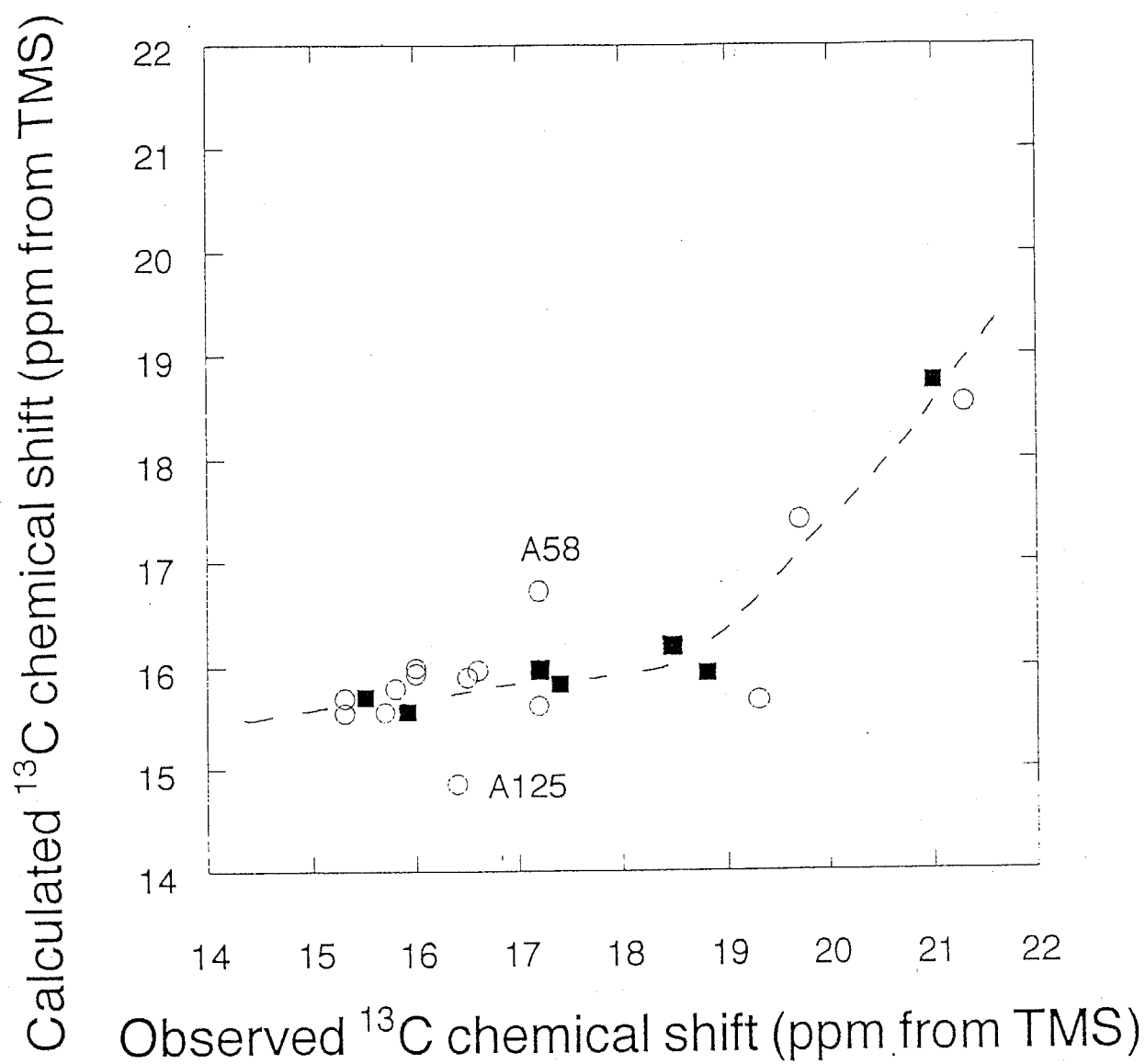


Figure 5.5: Comparison of the calculated chemical shifts with the observed shifts of the L-alanine residue C_β -carbons in some peptides in the solid state (solid square) and in RNaseH in the solution state (open square).

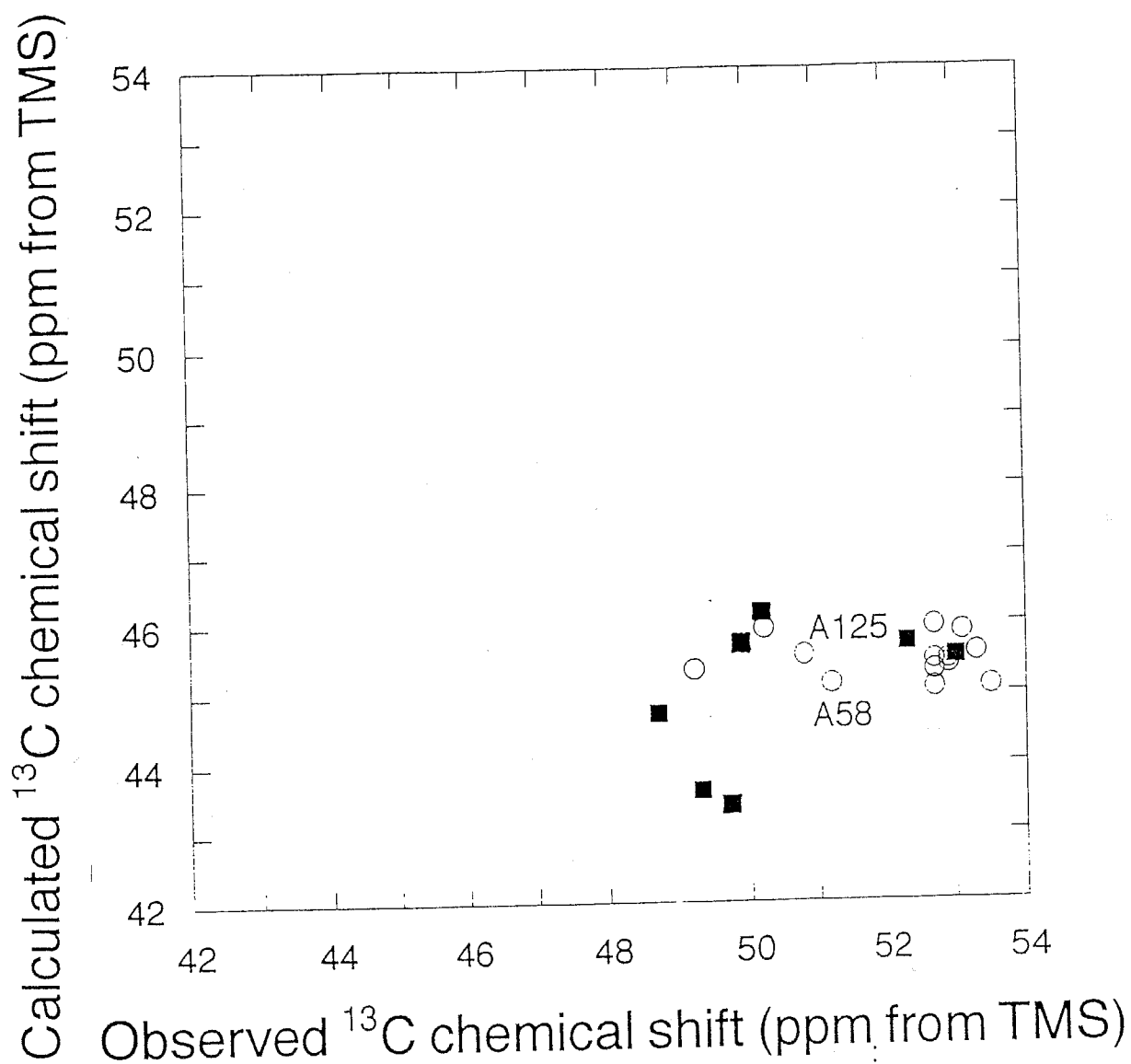


Figure 5.6: Comparison of the calculated chemical shifts with the observed shifts of the L-alanine residue C_α -carbons in some peptides in the solid state (solid square) and in RNaseH in the solution state (open square).

Chapter 6

Determination of Intermolecular Homonuclear Distance of α -Glycyl-glycine by XY8-DRAMA Sequence

It is well known that one needs the knowledge of the higher-order structures of peptides and proteins in order to understand how these molecules significantly act in the biological system. The secondary structure is particularly important because it determines the shapes of peptides and proteins. There exist the characteristic domains such as α -helix, β -sheet, and β -turn, which are commonly found in proteins. In order to elucidate the structure of proteins, one needs information about the distances between these domains, say, inter-chain distances.

However, it is difficult to determine highly accurate inter-chain distances by X-ray diffraction study even if one use a single crystalline sample. This is because the R-factor obtained by X-ray study should be inevitably large for polypeptides and proteins. This is originated by the fact that the numbers of geometrical parameters which must be determined are over 10000 for larger proteins; therefore, the distances determined include large experimental errors. For example, the X-ray diffraction study of poly(L-alanine) shows the large experimental error on the inter-chain distances in the β -sheet domain.⁷⁵) And, the X-ray crystallographic structure of Ribonuclease H (RNase H) from E.Coli have a quite large R-factor($R_f=0.19$)⁷⁶) and the amide-amide type($>N-H \cdots O=C<$) hydrogen-bond distances between the nitrogen and the oxygen atoms ($R_{N \cdots O}$) were rather longer($R_{N \cdots O} = 3.0 \sim 3.4 \text{ \AA}$) than the usual distances found in polypeptides and oligopeptides ($R_{N \cdots O} = 2.7 \sim 3.1 \text{ \AA}$). This is because most errors in the distances determined experimentally are shifted to the hydrogen-bond distances which have beforehand large freedoms in the optimization procedures.

The distance geometry method with employing solution NMR techniques does not give sufficiently accurate inter-chain distances because the nuclear Overhauser enhancement (NOE) obtained by the solution NMR is proportional to r^{-6} (r : inter-proton distances); therefore, the longer the distances determined, the larger the experimental errors are. The recent developments on the solid state NMR spectroscopy enable one to determine the internuclear distances regardless of whether one use a crystalline sample or not. The dipolar restoration at the magic angle (DRAMA) were developed for the purpose of detection of the homonuclear dipolar couplings in rotation solids.³⁵)

The DRAMA method works well, however, only when the sample contains homonuclear spin pairs of which isotropic resonance frequencies are identical to each other and also the chemical shift anisotropy(CSA) is not large. Therefore, the DRAMA method could not determine the coupling between carbonyl-carbon pairs. Gullion presented that the rotor synchronized XY-8 π -pulse scheme estimate transverse magnetizations(i.e., X,Y-magnetizations) equivalently, which leads to compensate the pulse imperfection and the resonance frequency offset.⁷⁷ Klug et al.⁷⁸ combined the DRAMA sequence with the XY-8 p-pulse scheme. Here, we tried to determine the ^{13}C - ^{13}C intermolecular homonuclear dipolar coupling in 10And we also performed the XY-8 DRAMA measurements by using natural abundance Gly-Gly in order to estimate the effect of the coupling between the labeled site and the natural abundance ^{13}C nuclei.

6.1 Solid State NMR Measurements

We made solid state NMR measurements by a home-built spectrometer which is operated at 50.3MHz for the ^{13}C channel. We used H_1 field intensity of 38kHz for cross-polarization and 98kHz for ^1H - ^{13}C heteronuclear decoupling. We employed 2ms cross-polarization contact time and 35+47ms filter delay before acquisition (The observation gate was opened at 47ms before acquisition). The magic angle spinning rate was 3125Hz. Figure 6.1 shows the pulse sequences for XY-8 DRAMA (a: rotor synchronized Harn echo, b: a XY-8 DRAMA full echo, and c: a XY-8 DRAMA dephase echo). We performed the experiments for 16, 32, 48, 64, 80, 96 rotor cycles. Table 6.1

shows the phase cycling for quadrature detection.

Figure 6.2 a and b show the rotor synchronized Hahn echo and the ^{13}C XY-8 DRAMA full echo spectra of 10 respectively. By using the phase cycling shown in Table 6.1, we were able to obtain the spectra with no significant phase errors. The XY-8 DRAMA full echo intensity of the Gly-1 carbonyl-carbon was about 90%. The decrease of signal intensity with increasing the rotor cycles is due to the natural T_2 decay. Figure 6.2 c shows the XY-8 DRAMA dephase echo spectra. No phase errors were observed even when we used the sequence for 96 rotor cycles, which has 1008 ^{13}C π -pulses. The ratio (S/S_0) of the XY-8 DRAMA dephase echo intensity (S) to the full echo intensity (S_0) against rotor cycles (N_c) are shown in Figure 6.3. We performed the experiments with three carrier frequencies: on-resonance, -0.45kHz off-resonance, and +2.00kHz off-resonance for Gly-1 carbonyl-carbon. Figure 6.3 shows that the carrier offset frequencies does not affect on the ratio of the S/S_0 .

6.2 Determination of Intermolecular Distances of Peptides

In order to estimate the homonuclear dipolar coupling, we calculated XY-8 DRAMA dephasing under δ -function pulses assumption. The nearest- and the next-nearest neighbor distances are 4.8Å and 5.6Å, respectively (Figure 6.4). These are corresponding to the dipolar coupling of 68Hz and 43Hz, respectively. Figure 6.3 shows that we can determine the intermolecular ^{13}C - ^{13}C distance for the initial XY-8 DRAMA dephasing ($N_c \leq 48$). For larger

rotor cycles, more dephasing occurred because of the dipolar couplings between the ^{13}C labeled site and the natural abundance carbonyl-carbons of both Gly-1 and Gly-2. In order to make it sure, we performed the same experiments by using natural abundance version of Gly-Gly(Figure 6.5). The values of S/S_0 for 64, 80, 96 rotor cycles are 0.94, 0.89, 0.84, respectively. Figure 6.5 shows that we cannot ignore the natural abundance effect on the S/S_0 . However, we were able to determine the ^{13}C - ^{13}C homonuclear distance in peptides for performing the experiments for small rotor cycles($N_c \leq 48$). The residual dipolar coupling between the ^{13}C carbonyl-carbon and the directly bonded amide ^{14}N causes the slight splitting and the broadening of the Gly-1 carbonyl-carbon signal(Figure 6.2), it does not seem to affect on the S/S_0 of XY-8 DRAMA. This way, the XY-8 DRAMA method will be useful to elucidate the structures of peptides and proteins in the solid state.

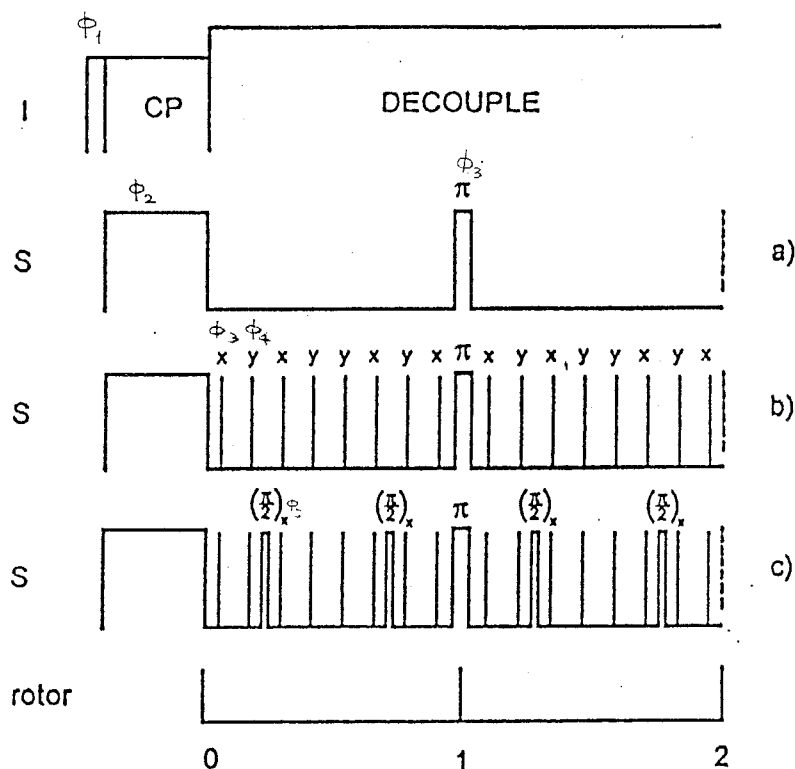


Figure 6.1: Pulse sequences for an I-S matched spin-lock, cross-polarization transfer (with spin-temperature alternation) followed by (a) a rotor synchronized Hahn echo, (b) a compensated DRAMA full echo, and (c) a compensated DRAMA-dephased echo. Phase alternation of the refocusing Hahn π pulse after odd-numbered rotor cycles and that of the eight equally spaced π pulses during each rotor period of the compensated DRAMA sequences follow the XY-8 scheme. All dephasing $\pi/2$ pulses have the same phases. The illustration is for two rotor cycles.

Table 6.1 Phase cycling for DRAMA experiments. ϕ_i ($i=1,2,3,4,5,6$) are defined in Figure 6.1.

ϕ_1	ϕ_2	ϕ_3	ϕ_4	ϕ_5	ϕ_6
x	x	x	y	x	x
-x	y	y	x	y	-y
-x	x	x	y	x	-x
x	y	y	x	y	y
-x	-x	x	y	x	x
x	-y	y	x	y	-y
x	-x	x	y	x	-x
-x	-y	y	x	y	y

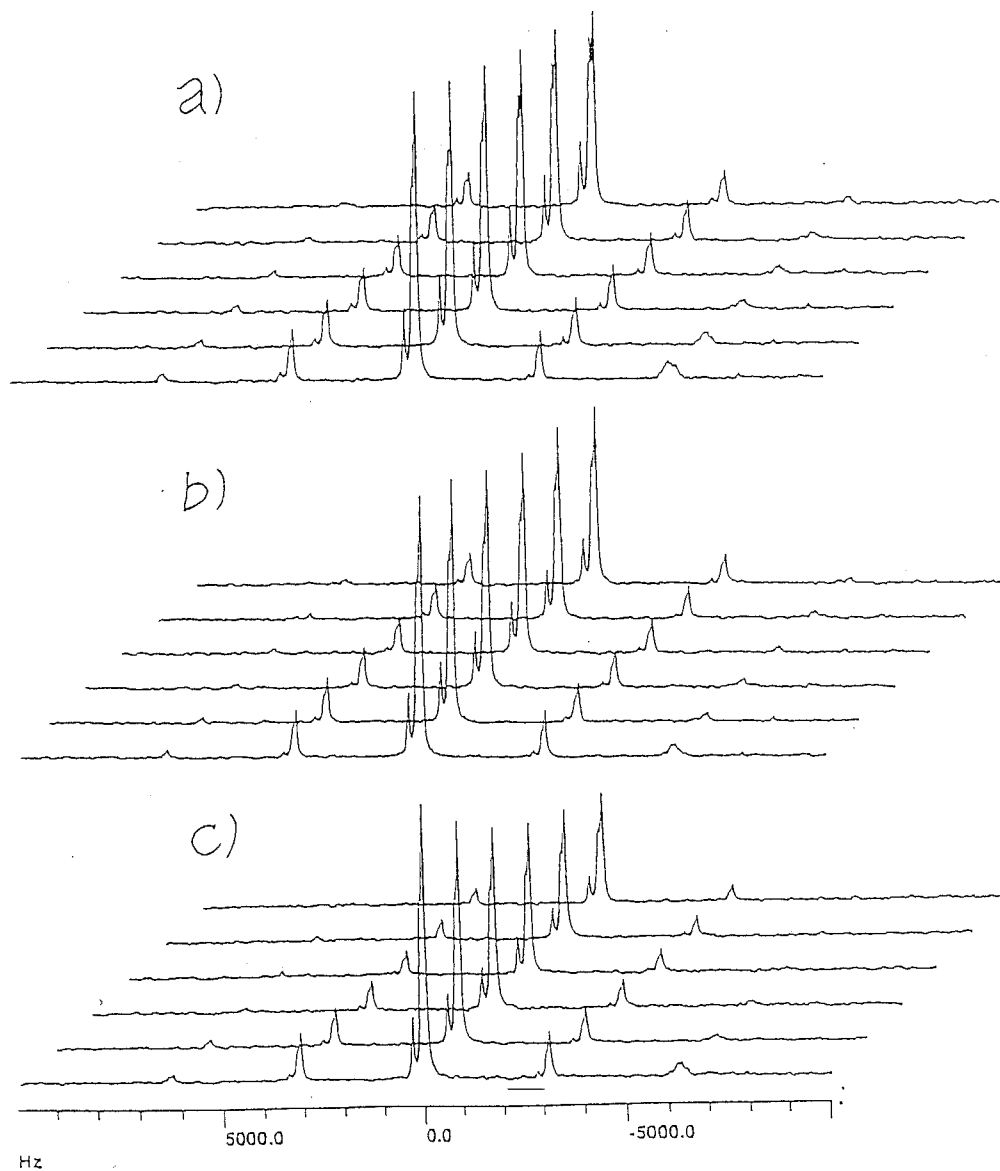


Figure 6.2: 50.3MHz ^{13}C cross-polarization magic-angle spinning spectra of 10% labeled $[1-^{13}\text{C}]\alpha$ -glycyl-glycine measured by (a) a rotor synchronized Hahn echo, (b) a XY8-DRAMA full echo(S_0), and (c) a XY8-DRAMA-dephased echo(S) sequences, respectively. The spectra are plotted as a function of the rotorcycles(N_C). Magic-angle spinning was at 3205Hz. The ^{13}C rf field intensity was 38kHz and ^1H decoupling field intensity was 89kHz. The ^{13}C carrier frequency was at the Gly-1 carbonyl-carbon signal.

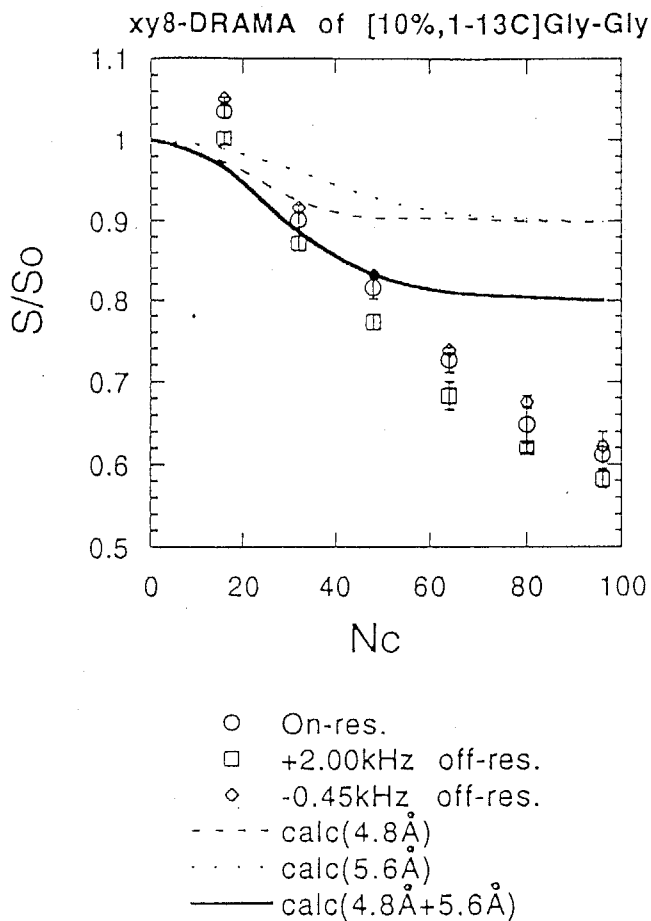


Figure 6.3: XY8-DRAMA dephasing (S/S_0) for [10%,1- ^{13}C]glycyl-glycine with the magic-angle spinning at 3205Hz. The ^{13}C carrier frequency was at on-resonance for Gly-1 carbonyl-carbon (open circle), +2.00kHz off-resonance (open square), and -0.45 kHz off-resonance (open diamond). Calculated DRAMA dephasing assumed δ -function pulses and two dipolar ^{13}C - ^{13}C couplings of 68Hz (4.8 Å) and 43Hz (5.6 Å). The calculation was performed for the pulse sequence in Figure 6.1(c) and is independent of all shift tensors.

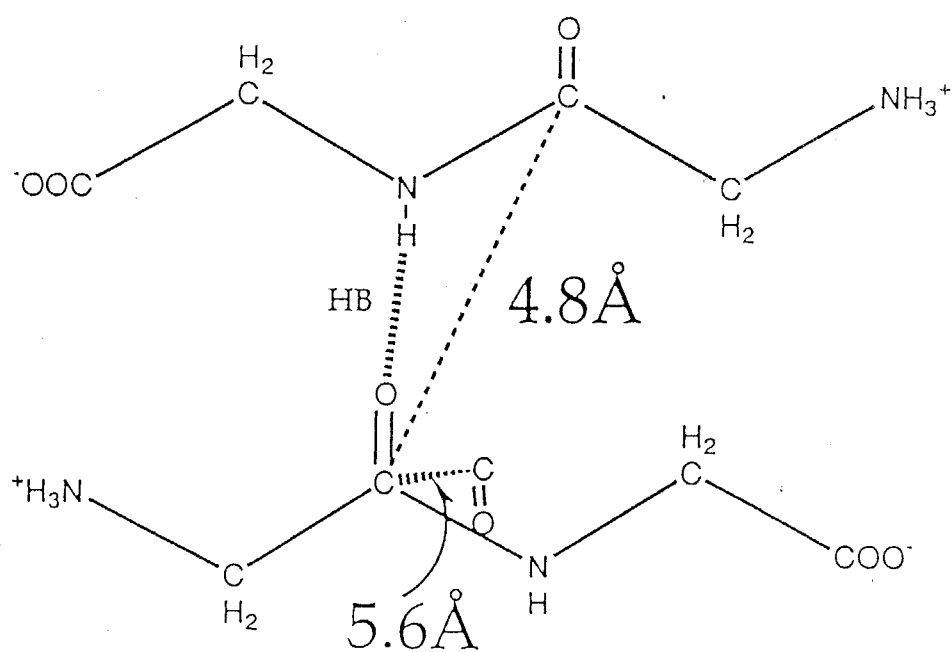


Figure 6.4: Molecular structure of α -glycyl-glycine in the crystalline state.

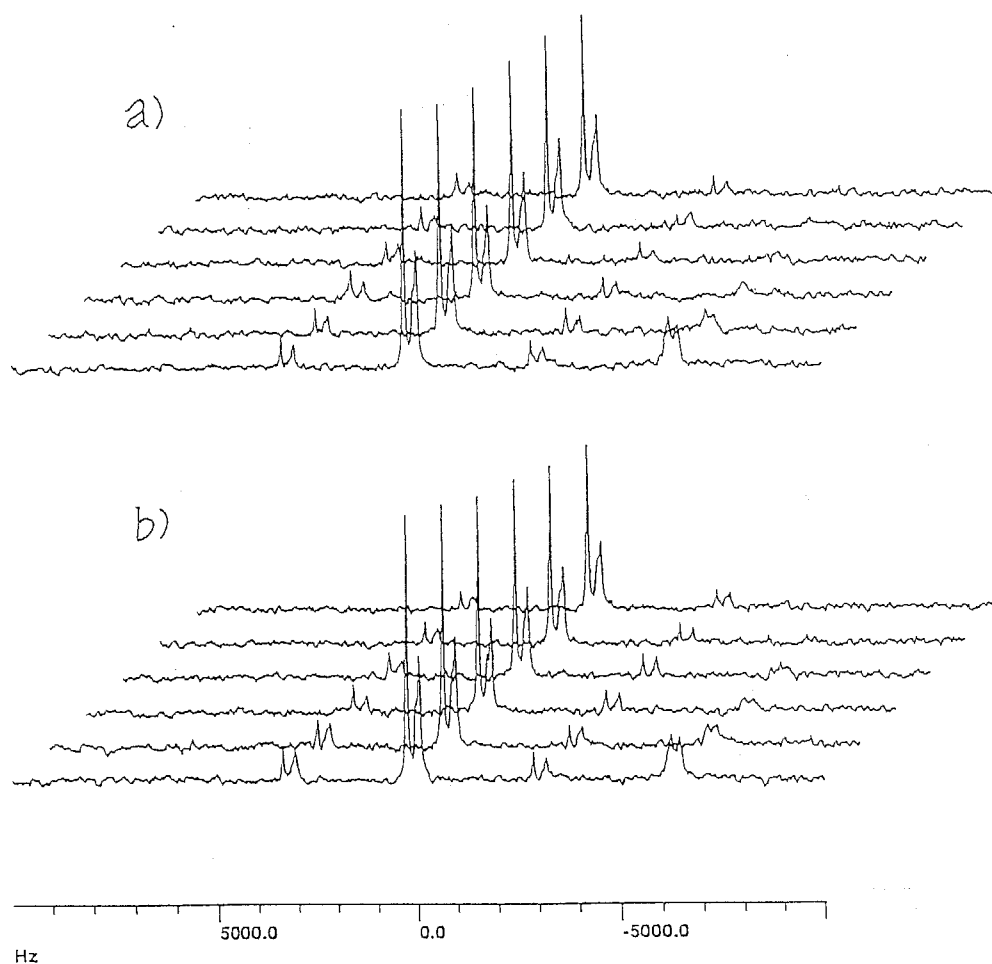


Figure 6.5: Control test for XY8-DRAMA pulse sequences. ^{13}C natural abundance version of glycyl-glycine was used for this purpose. For the small rotor cycles ($N_c \leq 48$), the effect of the natural abundance ^{13}C on S/S_0 was able to be ignored. (a) A XY8-DRAMA-full echo and (b) a XY8-DRAMA-dephased echo were shown; N_c is the number of rotor cycles.

Chapter 7

Conclusion

In Chapter 1, we described the current situation of structural study of proteins, and refer to the necessity of a novel method for this purpose. Particularly, the X-ray diffraction method is not necessarily powerful for structural study for a large molecular weight, and also the distance geometry method with the solution NMR technique is poor for determination of inter-chain distances such as hydrogen-bond length. These defects for both methods come from the lack of the number of data obtained from the experiments. Thus, we propose, as a novel method, a structural study of peptides by the solid state NMR with chemical shielding calculation.

In Chapter 2, we introduced two kinds of methods for determination of principal values for chemical shift tensor. One is the powder pattern analysis, and the other is the magic-angle spinning sideband analysis, namely, the Herzfeld-Berger analysis. We demonstrated that the Herzfeld-Berger analysis is more applicable than the powder pattern analysis, in the case of ^{13}C solid

state NMR measurements of peptides. We also made interpretation for the determination of internuclear distances of a homonuclear spin pair such as ^{13}C - ^{13}C by the reintroduction of magnetic dipole coupling in MAS experiments. In order to understand the correlation between ^{13}C chemical shift of peptides and molecular structure, we made chemical shielding calculation. For this purpose, we describe the two theories, FPT-INDO and 4-31G GIAO-CHF methods.

In Chapter 3, we described the procedures for peptides synthesis that were performed in this thesis, and the detailed conditions for the solid state NMR measurements.

In Chapter 4, we described the results regarding hydrogen-bonding effect on the chemical shift for L-alanine residue carbonyl-carbon. We found that the observed isotropic ^{13}C chemical shift (δ_{iso}) of L-Ala carbonyl-carbon in the amide-type hydrogen-bond, moves linearly downfield with a decrease of hydrogen-bond length. Such downfield shift is predominantly governed by the δ_{22} . The δ_{11} moves somewhat upfield, and the δ_{33} is not sensitive to the change of $R_{N...O}$. These results could be justified by the chemical shielding calculation with molecular orbital method. Further, the calculation shows that the δ_{22} (corresponding to the observed δ_{22}) lies along the amide carbonyl-bond and is the most sensitive principal value of the ^{13}C carbonyl chemical shift tensor. The above results are of use in analyzing ^{13}C solid state NMR studies of polypeptides and proteins. Although there exists the experimental relation that ^{13}C chemical shift for the L-alanine residue carbonyl-carbon in solid peptides linearly moves to downfield with the decrease of $R_{N...O}$, we could not find such relation on ^{13}C chemical shift of the

L-alanine carbonyl-carbon in ribonuclease H in the aqueous solution. This is due to the facts that $R_{N...O}$ s determined by X-ray diffraction study inevitably include large experimental errors. Then, it is useful to utilize chemical shifts of the carbonyl-carbons in peptides and larger proteins as an indication of hydrogen-bond length.

In Chapter 5, we showed that ^{13}C chemical shifts of the L-alanine residue C_β -carbons in peptides in the solid state and in proteins in the aqueous solution give information about the dihedral-angle of the main-chain of L-alanine moiety. However, hydrogen-bonded structure as well as the dihedral-angles complicatedly affects ^{13}C chemical shift of the C_α -carbon. These results were extracted by the 4-31G-GIAO-CHF calculation on ^{13}C chemical shift.

In Chapter 6, we examined the compensated XY-8 dipolar restoration at magic angle (XY-8 DRAMA) for 10 polycrystalline dipeptide. The XY-8 DRAMA sequence was used for multiples of 16 rotor cycles. By using the results for small rotor cycles ($N_c \leq 48$), we were able to determine the inter chain distances between carbonyl-carbons in this peptide. And also it was found that, as for many rotor cycles, we could not ignore the dipolar coupling between the labeled site and the natural abundance ^{13}C nuclei of both of Gly-1 and Gly-2.

Chapter 8

Future Prospect

In this chapter, the author should like to refer to future possibilities of the solid state NMR spectroscopy for structural elucidation of biological molecules such as proteins.

Firstly, NMR chemical shift will come to be important in the field of structural biology. So far, a great deal of efforts has been devoted to the complete assignments of NMR signals for several protein solutions. These assignments has, however, been utilized to NOE-based distance constraints for building up the three-dimensional structure of proteins. The more progressive utilization of chemical shift will increasingly be made for especially large proteins of which three-dimensional structure would not be able to be determined by the only conventional NOE-based distance-geometry method. Furthermore, as can be seen in chapter 5, chemical shift involves the information about the interaction between solvent molecules and the specific site of an amino acid residue. Therefore, one will be able to address the problem

of how the specific amino acid interacts with the other site or molecules, through the observation of chemical shift. This will gain the further insight on the biological events from the viewpoint of molecular level.

Secondly, the high-resolution solid state NMR spectroscopy will offer one information about detailed molecular structure of the heterogeneous system including proteins, lipid, and saccharides. Particularly, the nuclear magnetic dipolar coupling measured by the solid state NMR provides the direct information about internuclear distances such as ^{13}C - ^{13}C , ^{13}C - ^{15}N , ^{13}C - ^{19}F , ^{13}C - ^{31}P , and so on. Since the solid state NMR spectroscopy, in principle, involves no restrictions for performing the structural analysis of the heterogeneous systems, one will be able to detect various biological events such as the protein-protein, protein-lipid, protein-DNA, and protein-saccharide interactions in the solid state. Proteins are often embedded on the membranes and immobilized like solid materials. Therefore, from the viewpoint of molecular mobility, situations are often quite different from that can be seen in protein solutions. For such a system where, in general, the X-ray diffraction cannot be available, the solid state NMR will come to be a powerful methodology for structural investigations.

Thirdly, it seems to be valuable to refer to the prospect concerning the chemical shielding calculation by the molecular orbital methods. In associated with the recent rapid developments of computational capability, one can come to carry out chemical shielding calculation with high accuracy. However, in the case that one seeks to know what kind of chemistry or physics is really going on the system considered, the semi-empirical chemical shielding calculation might be sufficient to understand it. Therefore, one should select

the calculation method in accordance with his requirement.

Fourthly, the chemical shielding calculation offers the information about not only the shielding tensor components but also the orientation of the chemical shielding tensor with respect to the molecular fixed frame. However, at this point, the experimental techniques for determination of the small anisotropy and the orientation are not established well; particularly, it is difficult to determine the orientation for the nuclei of which the chemical shift anisotropy is small. The chemical shift tensor for the L-alanine residue α -carbon is included in this case. The switching angle sample spinning(SASS) method is, of course, the well-established, however, the modification of the NMR probe is needed. One really seeks an easy alternative method for the determination of the tensor components and the orientation of chemical shift tensor with small anisotropy.

Appendix

A: The Powder Averaging Procedure in the Magic-angle Spinning Sideband Spectrum Simulation

In this thesis, we have tried to determine the principal values of ^{13}C chemical shift tensor in L-alanine residue carbonyl-carbon in peptides. In order to make it, we employ the Herzfeld-Berger analysis instead of the powder pattern analysis. Hereafter, describe details of the spectrum simulation, particularly arguments regarding powder averaging procedures. From the viewpoint of computation, since time consuming is a vital problem, one has to endeavor to diminish the computation time. The question comes out from this viewpoint is how many crystalline orientations should be taken account for the powder averaging that we try to perform.

Figure A.1 a-c show the comparison between the powder averaging by 605 orientations, that by 4851 orientations, and that by 115351 orientations; 605 is the multiplication of 11 for α , 5 for β , and that by 11 for γ orientations,

4851 is 21 by 11 by 21, and 115351 is 61 by 31 by 61. The principal values for the chemical shift tensor are 243,193,94 ppm. The static magnetic field is 67.8MHz for 13 , and the MAS rate is 1600Hz. From this figure, 4851 orientations would be enough to build up the spinning sideband spectrum.

One might have a question about why all the spinning sidebands have the same phase. Figure A.2 a-d shows the spectrum simulations for the single crystal of which Euler angles are $(\alpha, \beta, \gamma) = (30^\circ, 45^\circ, 60^\circ), (-30^\circ, 45^\circ, 60^\circ), (30^\circ, -45^\circ, 60^\circ)$, and $(30^\circ, 45^\circ, -60^\circ)$. The other parameters are the same as those in Figure A.1. From this figure, each spinning sideband has the different phases, that is the mixture of the real part and the imaginal part of the complex signals. Figure A.3 a and b shows the spectrum partially averaged by α and γ , respectively. The number of orientations for each averaging is 61. From this figure, the averaging by γ does not make the absorptive spectrum, but the averaging by α does. If the complete averaging is desired, one needs the further averaging by β .

B: Remarks on the Behavior of the Chemical Shift Tensors for L-alanine Residue Carbonyl-, C_α -, and C_β -carbons by Molecular Orbital Diagram

L-Alanine Residue Carbonyl-carbon

The amide-amide type hydrogen-bonding in solid peptides causes

downfield shift on the mid-field principal value(δ_{22}) of chemical shift tensor for the L-alanine carbonyl-carbon; the σ_{22} is nearly aligned to the carbonyl-bond. That is, decreasing the hydrogen-bond length($R_{N...O}$) renders the chemical shielding diminished, which is aligned to the carbonyl-bond. In order to gain the further insight, we try to describe this de-shielding by MO diagram for L-alanine residue carbonyl-group. Generally, decreasing the differences between two specific energy levels that would contribute to the shielding, causes de-shielding on the paramagnetic contribution. This is expressed by the following equation:

$$\sigma^p \propto -\frac{1}{\Delta E} \quad (8.1)$$

When the hydrogen-bonding is formed, the energy level for the n-orbital that is spreaded around the outside of carbonyl-bond will have a lower energy level than that in which there exists no hydrogen-bond, because the hydrogen-bonding enlarges the overlap integral between the n-orbital and the amide-hydrogen s-orbital(shown in Figure B.1). Moreover, the hydrogen-bonding also diminishes the double-bond character of the carbonyl-bond, which causes the energy level of the antibonding orbital(π^* -orbital) immensely lower(Figure B.1). From these, we might be able to say that the n- π^* transition energy would be decreased by formation of the hydrogen-bond, and the decrease of n- π^* transition energy renders the σ_{22} downfield shifted. However, since conventionally, it is well known that hydrogen-bonding causes blue-shift on the n- π^* transition energy, the above mentioned discussion conflicts this. Then, the more accurate estimation of the n- π^* transition energy is needed.

L-Alanine Residue C_α - and C_β -carbon

- In section 6, we described the explanation for the chemical shift behavior of the L-alanine residue C_β -carbon with respect to variation of the main-chain dihedral-angles, by invoking the differences in the C_α - C_β bond length. In general, the paramagnetic contribution of a specific principal value ($\sigma_{\beta\beta}$) ($\beta = x$ or y or z) for a chemical shift tensor is dominantly raised from the interaction between the 2p-orbital perpendicular to the $\sigma_{\beta\beta}$ and the external magnetic field. This interaction is called as the magnetic dipole coupling, and expressed as $\langle \phi_\nu | \mathbf{L}_{B\beta} / r_B^3 | \phi_\lambda \rangle$; the notation is the same as the defined in section 2. On the other hand, the diamagnetic contribution of the principal value is dominated by $\langle \phi_\lambda | (\mathbf{r}_\lambda \cdot \mathbf{r}_B \delta_{\beta\beta} - (r_\lambda)_\beta (r_B)_\beta) / r_B^3 | \phi_\lambda \rangle$. Therefore, the diamagnetic contribution is largely due to atomic orbitals parallel to the $\sigma_{\beta\beta}$. As regards the C_α -carbon, the diamagnetic contribution of the σ_{33} is largely affected by changes in the main-chain dihedral-angles, especially in the comparison between the α_R -helix and the β_A -sheet main-chain dihedral-angles. The interaction involving the atomic-orbitals align to the σ_{33} would be, therefore, important for one to understand the results. However, the explicit geometrical differences around the C_α -carbon portion in the α_R -helix and β_A -sheet main-chain dihedral-angles could not be seen. This problem still remains as a future work.

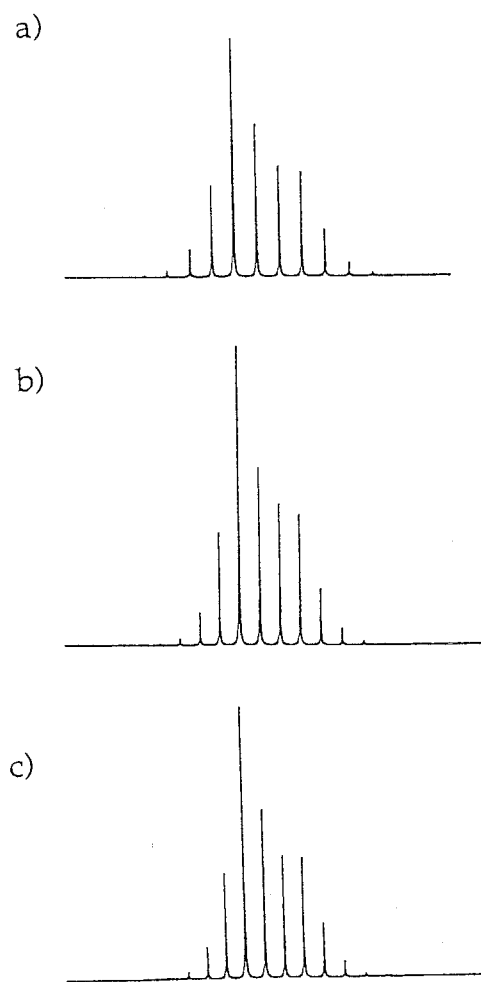


Figure A.1: The comparison of the 67.8MHz MAS simulation spectra for several degrees of powder averaging. a) 605 $[(\alpha, \beta, \gamma)=(9, 5, 9)]$, b) 4851 $[(\alpha, \beta, \gamma)=(21, 11, 21)]$, and c) 115351 orientations $[(\alpha, \beta, \gamma)=(61, 31, 61)]$. The principal values of the chemical shift tensor were 243, 193, 94 ppm, and MAS rate was 1600Hz.

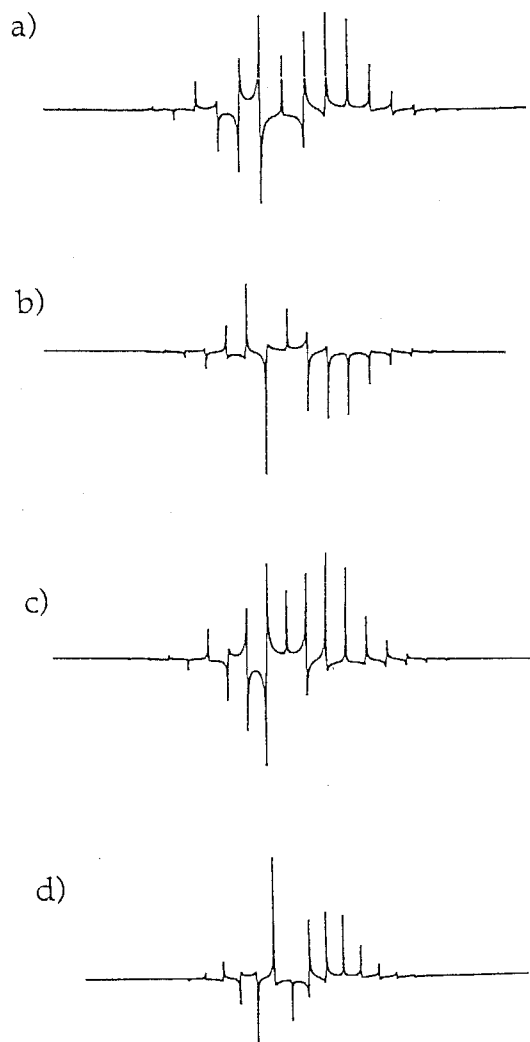


Figure A.2: The 67.8MHz MAS simulation spectra for the single crystal of which orientations are a) $(\alpha, \beta, \gamma) = (30^\circ, 45^\circ, 60^\circ)$, b) $(\alpha, \beta, \gamma) = (-30^\circ, 45^\circ, 60^\circ)$, c) $(\alpha, \beta, \gamma) = (30^\circ, -45^\circ, 60^\circ)$, d) $(\alpha, \beta, \gamma) = (30^\circ, 45^\circ, -60^\circ)$. The other parameters were the same as those in Figure A.1.

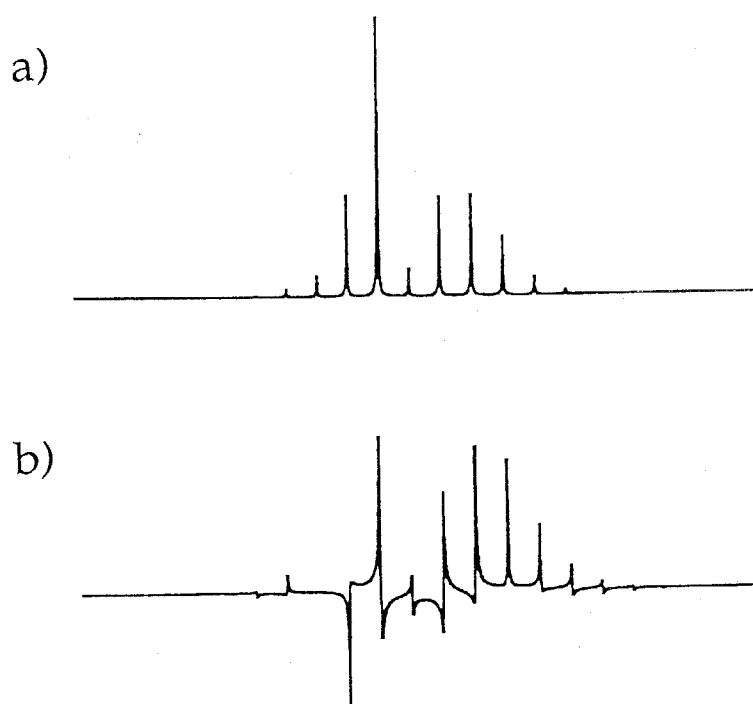


Figure A.3: The 67.8MHz MAS simulation spectra partially averaged by α and γ . a) $(\alpha, \beta, \gamma) = (\text{averaged}, 45^\circ, 60^\circ)$, b) $(\alpha, \beta, \gamma) = (30^\circ, 45^\circ, \text{averaged})$. For each averaging, single crystals of 61 orientations were accumulated. The other parameters were the same as those in Figure A.1.

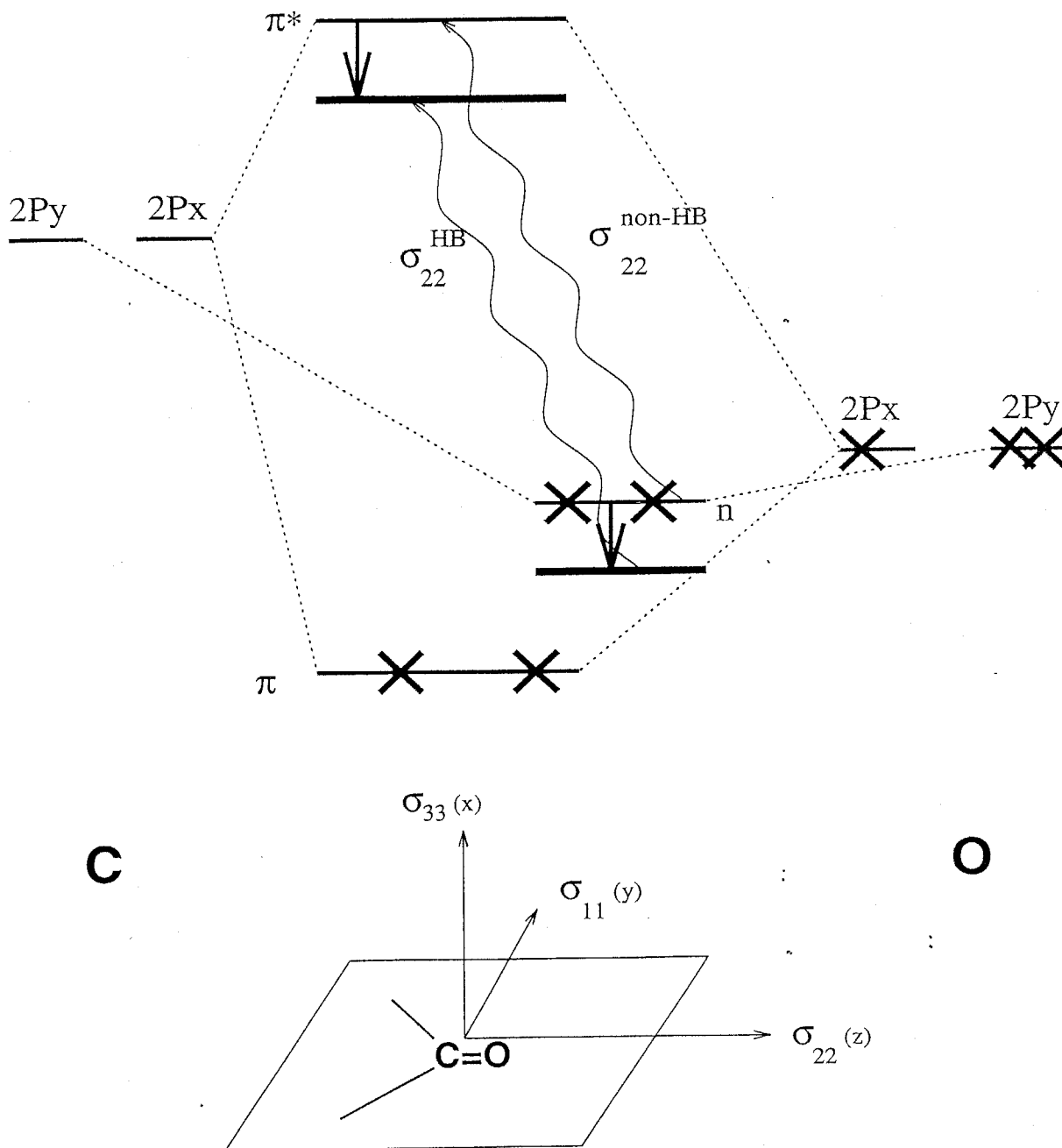


Figure B.1: Partial MO diagram for the carbonyl-group. The $n\text{-}\pi^*$ single electron excitation gives the main contribution to the σ_{22}^{HB} , of which principal axis is parallel to the carbonyl-carbon.

Bibliography

- [1] H.Saito and I.Ando, *Annu.Rep.NMR Spectrosc.*,**21**,209(1989)
- [2] J.W.Pflugrath, G.Wiegand, and R.Huber, *J.Mol.Biol.*, **189**, 383 (1986);
A.D.Kline, W.Braun, and Kurt Wuthrich, *J.Mol.Biol.*, **189**, 377 (1986)
- [3] I.Ando, H.Saito, R.Tabeta, A.Shoji, and T.Ozaki, *Macromolecules*, **14**,
457 (1984)
- [4] P.L.Huyskens, W.A.P.Luck, T.Zeegers- Huyskens (Eds.), "*Intermolecular Forces*," Springer-Verlag(Berlin),1991
- [5] B.H.Meier, F.Graf, and R.R.Ernst, *J.Chem.Phys.*,**76**, 15(1982)
- [6] F.Imashiro, S.Maeda, K.Takegoshi, T.Terao, and A.Saika
Chem.Phys.Lett.,**92**, 642(1982)
- [7] F.Imashiro, S.Maeda, K.Takegoshi, T.Terao, and A.Saika
Chem.Phys.Lett.,**99**, 189(1982)
- [8] B.Shröter, H.Rosenberger, and D.Hadži, *J.Molecular Struct.*,**96**,
301(1983)

-
- [9] K.Takegoshi, A.Naito, and C.A.McDowell, *J.Magn.Reson.*, **65**, 34(1985)
- [10] G.A.Jeffrey and Y.Yeon, *Acta Cryst.*, **B42**, 410 (1986)
- [11] R.K.Harris, P.Jackson, L.H.Merwin, and B.J.Say, and G.Hägele, *J.Chem.Soc.Faraday Trans. I.*, **84**, 3649(1988)
- [12] R.Kaliaperumal, R.E.J.Sears, Q.W.Ni, and J.E.Furst, *J.Che.Phys.*, **91**, 7387(1989)
- [13] S.Ando, I.Ando, A.Shoji, and T.Ozaki, *J.Am.Chem.Soc.*, **110**,3380(1988)
- [14] E.R.Andrew, A.Bradbury, and R.G.Eades, *Nature*, **182**, 1659 (1958); I.J.Lowe, *Phys.Rev.Lett.*, **2**,285(1959)
- [15] J.Herzfeld and A.Berger, *J.Chem.Phys.*, **73**,6021(1980)
- [16] P.D.Ellis, G.E.Maciel, and J.W.McIver, Jr., *J.Am.Chem.Soc.*, **94**, 4069 (1972); I.Ando and G.A.Webb, "*Theory of NMR Parameters*," Academic press(London),1983
- [17] R.Ditchfield, *Molecular Physics*, **27**,789(1974); K.Wolinski, J.F.Hinton, and P.Pulay, *J.Am.Chem.Soc.*, **112**,8251(1990)
- [18] R.R.Ernst, G.Bodenhausen, and A.Wokaun, "*Principles of Nuclear Magnetic Resonance in One and Two dimentions*," Oxford(New York), 1987

-
- [19] A.Pines, M.G.Gibby, and J.S.Waugh, *J.Chem.Phys.*, **56**, 1776(1972)
- [20] N.Bloembergen and T.J.Rowland, *Acta Metall*, **1**, 731 (1953)
- [21] J.Fenzke, B.Maess, H.Pfeifer, *J.Magn.Reson.*, **88**, 172(1990)
- [22] S.Vega, E.T.Olejniczak, and R.G.Griffin, *J.Chem.Phys.*, **80**, 4832(1984)
- [23] J.H.Shirley, *Phys.Rev.B*, **B138**, 979(1965)
- [24] D.R.Dion and J.O.Herschfelder, *Adv. in Chem. Phys.*, **35**, edited by I.Prigogine and S.Rice, Wiley, New York(1976)
- [25] Y.Zur, M.H.Levitt, and S.Vega, *J.Chem.Phys.*, **78**, 5293(1983)
- [26] M.M.Maricq, *Phys.Rev. B*, **25**, 6622(1982)
- [27] M.Maricq and J.S.Waugh, *J.Chem.Phys.*, **70**, 3300(1979)
- [28] D.P.Raleigh, M.H.Levitt, R.G.Griffin, *Chem.Phys.Lett.*, **146**, 71(1988)
- [29] D.P.Raleigh, A.C.Kolbert, T.G.Oas, M.H.Levitt, R.G.Griffin, *J.Chem.Soc.Fraday Trans. 1*, **88**, 3691(1988)
- [30] D.P.Raleigh, A.C.Kolbert, M.H.Levitt, R.G.Griffin, *Israel J. Chem.*, **28**, 263(1988)
- [31] D.P.Raleigh, F.Creuzet, S.K.Gupta, A.C.Kolbert, M.H.Levitt, R.G.Griffin, *J.Am.Chem.Soc.*, **111**, 4502(1989)
- [32] A.C.Kolbert, D.P.Raleigh, M.H.Levitt, R.G.Griffin, *J.Chem.Phys.*, **90**, 679(1989)

-
- [33] A.C.Kolbert, H.J.M. de Groot, M.H.Levitt, M.G.Munowitz, J.E.Roberts, G.S.Harbison, J.Herzfeld, and R.G.Griffin, *Multinuclear Magnetic Resonance in Liquids and Solid-Chemical Applications*, 339, Academic Press(1990)
- [34] M.H.Levitt, D.P.Raleigh, F.Creuzet, and R.G.Griffin, *J.Chem.Phys.*, **92**, 6347(1990)
- [35] R.Tycko and G.Dabbagh, *Chem.Phys.Lett.*, **173**, 461(1990)
- [36] M.H.Levitt, T.G.Oas, R.G.Griffin, *Israel J. Chem.*, **28**, 271(1988)
- [37] T.G.Oas, R.G.Griffin, and M.H.Levitt, *J.Chem.Phys.*, **89**, 692(1988)
- [38] T.Gullion and J.Schaefer, *J.Magn.Reson.*, **81**, 196(1989)
- [39] Y.Pan., T.Gullion, and J.Schaefer, *J.Magn.Reson.*, **90**, 330(1990)
- [40] Y.Pan and J.Schaefer, *J.Magn.Reson.*, **90**, 341(1990)
- [41] G.R.Marshall, D.D.Beusen, K.Kociolek, A.S.Redlinski, M.T.Leplawy, Y.Pan, and J. Schaefer, *J.Am.Chem.Soc.*, **112**, 963(1990)
- [42] T.Gullion and J.Schaefer, *Adv. in Magn.Reson.*, **13**, 57, Academic Press(1989)
- [43] A.M.Christensen, J.Schaefer, K.J.Kramer, *Magn.Reson. in Chem.*, **29**, 418(1991)
- [44] A.Schmidt, R.A.McKay, and J.Schaefer, *J.Magn.Reson.*, **96**, 644(1992)

-
- [45] A.W.Hing, S.Vega, and J.Schaefer, *J.Magn.Reson.*, **96**,205(1992)
- [46] T.Gullion and S.Vega, *Chem.Phys.Lett.*, **194**, 423(1992)
- [47] W. Zhu, C. A. Klug, and J.Schaefer, *J.Magn.Reson.*, **A108**, 121(1994)
- [48] O.Weintraub, S.Vega, CH.Hoelger, and H.H.Limbach, *J.Magn.Reson.*, **A110**, 12(1994)
- [49] F.A.Momany, R.F.McGuire, J.F.Yan, H.A.Scheraga, *J.Phys.Chem.*, **75**, 2286(1971)
- [50] H.Kurosu, G.A.Webb, and I.Ando, *Magn.Reson. in Chem.*, **30**,1122(1992)
- [51] N.Izumiya, T.Kato, M.Ohno, and H.Aoyagi, "Peptide Synthesis," Marzen(Tokyo), 1975
- [52] O.W.Howarth, *Prog.NMR Spectrosc.*,**12**,1(1978)
- [53] Y.Harada, and Y.Iitaka, *Acta Crystallogr.*, **B30**,1452(1974)
- [54] G.Valle, M.Crisma, F.Formaggio, C.Toniolo, and C.Jung, *Justus Liebigs Ann. Chem.*, 1055(1987)
- [55] V.Lalitha, and E.Subramanian, *Indian J.Pure Appl.Phys.*, **23**, 506 (1985)
- [56] P.G.Jones, L.Falvello, and O.Kennard, *Acta Crystallogr.*, **B34**, 1939 (1978)

-
- [57] S.Wo, P.Declercq, B.Tinant, and M.V.Meerssche, *Bull.Soc.Chim.Belg.*,
96, 515 (1987)
- [58] S.Arnott, and S.D.Dover, *J.Mol.Biol.*,30,209(1967)
- [59] S.J.Opella, and M.H.Frey, *J.Am.Chem.Soc.*, 101,5854(1979)
- [60] K.Morokuma, *Chem.Phys.Lett.*,19,129(1971)
- [61] C.J.Hartzell, M.Whitfield, T.G.Oas, and G.P.Drobny, *J.Am.Chem.Soc.*,
109,5966(1987)
- [62] T.Yamazaki, *Ph.D.Thesis*, Osaka University, 1992
- [63] W.Yang, W.A.Hendrickson, R.J.Crouch, and Y.Satow, *Science*, 249,
1398(1990)
- [64] K.Katayanagi, M.Miyagawa, M.Matsushima, M.Ishikawa, S.Kanaya,
H.Nakamura, M.Ikehara, T.Matsuzaki, and K.Morikawa, *J.Mol.Biol.*,
223, 1029 (1992)
- [65] J.Deisenhofer and W.Steigemann, *Acta Crystallogr., Sect.B*, 31, 238
(1975)
- [66] E.Tuchen, and P.E.Hansen, *Biochemistry*, bf 27,8568(1988)
- [67] R.Bosh, K.P.Voges, G.Jung, and W.Winter, *Acta Crystallogr., Sect.C*,
39, 481(1983)
- [68] M.E.Kamwaya, O.Oster, and H.Bradaczek, *Acta Crystallogr., Sect.B*,
38, 172(1982)

-
- [69] S.Arnott, and S.D.Dover, *J.Mol.Biol.*, **30**, 209(1967)
- [70] S.Arnott, S.D.Dover, and A.Elliott, *J.Mol.Biol.*, **30**, 201(1967)
- [71] B.Lotz, and H.D.Keith, *J.Mol.Biol.*, **61**, 201(1971)
- [72] T.Konishi, and M.Kurokawa, *Sen'i Gakkaishi*, **24**, 550(1968)
- [73] D.B.Chesnut, *Annu.Rep. NMR Spectrosc.*, bf 21, 51(1989)
- [74] A.Naito, S.Ganapathy, K.Akasaka, and C.A.McDowell, *J.Chem.Phys.*,
bf 74, 3190(1981)
- [75] S.Arnott, S.D.Dover, and A.Elliott, *J.Mol.Biol.*, **30**, 201(1967)
- [76] K.Katayanagi, M.Miyagawa, M.Matsushima, M.Ishikawa, S.Kanaya,
H.Nakamura, M.Ikehara, T.Matsuzaki, and K.Morikawa,
J.Mol.Biol., **223**,1029(1992)
- [77] T.Gullion, *J. Magn.Reson.*, **89**, 479(1990)
- [78] C.Klug, W.Zhu, M.Merritt, and J.Schaefer, *J.Magn.Reson.*, in press

Acknowledgments

The author would like to express his gratitude for Professor Isao Ando to support this work and make innumerable helpful discussion. Prof. Akira Shoji and Associate Prof. Takuo Ozaki are acknowledged for their helpful suggestion regarding peptides synthesis.

It is also grateful for Dr. Hiromichi Kurosu, Research Associate, Department of Polymer Chemistry, Dr. Hiroaki Yoshimizu, Research Associate, Department of Material Science, Nagoya Institute of Technology, Dr. Hidekazu Yasunaga, Research Associate, Department of Polymer Science, Kyoto Institute of Dr. Shigeki Kuroki, Koubunshi-sozai Center.

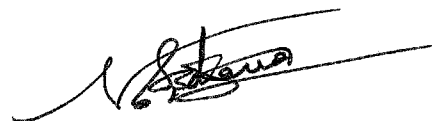
The author gives his thanks to Ms. Mizuyo Kikuchi and Mr. Masato Sone as well.

Ms. Chiyoko Watanabe should be acknowledged for their making arrangements for NMR measurements. The author would like to express his gratitude for Ms. Keiko Tamura to do with troublesome office work. The author would like to express his ultimate gratitude to all of staffs at Ando lab.

The author should like to express his gratitude for Prof. Yoshio Inoue, Associate Prof. Minoru Sakurai, and Assistant Prof. Naoko Yoshie to enable

the author this dissertation. It is grateful for all the colleagues at Inoue-Sakurai group to discuss his research work.

The author is indebted the Fellowships of the Japan Society for the Promotion of Science for Japanese Junior Scientists and also thank Professors Jacob Schaefer and Isao Ando to enable the author to perform this research work at the Department of Chemistry, Washington University in St. Louis.



Naoki Asakawa